AEDC-TR-70-235

INVESTIGATION OF FLAT-PLATE ASPECT RATIO EFFECTS ON RAMP-INDUCED, ADIABATIC, BOUNDARY-LAYER SEPARATION AT SUPERSONIC AND HYPERSONIC SPEEDS

J. Don Gray and R. W. Rhudy

ARO, Inc.

March 1971

VON KÁRMÁN GAS DYNAMICS FACILITY
ARNOLD ENGINEERING DEVELOPMENT CENTER
AIR FORCE SYSTEMS COMMAND
ARNOLD AIR FORCE STATION, TENNESSEE

140

NOTICES

When U. S. Government drawings specifications, or other data are used for any purpose other than a definitely related Government procurement operation, the Government thereby incurs no responsibility nor any obligation whatsoever, and the fact that the Government may have formulated, furnished, or in any way supplied the said drawings, specifications, or other data, is not to be regarded by implication or otherwise, or in any manner licensing the holder or any other person or corporation, or conveying any rights or permission to manufacture, use, or sell any patented invention that may in any way be related thereto.

Qualified users may obtain copies of this report from the Defense Documentation Center.

References to named commercial products in this report are not to be considered in any sense as an endorsement of the product by the United States Air Force or the Government.

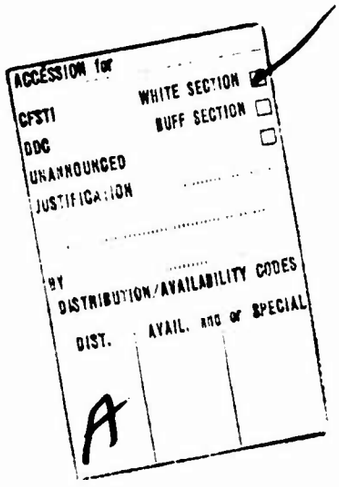

INVESTIGATION OF FLAT-PLATE ASPECT RATIO EFFECTS ON RAMP-INDUCED, ADIABATIC, BOUNDARY-LAYER SEPARATION AT SUPERSONIC AND HYPERSONIC SPEEDS

J. Don Gray and R. W. Rhudy
ARO, Inc.

FOREWORD

The work reported was done at the request of the Air Force Flight Dynamics Laboratory (AFFDL), Flight Dynamics Control Criteria Division, Air Force Systems Command (AFSC), under Program Element 62201F, Project 8219.

The results of the tests presented were obtained by ARO, Inc. (a subsidiary of Sverdrup & Parcel and Associates, Inc.), contract operator of the Arnold Engineering Development Center (AEDC), AFSC, Arnold Air Force Station, Tennessee, under Contract F40600-71-C-0002. The tests were conducted from December 10, 1969, to March 25, 1970, under ARO Project No. VT0036, and the manuscript was submitted for publication on June 16, 1970.

This technical report has been reviewed and is approved.

Emmett A. Niblack, Jr.
Lt Colonel, USAF
AF Representative, VKF
Directorate of Test

Joseph R. Henry
Colonel, USAF
Director of Test

ABSTRACT

An experimental investigation of the effects of flat-plate aspect ratio on both laminar and turbulent boundary-layer separations induced by ramps was conducted at free-stream Mach numbers of 6, 8, and 10. Reynolds numbers, based on flat-plate length, ranged from 0.06 million to 1.0 million (laminar) and from 2.6 million to 9.1 million (turbulent) at near-adiabatic model wall conditions. Local Mach number on the flat plate was varied by pitching the laminar model at all free-stream Mach numbers. Longitudinal surface pressure distributions at several spanwise stations were measured to define the lateral pressure gradients and the spanwise variation of the longitudinal extent of the separation region. Data are presented to support the conclusion that for a flat plate short enough (2.5 in.) to achieve laminar flow reattachment, it is required that the flat-plate aspect ratio be of the order of 3 to be assured of negligible effects induced by the finite span. Moreover, the results for the turbulent flow separation model (14 in. flat-plate chord) at Mach number 6 indicate that even the largest span model tested (28 in.) was not free of finite span effects and, therefore, that flat-plate sections with aspect ratio greater than 2 may also be required for turbulent separation investigations. Tabulated data are also presented in addition to the extensive plotted results.

CONTENTS

ILLUSTRATIONS

APPENDIXES

NOMENCLATURE

AR	Flat-plate aspect ratio, $2b/x_t$
b	Model semispan, in.
C	Chapman-Rubesin viscosity factor $(T/T_{wall})(\mu_{wall}/\mu)$
C_p	Pressure coefficient $(p - p_w)/(q_w)$
h	Side plate height at ramp trailing edge, in.
ℓ	Ramp surface length, in.
M	Mach number
P	Nondimensionalized pressure in Chapman-Curle coordinates, $1.75\left(\frac{Re_{\bar{o}}^{1/4}}{C^{1/4}M_w^{3/2}}\right)\left(\frac{p - p_{\bar{o}}}{p_{\bar{o}}}\right)$
p	Static pressure, psia
p_t'	Measured pitot probe pressure, psia
q	Dynamic pressure, psia
Re	Reynolds number based on local inviscid (u/ν) flat-plate conditions and length x
T	Temperature, °R
u/ν	Unit Reynolds number, $in.^{-1}$
X	Nondimensionalized distance in Chapman-Curle coordinates, $0.47\left(\frac{M_w^{1/2}\,Re_{\bar{o}}^{1/4}}{C^{1/4}T_{wall}/T_w}\right)\left(\frac{x - x_{\bar{o}}}{x_{\bar{o}}}\right)$
x	Streamwise surface distance measured from leading edge, in.
y	Vertical height measured from and normal to surface, in.
z	Spanwise distance from model centerline (see Fig. 1c), in.

α	Angle between flat plate and free stream, deg
δ	Boundary-layer thickness, in.
θ	Angle between ramp and flat plate, deg
μ	Dynamic viscosity, lb-sec/ft^2
$\bar{X}$	Hypersonic viscous interaction parameter, $M_w^3[C_w/Re]^{1/2}$

SUBSCRIPTS

c	Value at ramp leading edge
e	Value at side plate leading edge
$\bar{o}$	Value at the start of the interaction (see Fig. 11)
t	Tunnel stilling chamber conditions
to	Value at the onset of transition
w	Local inviscid value
δ	Value at the boundary-layer edge
∞	Free-stream conditions

SECTION I
INTRODUCTION

Over the last two decades a considerable number of experimental investigations of shock-wave-induced separation of laminar and turbulent boundary layers have been conducted using either ramps or external wedges to generate the pressure rise. The most noteworthy investigations were those of Gadd, Holder, and Regan (Ref. 1) and Chapman, Kuehn, and Larson (Ref. 2), both of which established the dominant influence of boundary-layer transition on the viscous interaction when it occurs during flow reattachment.

Although the question of lateral (spanwise) outflow from the interaction zone was considered in these early experimental investigations, no direct investigation of the influence of aspect ratio (AR) was undertaken until the experiments of Lewis (Ref. 3) at $M_\infty = 4$. It is to be noted that the existence of two-dimensional flow is crucial to a satisfactory evaluation of present theories for supersonic, adiabatic, laminar flow separation since they are all derived assuming the lateral velocity is zero. Lewis found that the centerline pressure distribution reached a limit when the lateral distance between vertical end plates was made equal to or greater than the distance from the flat-plate leading edge to the ramp hinge line. In an investigation at $M_\infty \geq 14$, Holden (Ref. 4) actually varied the flat plate aspect ratio as well as that corresponding to the distance between end plates, and he found that a limit was reached at an aspect ratio of 2. However, the results obtained by Rhudy (Ref. 5) with a model having an aspect ratio of 2.2 indicated that (1) pitching the model to reduce the local Mach number affected the spanwise flow uniformity, and (2) increasing the local Mach number beyond 6 (model unpitched) may also adversely affect the uniformity.

The present experimental investigation was undertaken to define the effects of (1) local Mach number, (2) Reynolds number, and (3) model attitude on the aspect ratio required to achieve uniform flow on the centerline of symmetry and which would be equivalent to that obtained with an infinite span flat-plate and ramp combination. The majority of the experiments were conducted using a one-piece ramp model designed to assure the separation of a laminar boundary layer and which had an aspect ratio as large as practical. The maximum aspect ratio was fixed by choosing a flat-plate length equal to one of those used by Lewis and making the span approximately equal to the width of the fairing doors in the continuous flow hypersonic tunnels. Starting with an aspect ratio of 11.2, the so-called "laminar" model span was successively halved (three times) at the conclusion of each

series of tests at free-stream Mach numbers of 6, 8, and 10. More limited tests were conducted with a two-piece model designed to investigate the effects of aspect ratio and Mach number on a turbulent boundary-layer separation. Because the tests were conducted at hypersonic Mach numbers, it was necessary that the flat plate be over a foot long to assure turbulent flow an adequate distance upstream of the adjustable ramp ($\theta \geq 30$ deg). For this reason, the maximum aspect ratio was limited to 2, and it was only halved one time to reduce the ratio of the so-called "turbulent" model. It should be noted that the span of both models was considerably less than the inviscid test core, except at $M_\infty = 10$ where they were nearly equal.

To deduce the two-dimensionality of the flow, the longitudinal surface pressure distribution was measured at several spanwise stations. From these data it was possible to define both the lateral pressure gradients and the quantitative change in the extent of the interaction.

The investigations were conducted in the von Kármán Gas Dynamics Facility (VKF) 50-in.-diam Hypersonic Wind Tunnels (B) and (C).

SECTION II
APPARATUS

2.1 MODELS AND SUPPORTS

Two basic models were designed and fabricated by AEDC. One model consisted of a 2.5-in.-chord flat plate with a fixed-angle ramp (9.5 deg) with a chord of 12 in. This model, shown installed in the wind tunnel in Fig. 1a, was used only for the investigations of laminar flow separations and is therefore referred to as the laminar model. The other basic model, Fig. 1b, had a 14-in.-chord flat plate with an 8-in.-chord ramp and available ramp angles of 30, 35, and 45 deg. This model was used for the turbulent investigation. A modification of the ramp support was made to this so-called turbulent model which extended the ramp chord to 14 in. and provided a ramp angle of 9.5 deg for use in the laminar investigation. One row of 0.093-in. steel balls, spaced 0.2 in. apart and 1.25 in. from the leading edge, was used to induce transition during tests with the larger ramp angles ($\theta \geq 30$ deg).

Both the laminar and turbulent models were designed so that the original 28-in. span could be reduced by cutting equal amounts from each side. This provided for laminar configurations with spans and aspect

ratios of 28 in. - 11.20, 14 in. - 5.60, 7 in. - 2.80, 3.4 in. - 1.35, and the special case, using the turbulent model, of 28 in. - 2.00. The turbulent model was designed for two spans and aspect ratios: 28 in. - 2.0 and 14 in. - 1.0.

Lower surface skirts were an integral part of all configurations, and removable upper side plates were provided for each configuration. These upper side plates were designed to start near the beginning of the ramp-induced interaction and extend to the trailing edge of the ramp. These side plates were made of 0.020-in. sheet metal, and the leading edges were beveled approximately 45 deg. A general sketch of all configurations is shown in Fig. 1c, and the dimensions for each are given below.

MODEL DIMENSIONS

Configuration	Aspect Ratio*	b, in.	x_c, in.	ℓ, in.	θ, deg	x_{c_2}, in.	h, in.
Laminar Models	11.20	14.0	2.5	12.0	9.5	1.0	1.5
	5.60	7.0	2.5	12.0	9.5	1.0	1.5
	2.80	3.5	2.5	12.0	9.5	1.0	1.5
	2.00	14.0	14.0	14.0	9.5	7.0	1.0
	1.35	1.7	2.5	12.0	9.5	1.0	1.5
Turbulent Models	2.0	14.0	14.0	0	---	---	---
	2.0	14.0	14.0	8.0	30	12.0	0.75
	2.0	14.0	14.0	8.0	35	10.0	0.75
	2.0	14.0	14.0	8.0	45	(No Side Plates)	
	1.0	7.0	14.0	8.0	35	10.0	0.75

*Aspect ratio = AR = $2b/x_c$

The laminar model was originally instrumented with 173 pressure taps distributed among nine longitudinal rows and nine thermocouples located as shown in Table Ia of Appendix I. The turbulent model (x_c = 14 in.) originally had 130 pressure taps distributed among five longitudinal rows as given in Table Ib, Appendix I.

Because of limitations of the pressure measuring systems and the absence of some of the taps after the model had been cut, only a portion of these taps were used for any configuration. The instrumentation rows used and the corresponding relative spanwise locations for each configuration are given in Table Ic, Appendix I. All of the pressure taps were 0.015-in. ID except ten on the laminar model, five of which were 0.030-in. ID and five of which were 0.062-in. ID. These larger diameter taps were used, early in the tests, to determine if the orifice diameter had any effect on either the response time or the precision of measurement in the region of separation. These checks showed, however, that the pressure stabilized as quickly with the 0.015-in. taps as

with the larger diameters, and that the measured values were the same. This constant stabilization time is attributed to the very short length of small diameter (see insert in Fig. 1c). After these checks, the large diameter taps were no longer used. The thermocouples were used to monitor the general level of model surface temperature; nine were provided for the laminar model and six for the turbulent one.

Both models were attached to model mounting equipment (a 12-deg bent sting in most cases) by an offset bracket which bolted to the lower surface of the model and aligned the upper surface of the flat plate parallel to the centerline of the sting. The mounting equipment provided for flat plate pitch angles from 0 to 25 deg and for vertical positioning from 2.7 in. below the tunnel centerline to 3.2 in. above centerline.

2.2 INSTRUMENTATION

Model surface pressures were measured at M_∞ = 6 and 8 with 1-psid transducers on the forward plate and 15-psid transducers on the ramp. At M_∞ = 10, 1- and 15-psid transducers were switched in and out of the system automatically to allow measuring to the best precision. All transducers were referenced to near vacuum.

The pitot pressure measurements were made with a 0.026-in.-high oval probe connected to a 15-psid transducer which had a variable reference from near vacuum to atmospheric pressure. This reference pressure was measured by either a 1- or 15-psid transducer.

From repeat calibrations the estimated precision of the pressure measurements was ±0.1 percent of transducer rating except for (1) the 1-psid transducers at M_∞ = 10, where the precision was ±0.0002 psia or ±1.0 percent, whichever was greater, and (2) the pitot pressure, where the precision was ±0.01 psia or ±1.0 percent, whichever was greater.

The probe drive mechanism allowed the probe to be positioned with an estimated precision of ±0.010 in. in the x direction, ±0.003 in. in the y direction and ±0.050 in. in the z direction.

The precision of the temperature measurements, using Chromel®-Alumel® thermocouples, was ±2°F or ±0.5 percent, whichever was greater. Model flow-field shadowgraphs (parallel beam) were obtained during all tests. High-speed schlieren motion pictures (1000 frames per second) were taken during some tests with the turbulent model.

2.3 WIND TUNNELS

The tunnels (Hypersonic Wind Tunnels (B) and (C)) are continuous, closed-circuit, variable density wind tunnels with axisymmetric, contoured nozzles and 50-in.-diam test sections. Tunnel B was operated at a nominal Mach number of 6 or 8 at stagnation pressures from 30 to 285 and from 50 to 800 psia, respectively, at stagnation temperatures up to 1350°R. Tunnel C was operated at a nominal Mach number of 10 at stagnation pressures from 250 to 2000 psia at 1900°R stagnation temperature. The model may be injected into the tunnels for a test run and then retracted for model cooling or model changes without interrupting the tunnel flow.

SECTION III
PROCEDURE

3.1 TEST CONDITIONS AND METHODS

The tests were conducted at nominal free-stream Mach numbers of 6, 8, and 10 with Reynolds numbers, based on the length to the hinge line, from 0.06 million to 1.0 million for the laminar configurations and 2.6 million to 9.1 million for the turbulent configurations. In order to reduce the free-stream Reynolds number below that obtained during normal tunnel operation at $M_\infty = 6$, some runs were made with the stilling chamber temperature raised to approximately 1.5 times the normal. The normal tunnel operating conditions are shown in Figs. 2 through 4, and the conditions at which the present tests were conducted are indicated by symbols.

In order to obtain local Mach numbers on the flat plate lower than free-stream flow, the model was pitched to an angle of attack, α. The ratios used to calculate the local inviscid flow conditions (obtained from the graphs in Ref. 5) are listed below.

RATIOS OF LOCAL TO FREE-STREAM CONDITIONS

M_∞ (Nominal)	α, deg	M_w/M_∞	p_w/p_∞	$(\mu/\nu)_w/(\mu/\nu)_\infty$	T_w/T_∞
6	11.0	0.75	4.1	1.50	1.62
8	8.8	0.75	4.4	1.53	1.68
8	16.5	0.563	10.7	1.33	2.75
10	5.9	0.80	3.6	1.52	1.53
10	12.4	0.60	9.8	1.40	2.60

As stated previously, the two basic models were designed so that equal sections could be cut from each side in order to reduce the aspect ratio (AR). A complete range of Mach numbers and Reynolds numbers were covered using the full span (AR = 11.2) laminar model, and then the model was cut to half span (AR = 5.6). This procedure was repeated two more times for the laminar model. This same procedure was used for the turbulent model; however, because of the flat-plate size (2b = 28 in. and x_c = 14 in.) the span was only reduced one time. This provided for aspect ratios of 2.0 and 1.0.

Since the plate length of the turbulent model was intentionally restricted to keep the maximum aspect ratio as large as possible, boundary-layer trips were required to ensure a turbulent profile sufficiently far upstream of the ramp hinge line. Testing of the turbulent model was begun with pitot surveys on the model without a ramp at M_∞ = 8. Inasmuch as these data indicated that the profiles were at best transitional, subsequent tests were only conducted at M_∞ = 6.

Before data were recorded, the model was injected into the tunnel and allowed to soak until nominal equilibrium of the model surface temperatures was attained. In general these temperatures were of the order of 0.92 T_{t_∞} at Mach number 6, 0.90 T_{t_∞} at Mach number 8, and 0.78 at Mach number 10.

Before injection into the tunnel, the model was adjusted for zero roll to within ±0.1 deg using an inclinometer. After the model was injected into the airstream and allowed to reach the equilibrium wall temperature, zero pitch was set to within ±0.05 deg using an optical level and a scribe line on the model. All other pitch angles were set to within ±0.1 deg using the standard tunnel pitch mechanism. Model leading-edge yaw was checked on each installation and found to be within ±0.1 deg.

During the early stages of the laminar investigation at each Mach number, checks were made to determine the best position of the model, relative to the wind tunnel centerline, for obtaining uniform flow. As stated previously, the model mounting equipment allowed the model to be positioned from 2.7 in. below to 3.2 in. above the tunnel centerline, and the model could be mounted either with the instrumented surface up or down. While there appeared to be little or no effect of varying the model position at M_∞ = 8 or 10, it was determined, from the repeatability and uniformity of the data as well as from tunnel empty calibration data that the highest quality data were obtained when the model was either above or below the tunnel centerline at M_∞ = 6. All subsequent data, at M_∞ = 6, were obtained with the model positioned 2.7 in. above the centerline with the instrumented surface up.

3.2 SCOPE OF RESULTS

In order to investigate the effects of local Mach number, Reynolds number, model attitude, and aspect ratio, several configurations differing only in aspect ratio were tested over a wide range of free-stream Mach numbers and Reynolds numbers. Data were obtained with the same model both unpitched and pitched but at the same local Mach number and Reynolds number. A complete summary of the test matrix for the laminar configurations is given in Table II, Appendix I, and the tabulated data for the 11.2 aspect ratio configuration are given in Appendix II.

A 45-deg ramp angle was tested first on the turbulent model, since it was desired that the separation zone not be negligible. It was, in fact, so large that separation occurred upstream of the pressure taps and in a region where the boundary layer was in the early stages of transition. A 30-deg ramp was tested next and found to produce only a small separation zone. Therefore, the 35-deg ramp was finally tested and found to be satisfactory. A complete summary of the test matrix for the turbulent investigation is given in Table III of Appendix I, and tabulated surface pressure data for the 30- and 35-deg ramp configurations are given in Appendix II.

3.3 UNCERTAINTIES OF THE DATA

An evaluation of the influence of random measurement errors is presented in this section to provide a partial measure of the precision of the results contained in this report. No evaluation of the systematic measurement error (bias) is included here. Therefore, the precision of the test results was estimated using the estimated instrumentation precisions quoted in Section II, and the uncertainties in free-stream conditions given below, considering that the propagation of these independent measurement errors is closely approximated by a Taylor's series expansion.

The estimated uncertainties in free-stream Mach number (based on repeat calibrations) and stagnation pressure are presented below along with the corresponding estimates of the precision of pertinent free-stream conditions.

PERCENTAGE (±) OF UNCERTAINTIES IN FREE-STREAM CONDITIONS

Nominal Mach Number	M_∞	p_{t_∞}	p_∞	q_∞	$(u/\nu)_\infty$
6	0.5	0.7 to 1.0	3.2	2.3	2.2
8	0.1	0.2 to 0.4	0.9	0.7	1.6
10	0.2	0.3 to 0.5	1.4	1.1	1.7

The estimated random errors in the surface pressure measurements are presented below in terms of the ratio, p/p_w, for both the flat plate and ramp because of the significant differences in pressure at all test conditions. The ranges quoted correspond to those at maximum free-stream stagnation pressure and to those at the minimum pressure, values of which are presented in Section 3.1.

PERCENTAGE (±) OF UNCERTAINTIES IN SURFACE PRESSURE RATIO, p/p_w *

M_∞		$0 < x/x_c \leq 1$		$1 < x/x_c \leq 3$	
		p_{t_∞}, max	p_{t_∞}, min	p_{t_∞}, max	p_{t_∞}, min
6	6	3.2	8.3	4.0	32.0
	4.5	3.4	3.9	3.5	11.0
8	8	1.4	20.0	3.3	55.5
	6	1.6	4.7	1.9	18.0
	4.5	1.3	2.3	1.5	10.4
10	10	1.4	4.2	3.2	1.4
	8	3.0	3.0	2.6	2.3
	6	2.9	2.9	2.1	2.7

*The estimated uncertainty in the oblique shock pressure ratio, p_w/p_∞, was found to vary from 1.0 to 1.9 percent using the uncertainties quoted for M_∞ and ±0.1 deg for the deflection angle.

The estimated maximum uncertainty in surface pressure coefficient for the turbulent model at $x/x_c \approx 1$ is ±2.6 percent.

The uncertainties associated with the pitot pressure surveys were estimated for the condition of maximum stagnation pressure and for the appropriate local conditions ranging from those at the boundary-layer edge to those at the surface. They are listed below.

PERCENTAGE (±) OF UNCERTAINTY IN PITOT PROBE DATA

M_∞	M_w	$(p_t'/p_t)_w$		M	
		p_{t_∞}, max	p_{t_∞}, min	p_{t_∞}, max	p_{t_∞}, min
6	6	2.0	5.3	0.6	2.7
	4.5	1.8	2.2	0.3	1.1
8	8	1.3	10.0	0.8	5.0
	6	0.9	2.6	0.3	1.3

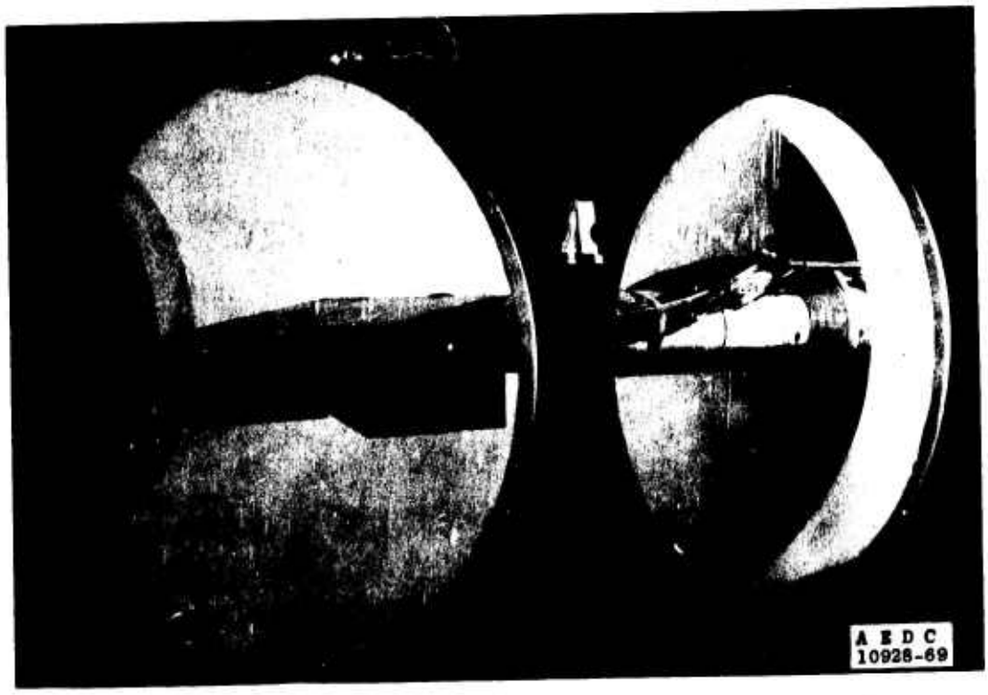

a. Laminar Model (AR = 5.6) Installed in Hypersonic Wind Tunnel B

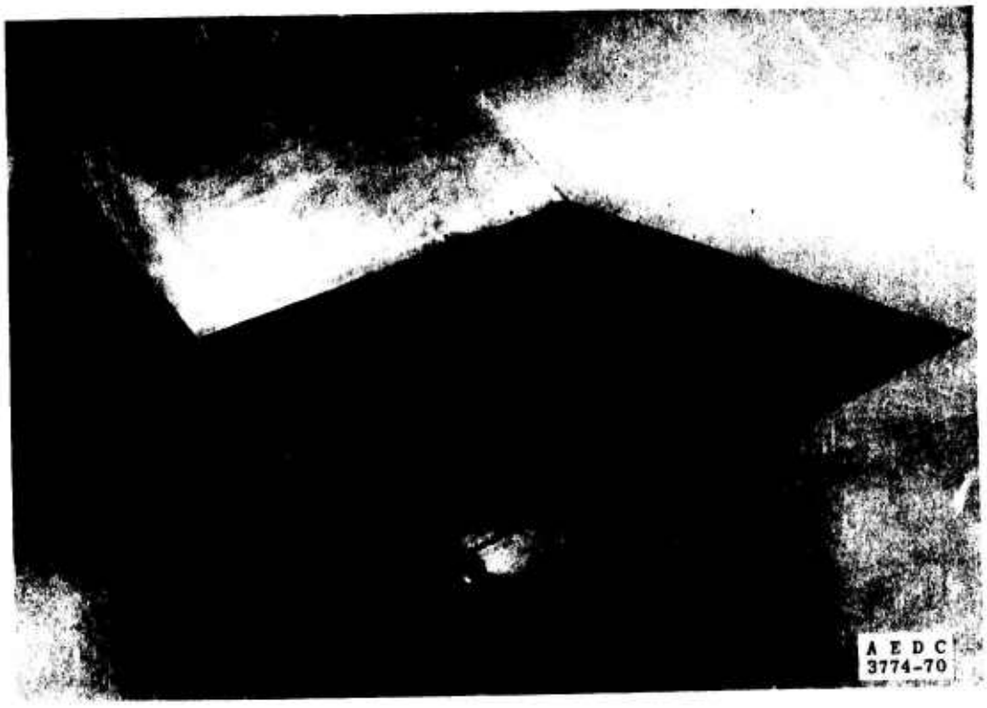

b. Turbulent Model Photograph, AR = 1.0

Fig. 1 Model Details

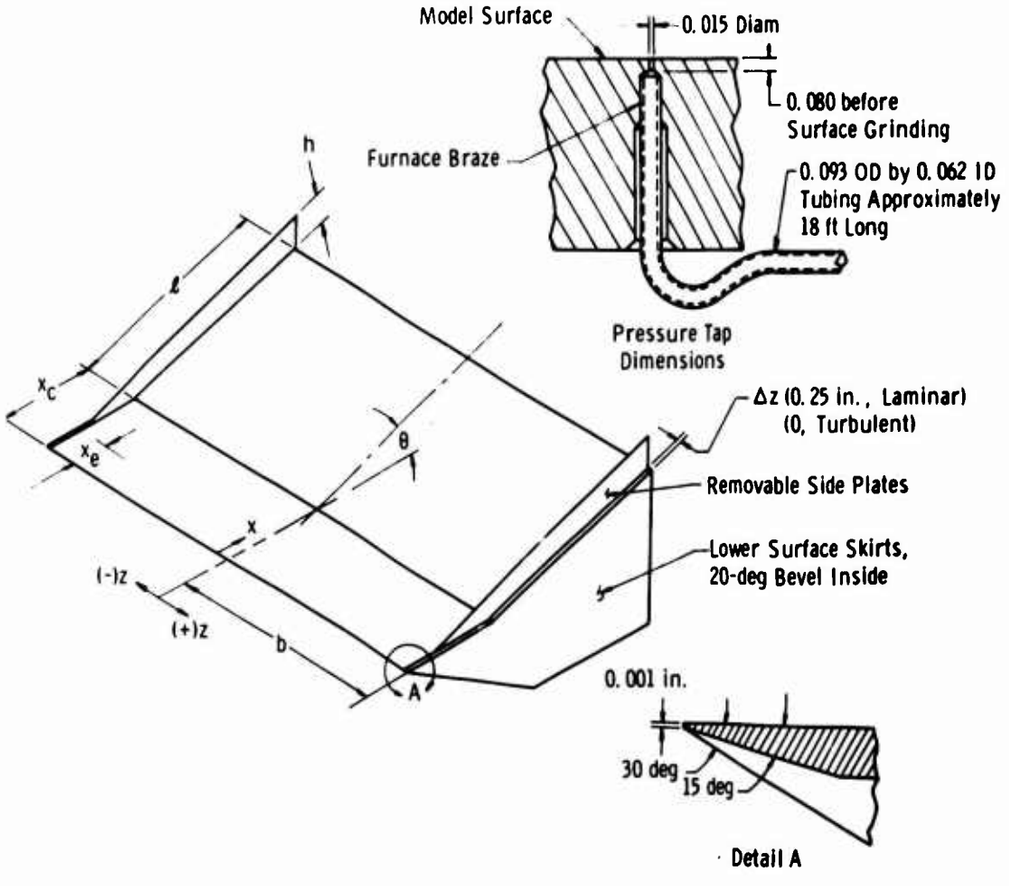

c. Geometry

Fig. 1 Concluded

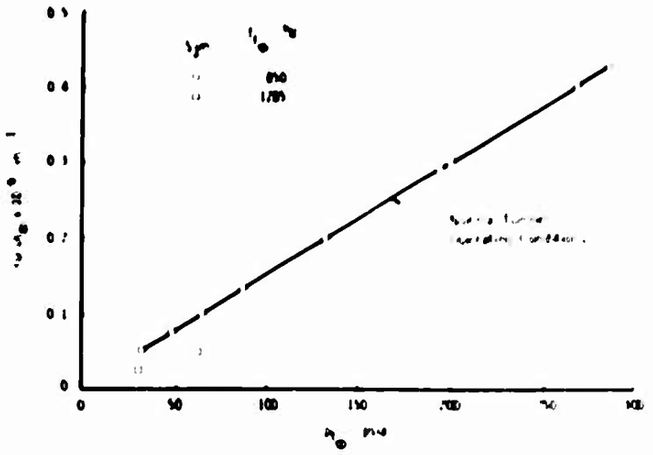

a. $M_\infty \approx 6$

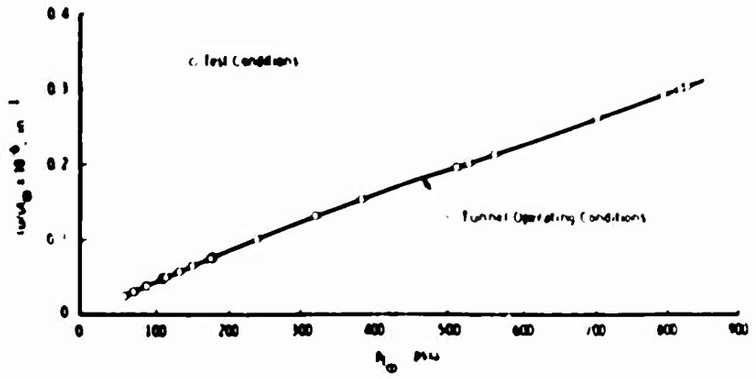

b. $M_\infty \approx 8$

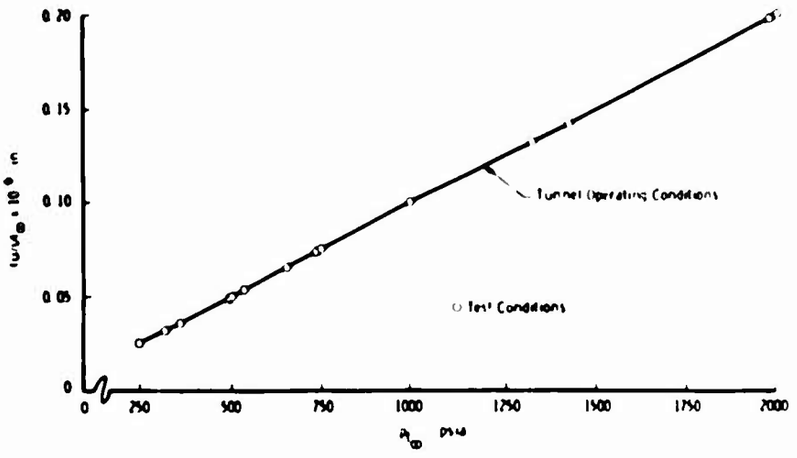

c. $M_\infty \approx 10$

Fig. 2 Free-Stream Unit Reynolds Number as a Function of p_{t_∞}

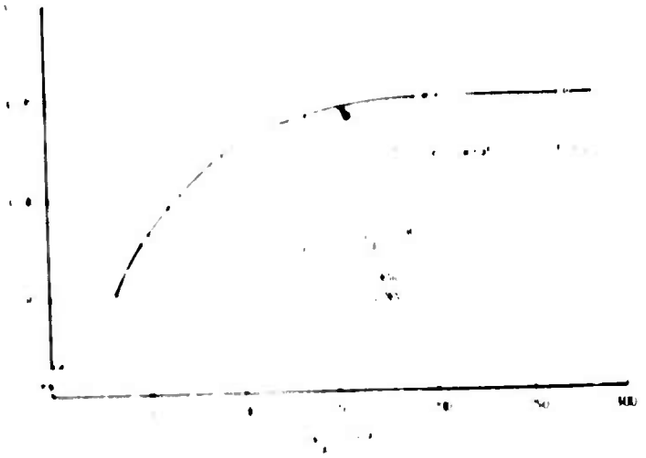

a. $M_\infty \approx 6$

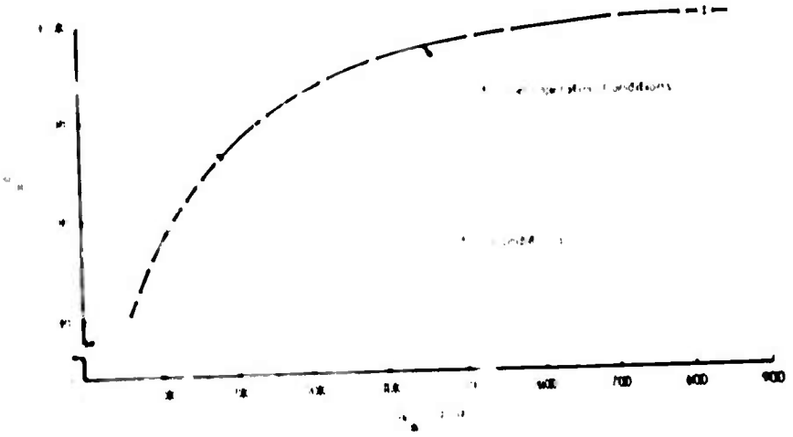

b $M_\infty \approx 8$

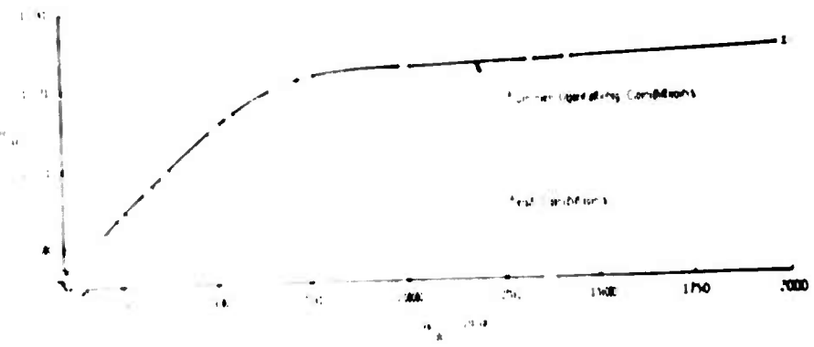

c $M_\infty \approx 10$

Fig 3 Free Stream Mach Number as a Function of p_{t_∞}

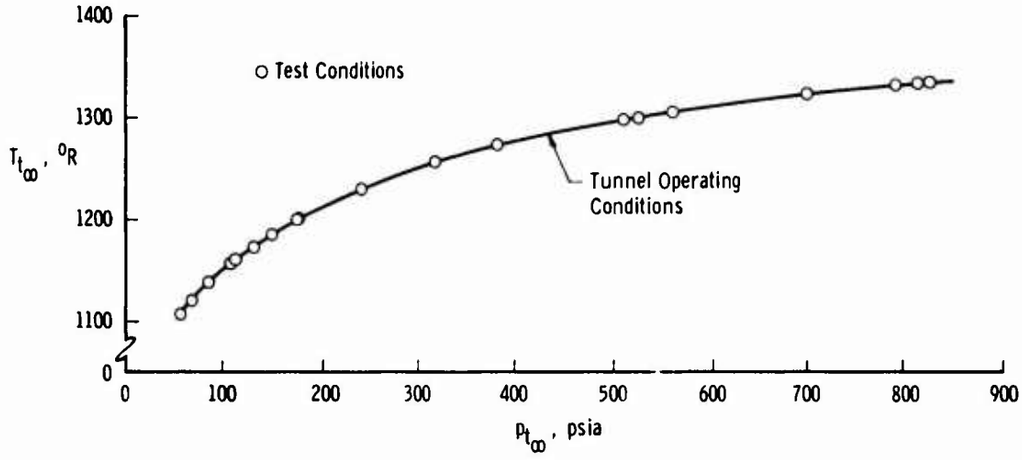

Fig. 4 Free-Stream Total Temperature as a Function of p_{t_∞} for $M_\infty \approx 8$

SECTION IV
RESULTS

4.1 LAMINAR FLOW MODEL

4.1.1 Influence of Reynolds Number and Mach Number

In order to demonstrate that a laminar flow reattachment could be obtained on the laminar model, this investigation was conducted over a wide range of Reynolds numbers at free-stream Mach numbers of 6, 8, and 10. The information used to judge if the boundary layer was laminar through reattachment was: (1) the location of the start of transition determined from shadowgraph photographs, and (2) the change in the centerline pressure distribution as Reynolds number was increased at a constant Mach number (Ref. 3).

Shadowgraph pictures for $M_W = M_\infty = 6$ at four Reynolds numbers are shown in Fig. 5 with the estimated value for the onset of boundary-layer transition indicated thereon. These photographs show that as the Reynolds number was increased from 0.13 to 0.50 million, the location of the start of transition moved forward on the ramp, but appears to always have been well downstream of reattachment (assumed to be upstream of $2x_c$). These transition locations are compared in Fig. 6 with an estimated curve for the onset of boundary-layer transition on a flat plate which was derived from data in Ref. 6. Because the results in Ref. 6 correspond to the end of transition, it was necessary to reduce the values by 50 percent* in order to correspond to the condition

*Pitot survey data in Ref. 6 indicate that the minimum pitot pressure occurs at no less than 50 percent of the location of the maximum.

of interest in this work. This figure indicates that the ramp deflection (9.5 deg) caused transition to occur much earlier than estimated for a flat plate (about 50 percent) but that it was never further upstream than $x \approx 4.9$ in. ($x/x_c = 1.96$) in this investigation ($Re_c = 1.0$ million). It was observed that, within the uncertainty in reading the shadowgraphs, the location of the onset of transition at all test conditions investigated is well represented by the data in Fig. 6 based upon local flow conditions, M_w and $(u/\nu)_w$.

The centerline pressure distribution for the 11.2 aspect ratio model at $M_w = M_\infty = 6$ and several Reynolds numbers is shown in Fig. 7. These data show that as Reynolds number was increased, the pressure gradient and maximum pressure ratio on the ramp were increased and, most importantly, the extent of the interaction on the flat plate increased. However, except at the lowest Reynolds number where there is little or no separation indicated, the maximum pressure ratio on the flat plate (sometimes referred to as the "plateau pressure") remained constant. The trend of an upstream movement of the beginning of the interaction for increased Reynolds number is sufficient evidence of the existence of laminar flow through reattachment (Ref. 3) for the entire Reynolds number range shown in Fig. 7. The location of the onset of transition, based on Fig. 6, is also well downstream of the probable reattachment location.

Longitudinal pressure distributions for $M_w = M_\infty = 8$ are presented in Fig. 8 for three spanwise locations ($z/b = 0$, 0.66 and 0.91) on the 11.2 aspect ratio model in order to show that the general trends observed on the centerline of symmetry are preserved to the vicinity of the tips. It may be noted, however, that there were significant changes in the level of the distributions off centerline (see Figs. 8b and c) at a fixed Reynolds number.

Centerline pressure distributions obtained at $M_w = M_\infty = 10$ for the range of Reynolds number investigated are presented in Fig. 9. These data also exhibit the trend which is characteristic of laminar flow reattachment. It may be noted that at $Re_c = 0.06$ million, the upstream influence (i.e., the start of the interaction) was not much more than 10 percent of the flat-plate length, whereas the length required to achieve the overall ramp pressure rise was essentially unchanged from that required at $Re_c = 0.5$ million.

The effects of Mach number on the longitudinal (centerline) distribution at a low and a high Reynolds number are illustrated in Fig. 10. It is evident from these data that although there were no drastic changes in the characteristic pressure distribution, the upstream influence of the

ramp decreased with Mach number increase. These results also show the ramp pressure gradient (as well as the maximum gradient on the flat plate) to be a relatively weak function of Mach number. It is perhaps more apparent in these figures that the ramp is the most substantially affected by the viscous interaction and that the extent of it increases with Mach number.

A summary of the data in terms of the relative extent of the interaction on the flat plate is presented in Fig. 11 to show simultaneously the effects of Reynolds number and Mach number. All of the data follow the same general trend with Reynolds number but over a much wider range than heretofore shown (e.g., data in Ref. 3 were judged transitional at $Re_c \gtrsim 0.3$ million).

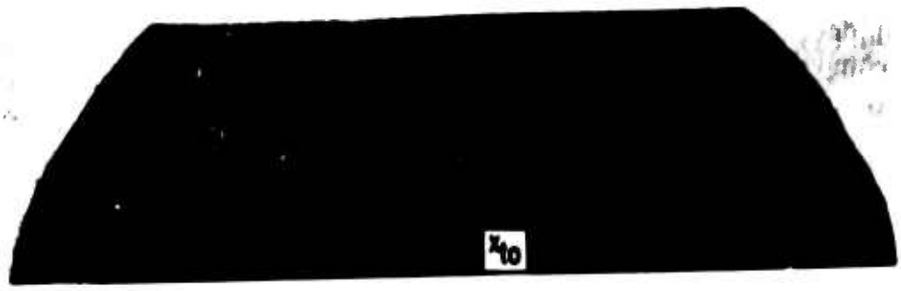

a. $Re_c = 0.13 \times 10^6$

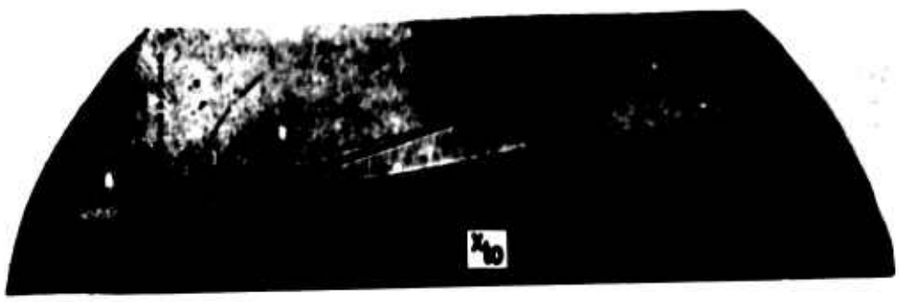

b. $Re_c = 0.19 \times 10^6$

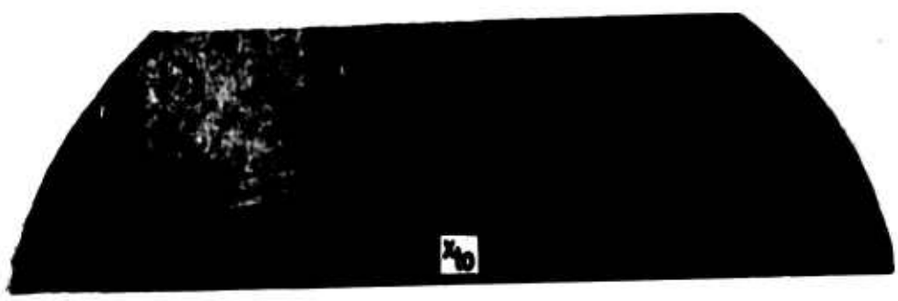

c. $Re_c = 0.25 \times 10^6$

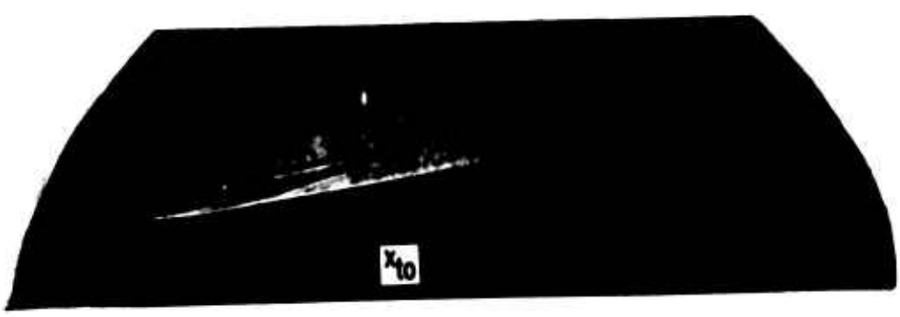

d. $Re_c = 0.50 \times 10^6$

Fig. 5 Shadowgraph Pictures of Transition Location on the Laminar Model at $M_\infty = 6$, AR = 5.6

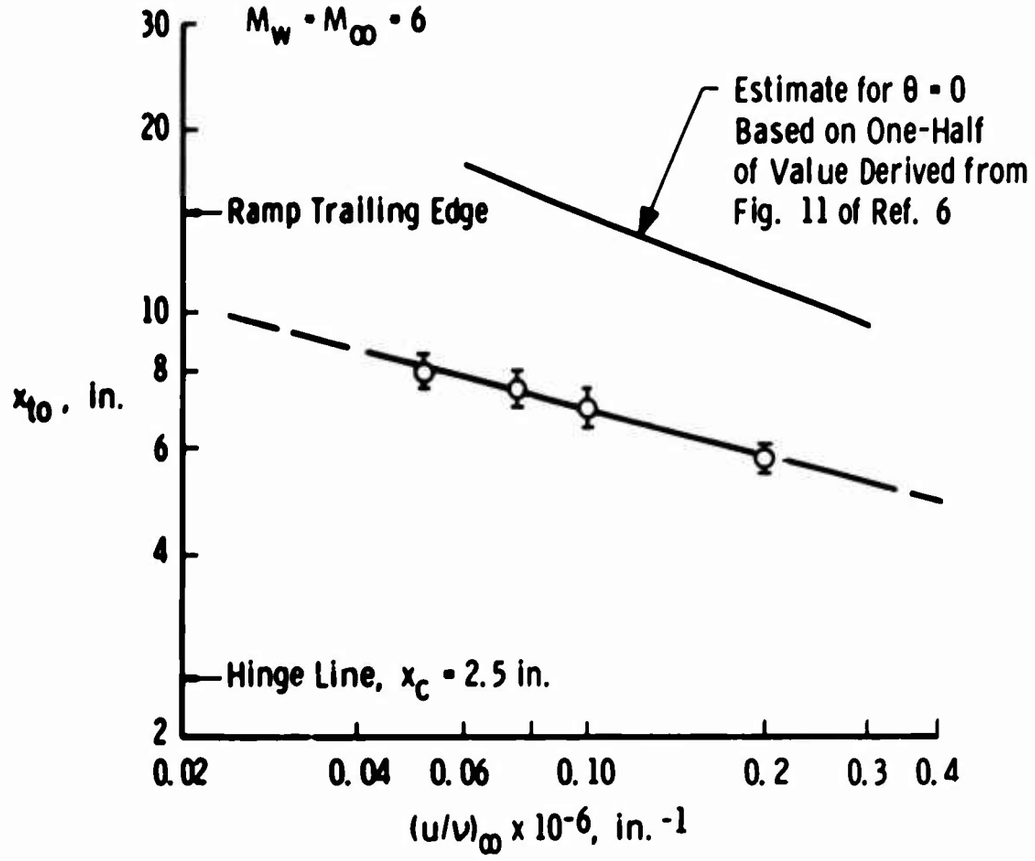

Fig. 6 Comparison of the Transition Location on the Laminar Model with that Estimated for a Flat Plate

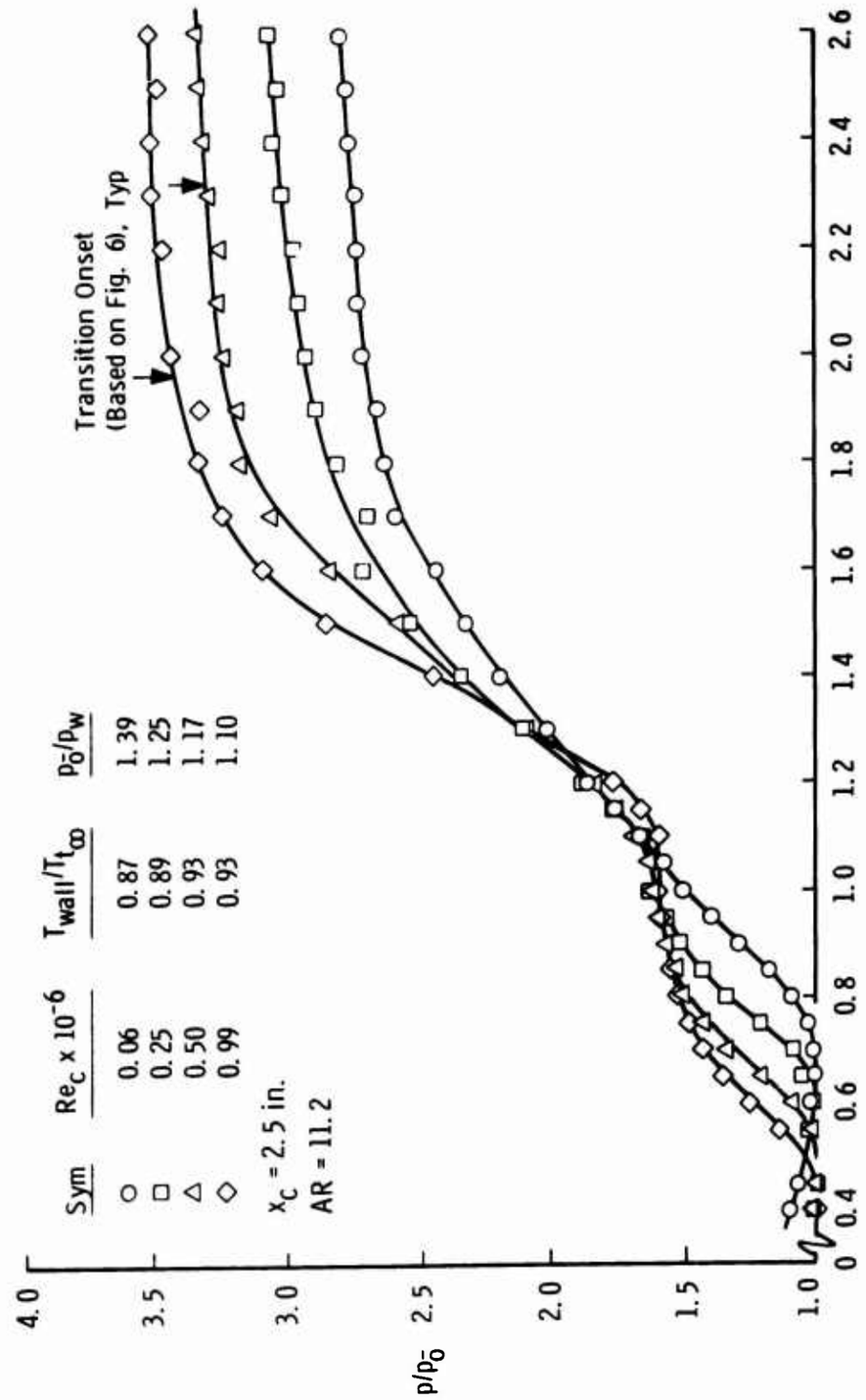

Fig. 7 Effect of Reynolds Number on Centerline Pressure Distributions at $M_w = M_\infty = 6$

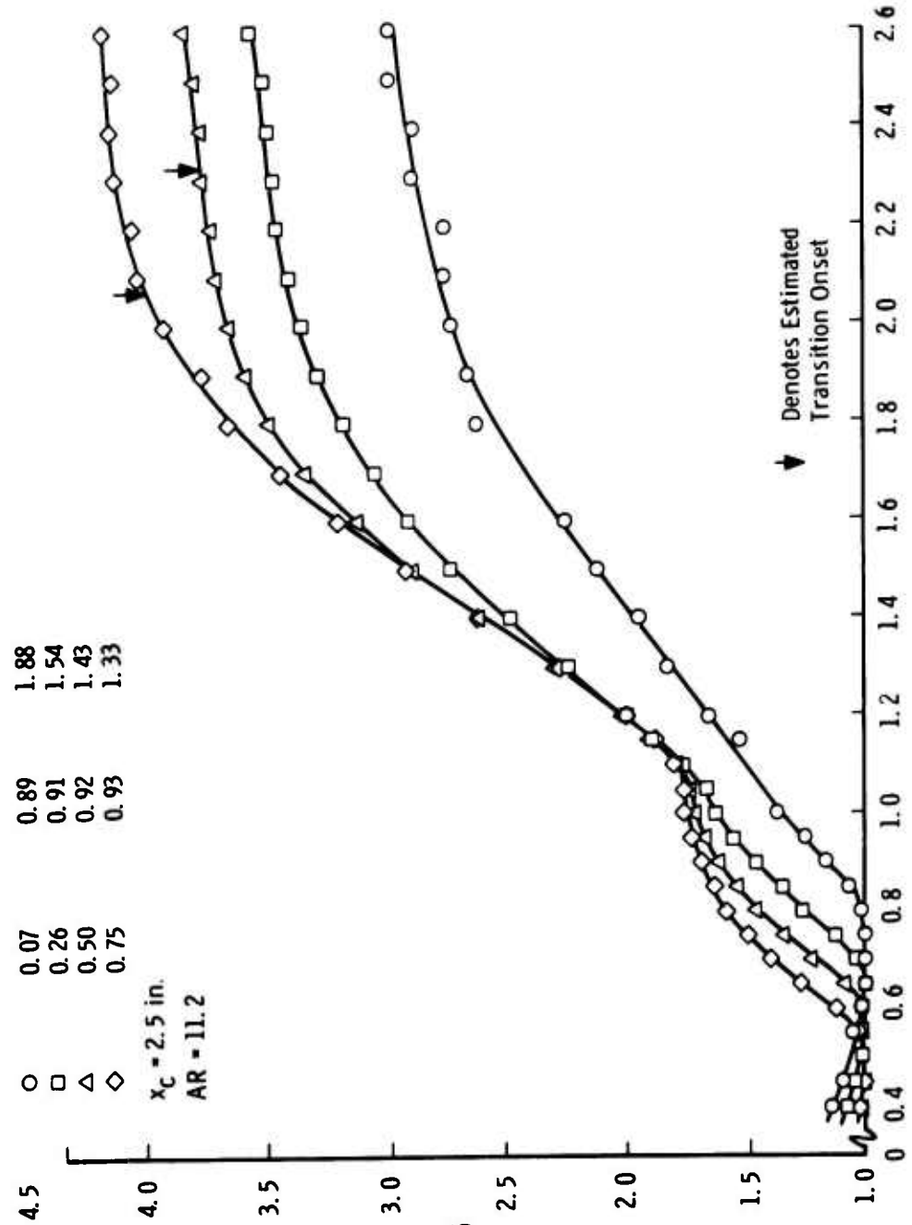

a. z/b = 0

Fig. 8 Effect of Reynolds Number on Longitudinal Pressure Distributions at $M_w = M_\infty = 8$

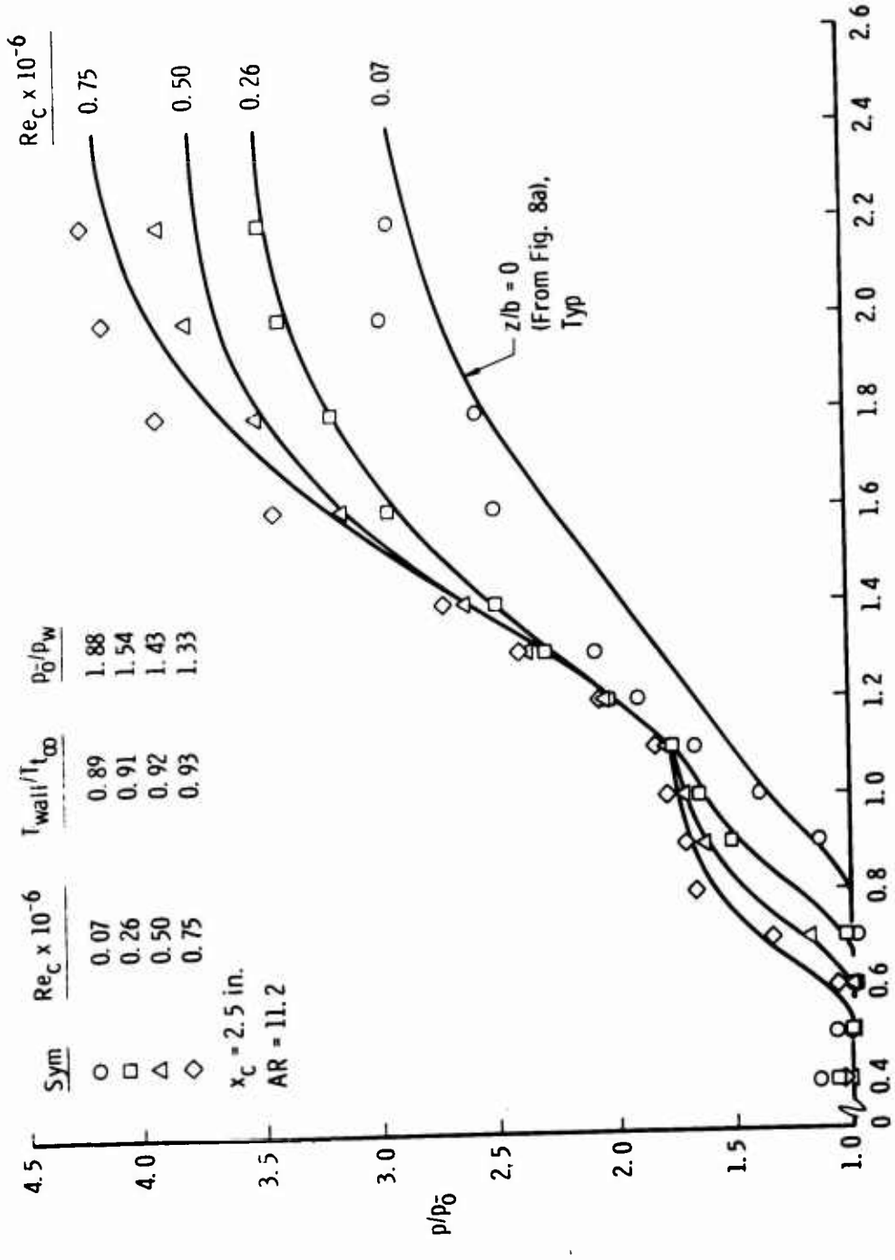

b. z/b = 0.661
Fig. 8 Continued

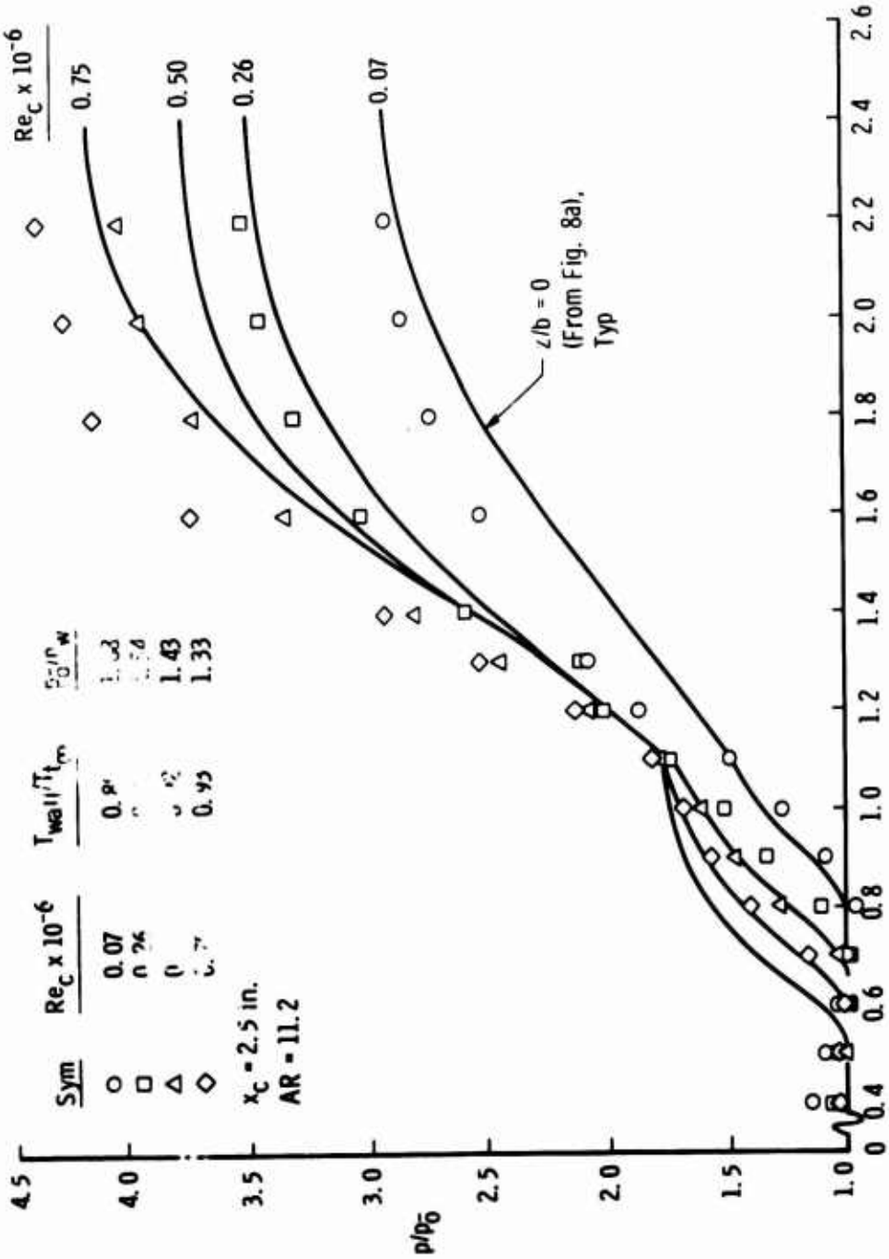

c. $z/b' = 0.911$

Fig. 8 Concluded

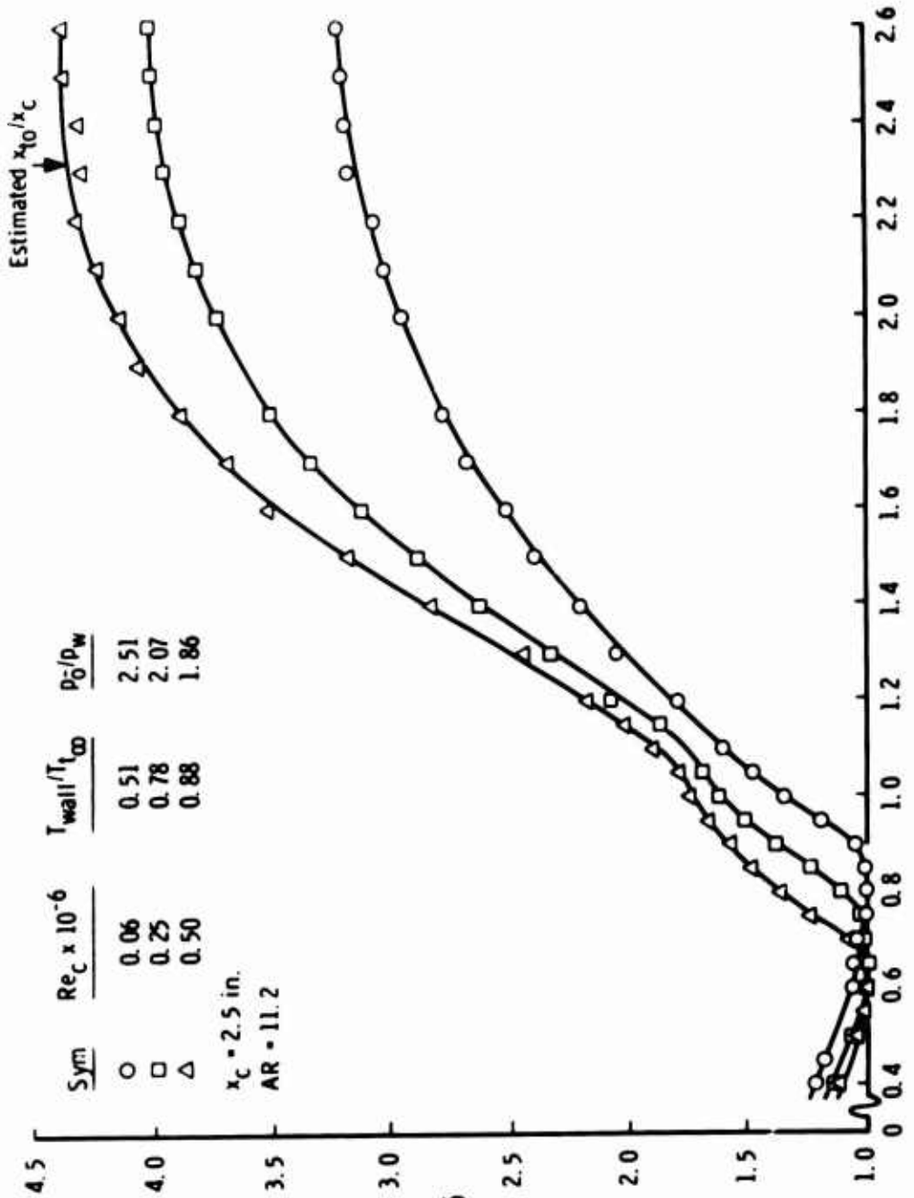

Fig. 9 Effect of Reynolds Number on Centerline Pressure Distributions at $M_\infty = M_{\infty,i} = 10$

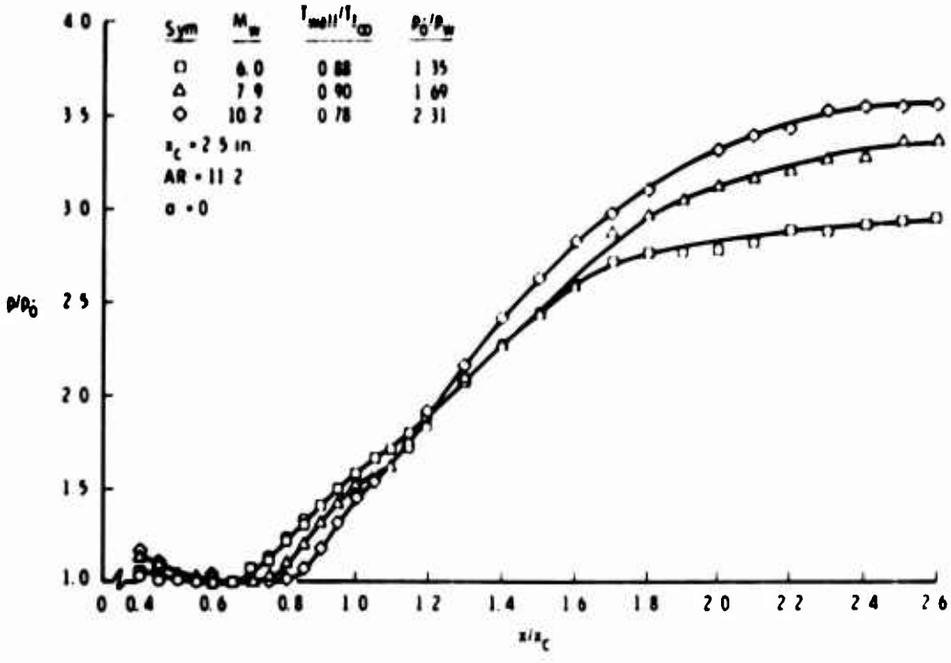

a. $Re_c = 0.13 \times 10^6$

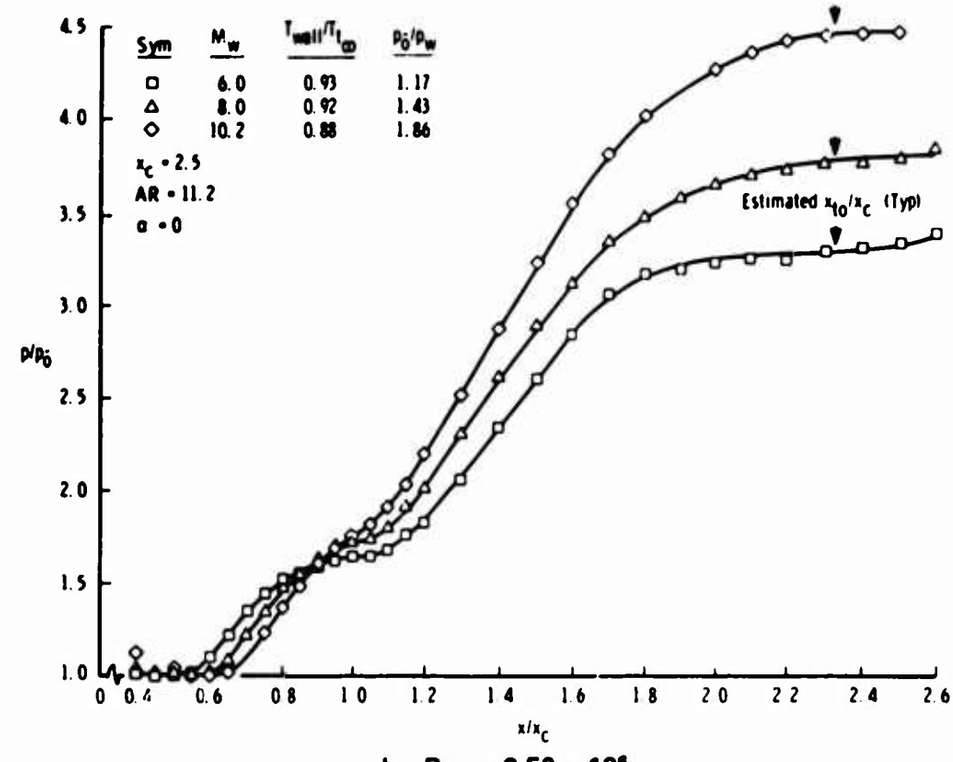

b. $Re_c = 0.50 \times 10^6$

Fig. 10 Effect of Mach Number on Centerline Pressure Distributions

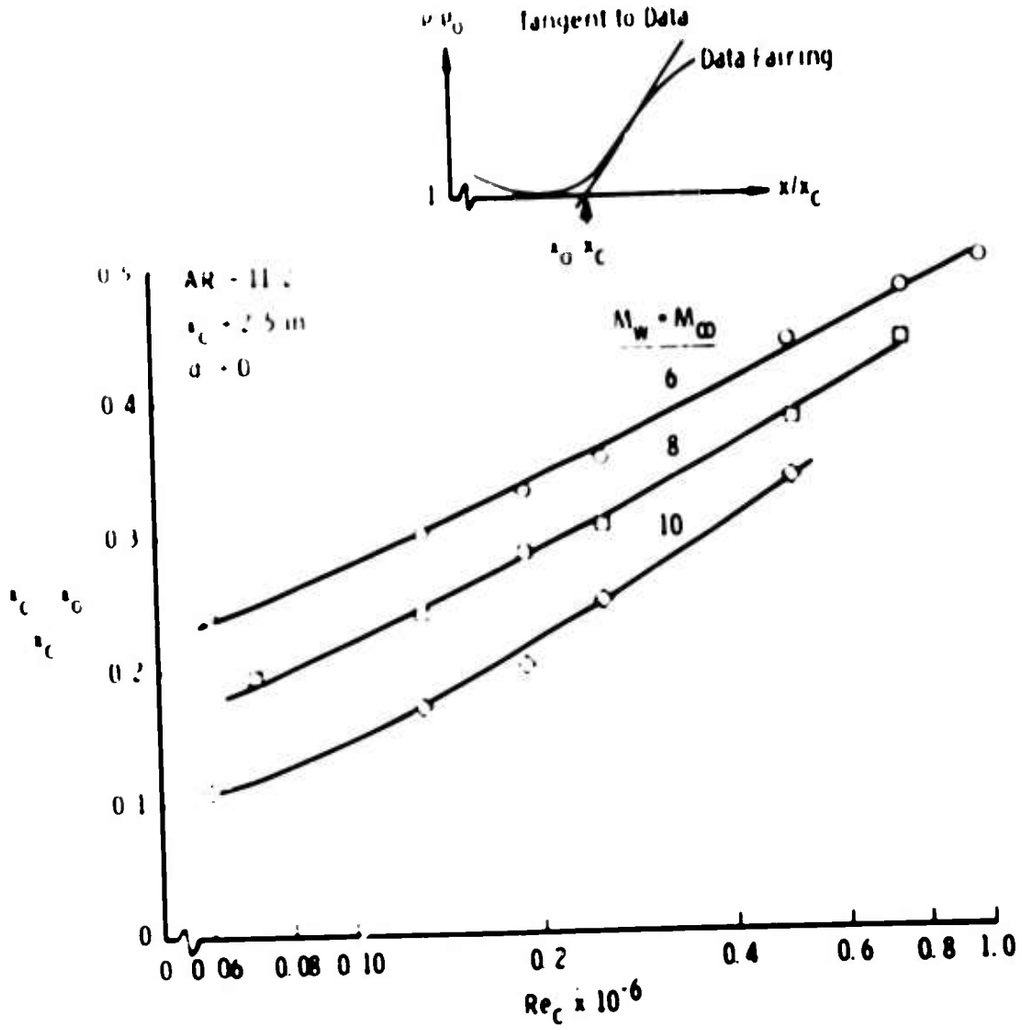

Fig. 11 Effects of Reynolds Number and Mach Number on Centerline Extent of the Separation Region

4.1.2 Influence of Angle of Attack

In order to obtain a lower than free-stream local Mach number, tests were made with the model pitched at free-stream Mach numbers of 6, 8, and 10. The tunnel stilling chamber conditions and model attitude were adjusted so that matching local Reynolds numbers were obtained for $M_w = 4.5$ at $M_\infty = 6$ and 8, for $M_w = 6$ at $M_\infty = 6$, 8, and 10, and for $M_w = 8$ at $M_\infty = 8$ and 10. The pitch angles used to obtain the desired local Mach numbers and the ratios between local and free-stream conditions may be found in Section 3.1.

Centerline pressure distributions for the 11.2 aspect ratio model at free-stream Mach numbers of 6 and 8, pitched to obtain $M_w = 4.5$ and $Re_c = 0.19$ million are shown in Fig. 12. Although these data were taken at the same local conditions, they show major differences in the extent of interaction scale on the flat plate and in the peak pressure ratio on the ramp. Measurements taken at $M_\infty = 6$ with the model at zero angle of attack but located above or below, the tunnel centerline yielded a significantly greater (10 percent) upstream extent than that obtained when the model was located on the tunnel centerline. This discrepancy at $\alpha = 0$ was felt to be caused by free-stream flow nonuniformities (which are a maximum on the centerline) and which can cause substantial changes in the model pressure distributions with the model pitched. However, it is considered that the most reasonable explanation for the decrease is associated with the lower overall pressure rise, because the scale of the upstream influence decreases with decreased overall pressure rise (i.e., an effective decrease in ramp angle). Data obtained for $M_w = 6$ at $M_\infty = 6$, 8, and 10 (Fig. 13) show much better agreement than the data for $M_w = 4.5$. In this case, the $M_\infty = 6$ data were obtained at $\alpha = 0$ with the model positioned 2.7 in. above the tunnel centerline. The extent of the interaction on the flat plate did, however, decrease slightly as free-stream Mach number was increased. The spanwise distributions at several longitudinal stations (Figs. 13b and c) show no significant differences at different free-stream Mach numbers. The model centerline pressure distributions obtained for $M_w = 8$ at $M_\infty = 8$ and 10 (Fig. 14) show a similar small sensitivity to a change in free-stream Mach number, as that obtained for $M_w = 6$.

A summary of the data in terms of the relative extent of the interaction, $(x_c - x_o)/x_c$, as a function of Reynolds number is presented in Fig. 15 for both the pitched (symbols) and unpitched (curves) model attitudes. These data for a given local Mach number, M_w, show that as M_∞ was increased a general decrease in the interaction length was obtained over the entire Reynolds number range. The one exception to

this trend occurred for M_w = 4 at Re_c = 0.75 million. The decrease in interaction length with an increase in Reynolds number at M_w = 4.5 is indicative of transitional reattachment at Re_c > 0.5 million.

Data from several runs with the model pitched and unpitched are shown in Fig. 16 as a function of the hypersonic viscous interaction parameter, $\bar{\chi}$. The α = 0 data show reasonable agreement with the weak interaction formula of Ref. 7, and are fairly uniform. The pitched data ($\alpha \neq 0$) show somewhat more scatter than the unpitched data and are in poorer agreement with the theory at $\bar{\chi} > 1.6$.

Estimates of the inviscid pressure rise were made, for the assumed flow model shown in Fig. 17, to illustrate the differences which might exist on a 9.5-deg ramp when pitching the model to vary the Mach number on the flat plate. The results (Fig. 17) show, for a given local Mach number, that increasing the free-stream Mach number, M_∞, can cause the peak ramp pressure ratio, p_3/p_1, to be significantly less than the isentropic (maximum) ratio. Because of the requirement for constant pressure across the slip line, these results indicate that an expansion fan should exist downstream of zone 2 and that its strength depends on both the free-stream Mach number and the local flat-plate Mach number. Shadowgraph pictures which show the slip-line dividing zones 3 and 4 are presented in Fig. 18 for a range of pitch attitudes and Mach numbers. It is also evident from these pictures that the expansion fan would be situated relatively near the hinge line (e.g., of the order of length x_c downstream), and could thus have an influence on the overall pressure rise achieved.

A comparison of the experimental results with the theoretical maximum pressure ratio is presented in Fig. 19. Because the "peak" pressure ratio measured on both pitched and unpitched models exceeded that corresponding to the actual ramp angle (θ = 9.5 deg), two additional deflection angles were included to show the magnitude of the discrepancy. In addition, a so-called asymptotic value (see sketch in figure) pertinent only to the pitched data was included. This latter ratio should approach the values given in Fig. 17, for p_3/p_1, which it is noted to do, generally. These data indicate that the effective ramp angle was about one-half degree greater than the actual angle, and this is presumed to be a result of a displacement thickness induced flow deflection on the ramp. One last point which these last three figures raise is the probability that the reduction in scale of upstream influence (shown especially in Fig. 14) observed with the model pitched could very likely have been caused by a reduction in the overall pressure rise (see the discussion of theoretical results in Section 4.1.4).

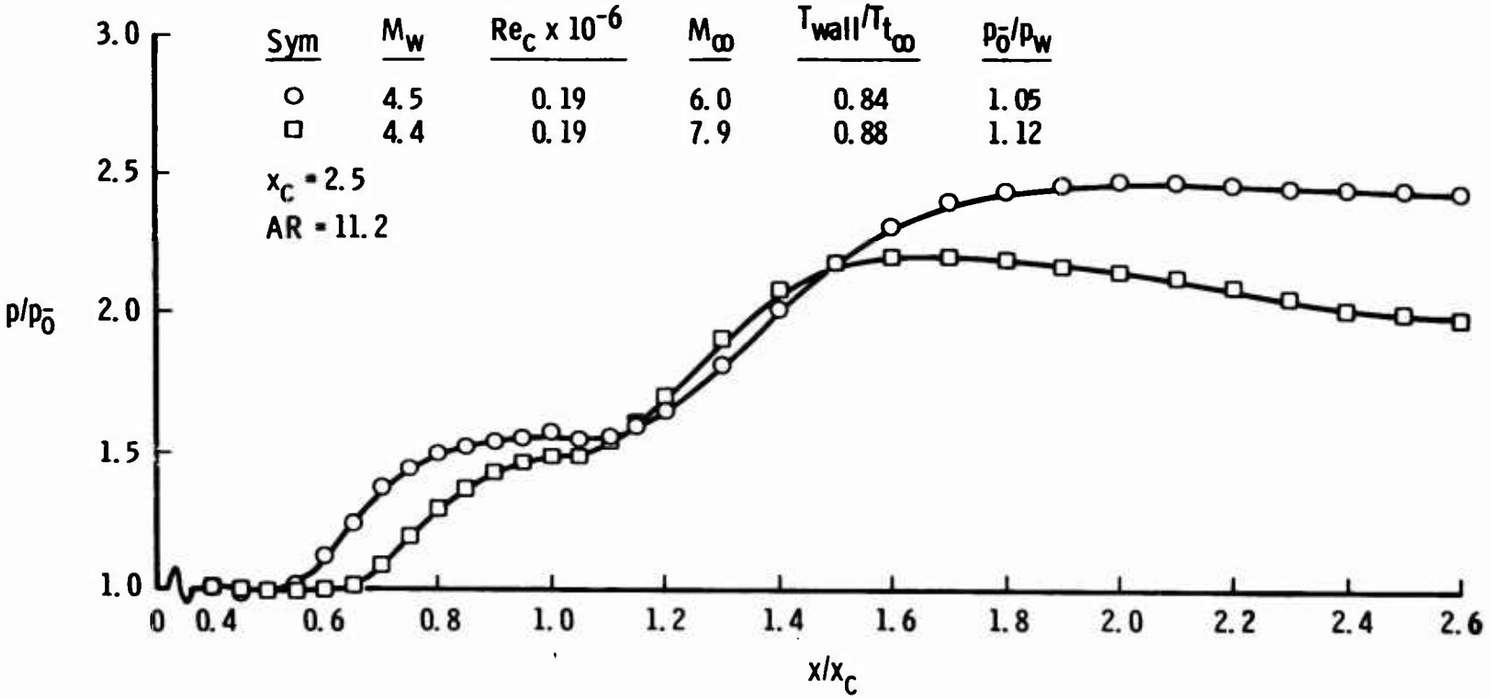

Fig. 12 Effect of Pitch on Centerline Pressure Distributions at M_w = 4.5

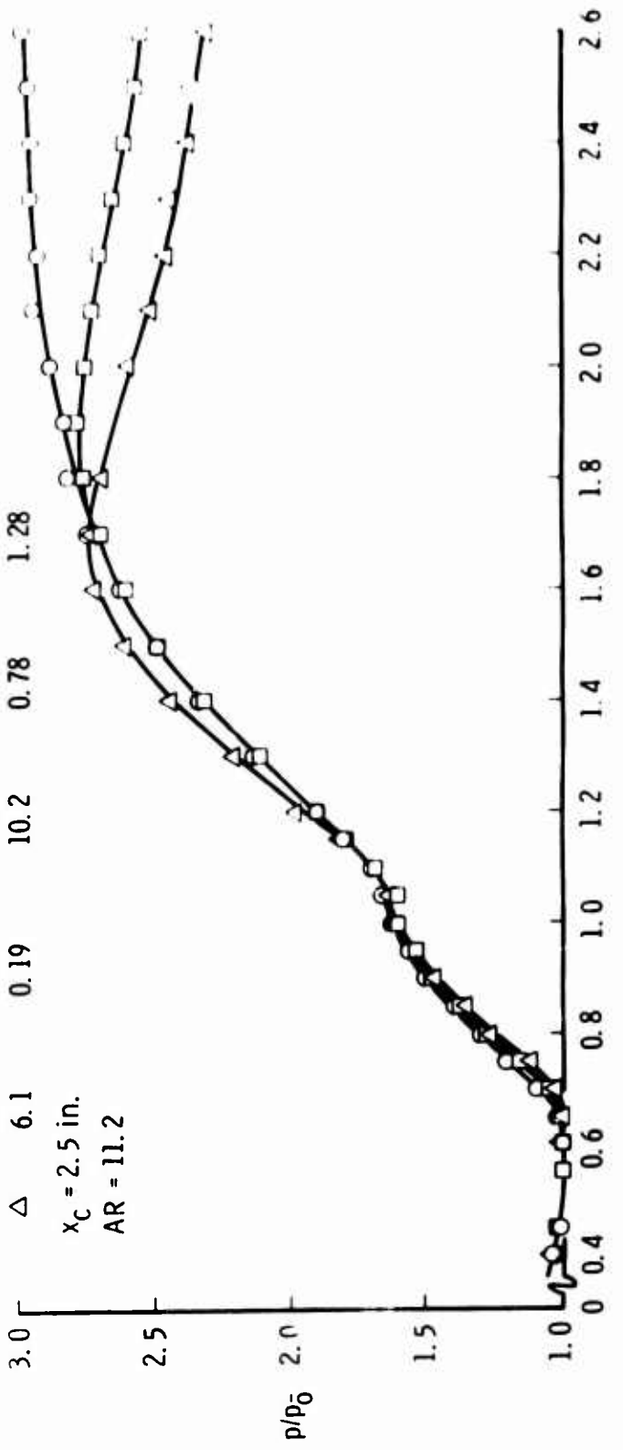

a. Longitudinal Centerline Distributions

Fig. 13 Effect of Pitch on Pressure Distributions at M_w = 6

Sym	M_w	$Re_c \times 10^{-6}$	M_∞	T_{wall}/T_{t_∞}	$p_{\bar{o}}/p_w$
○	6.0	0.19	6.0	0.92	1.27
□	5.9	0.20	7.9	0.89	1.25
△	6.1	0.19	10.2	0.78	1.28

x_t = 2.5 in.
AR = 11.2

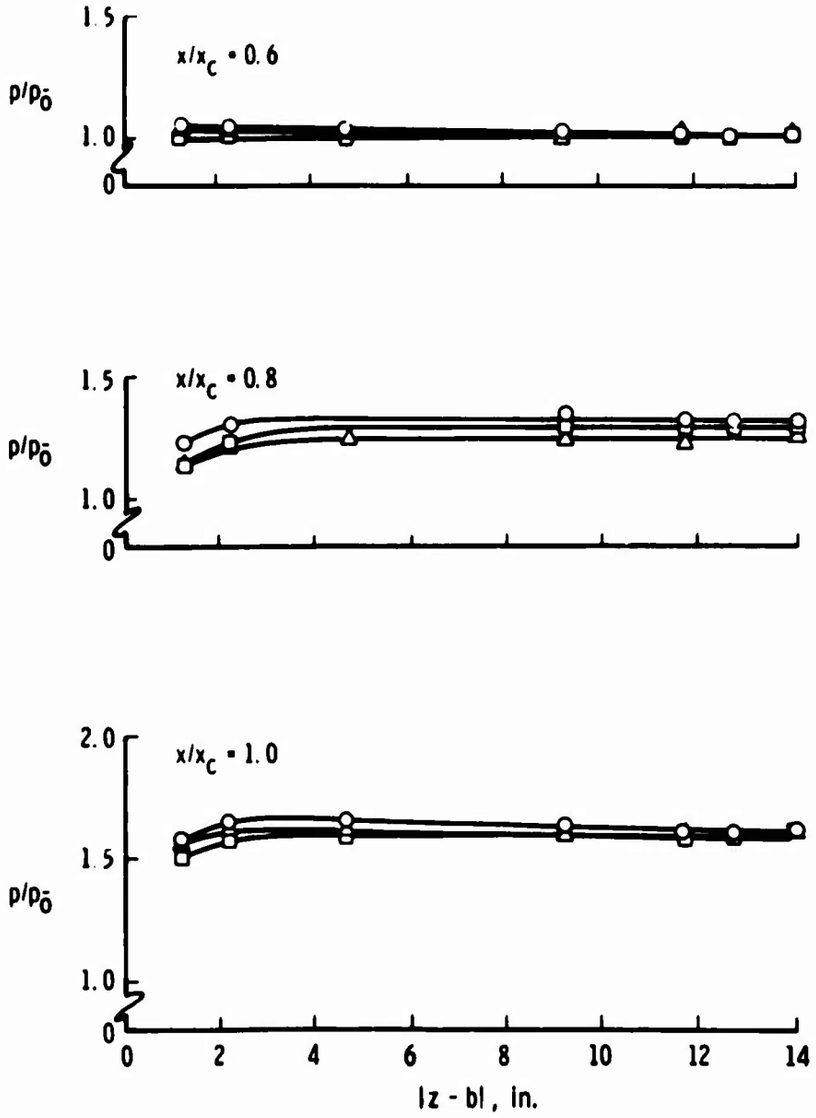

b. Spanwise Distributions on Flat Plate
Fig. 13 Continued

Sym	M_w	$Re_c \times 10^{-6}$	M_∞	T_{wall}/T_{t_∞}	$p_{\bar{o}}/p_w$
○	6.0	0.19	6.0	0.92	1.27
□	5.9	0.20	7.9	0.89	1.25
△	6.1	0.19	10.2	0.78	1.28

x_c = 2.5 in.
AR = 11.2

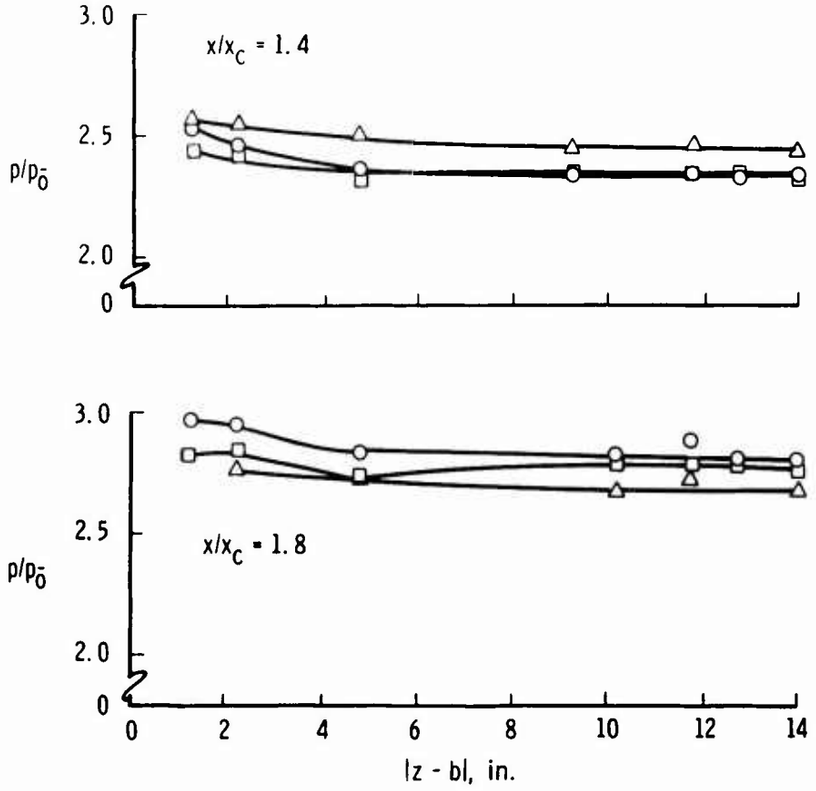

c. Spanwise Distributions on Ramp
Fig. 13 Concluded

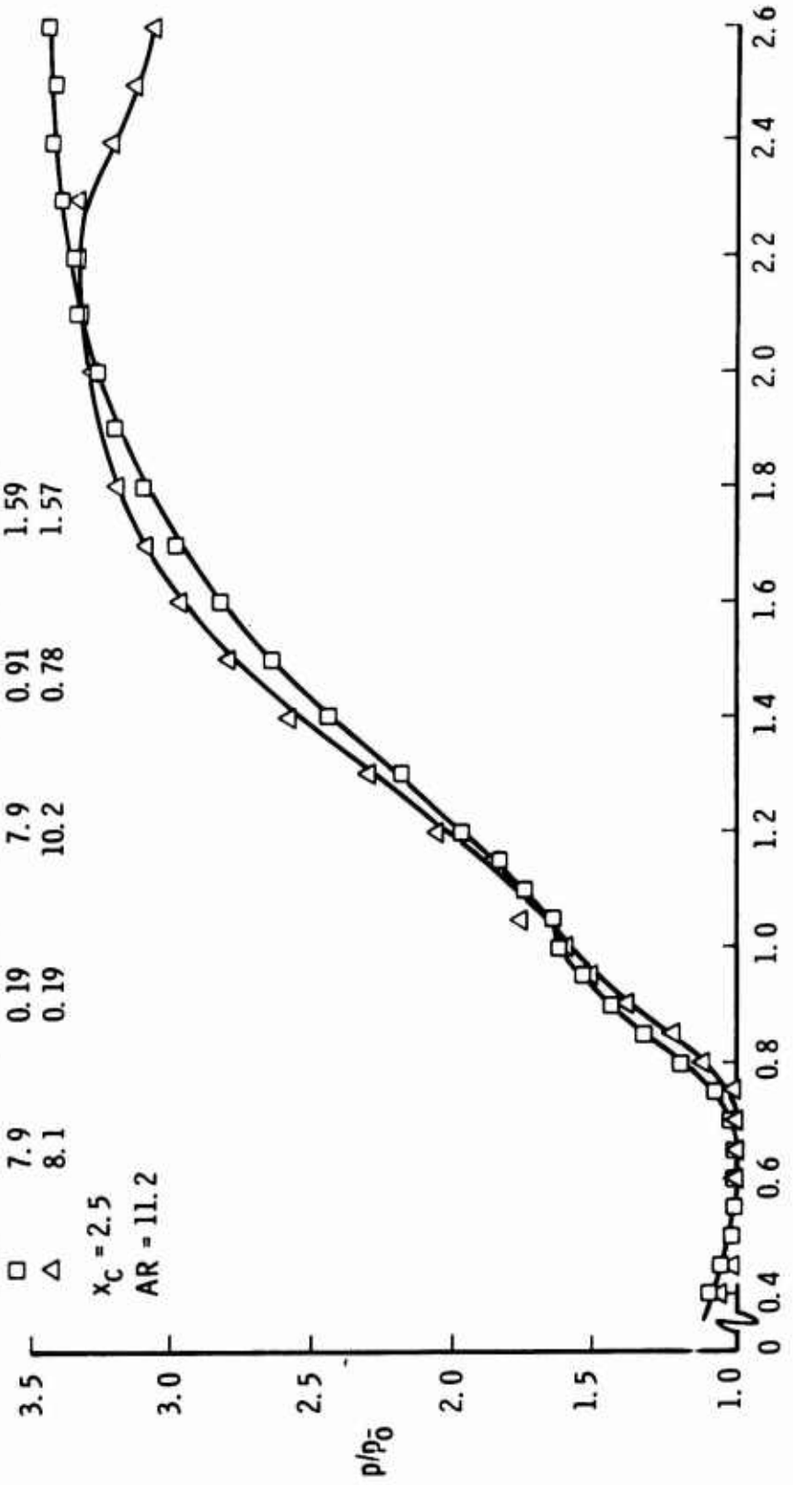

Fig. 14 Effect of Pitch on Centerline Pressure Distributions at M_w = 8

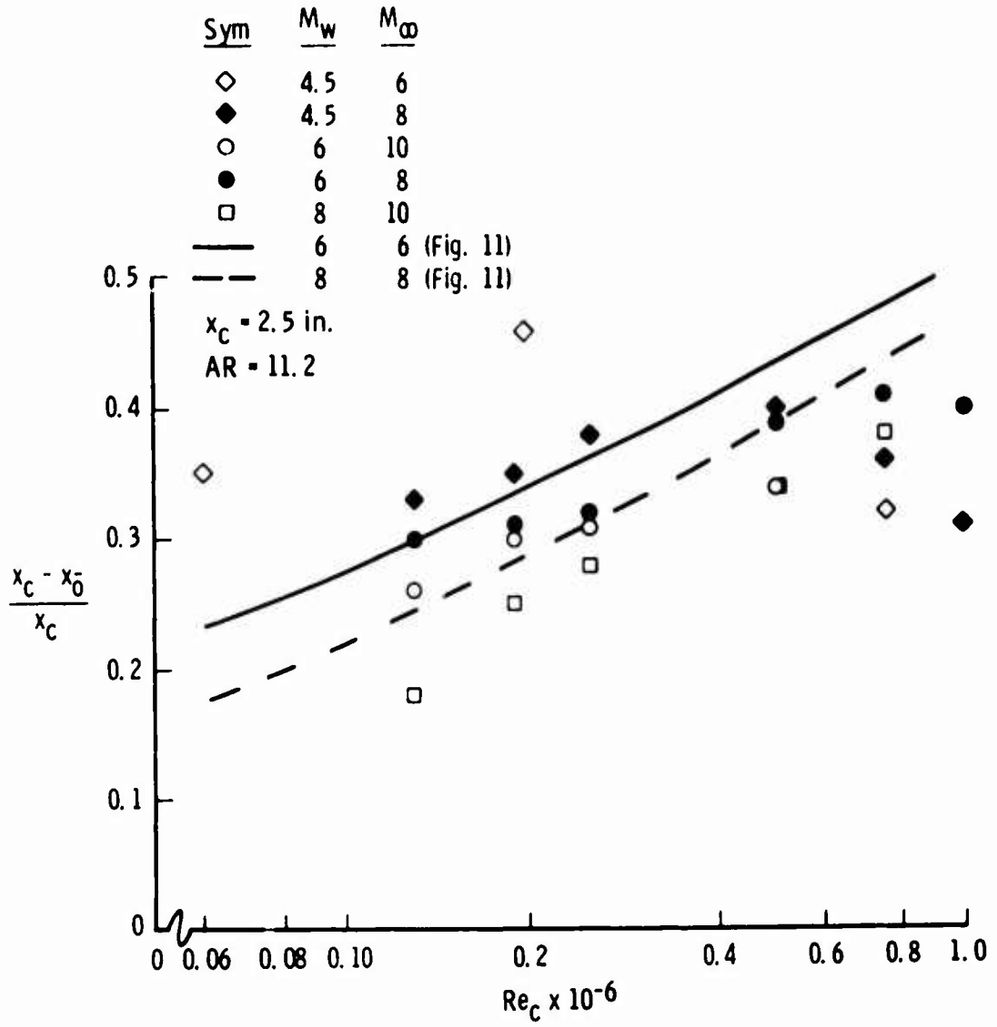

Fig. 15 Effect of Pitch on Centerline Extent of the Separation Region

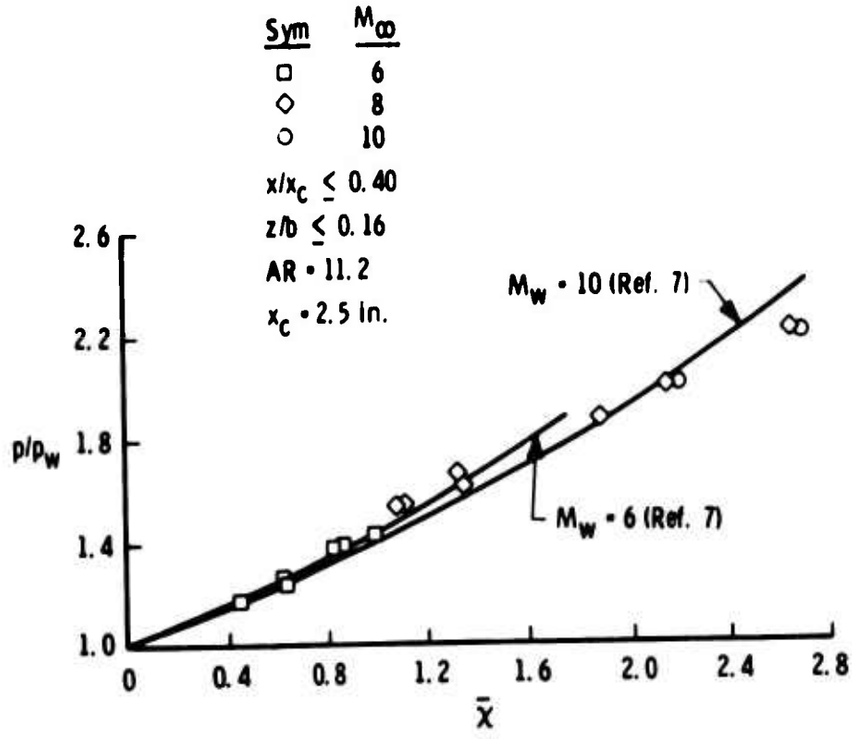

a. $\alpha = 0$

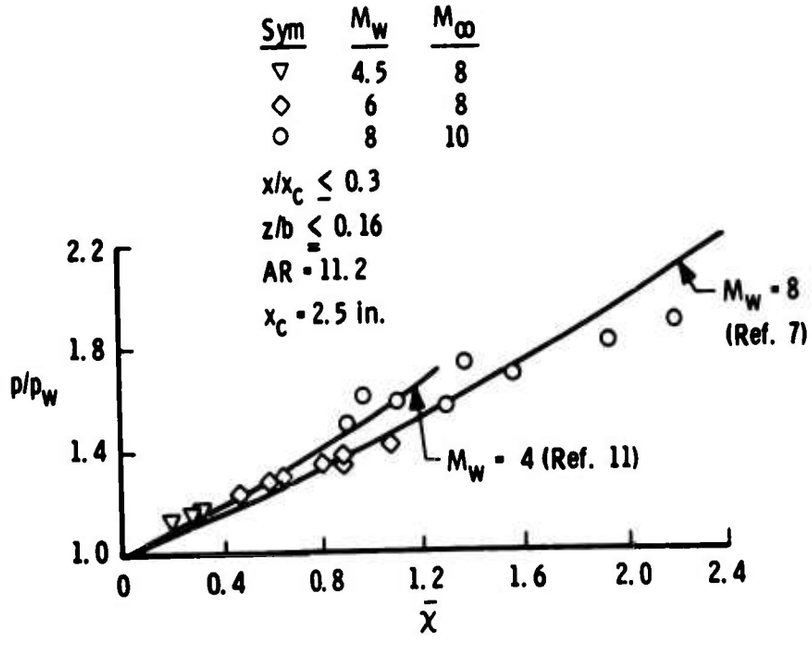

b. $\alpha > 0$

Fig. 16 Comparison of Flat-Plate Pressure Ratio with Weak Interaction Theory

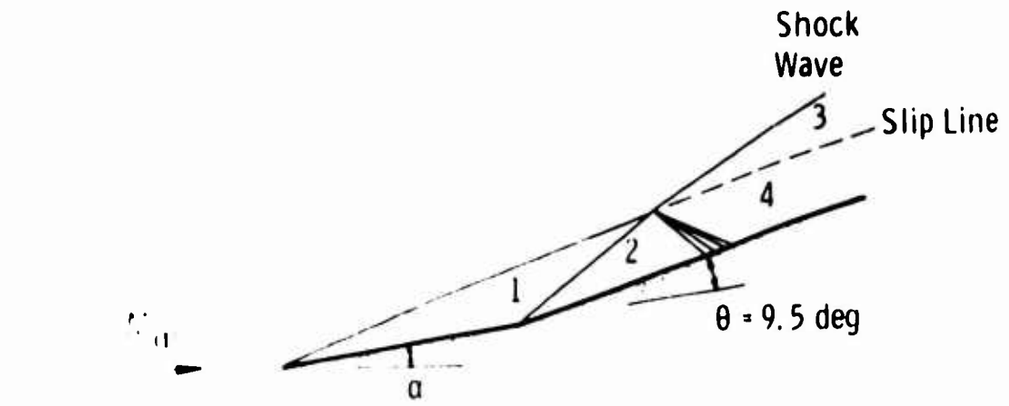

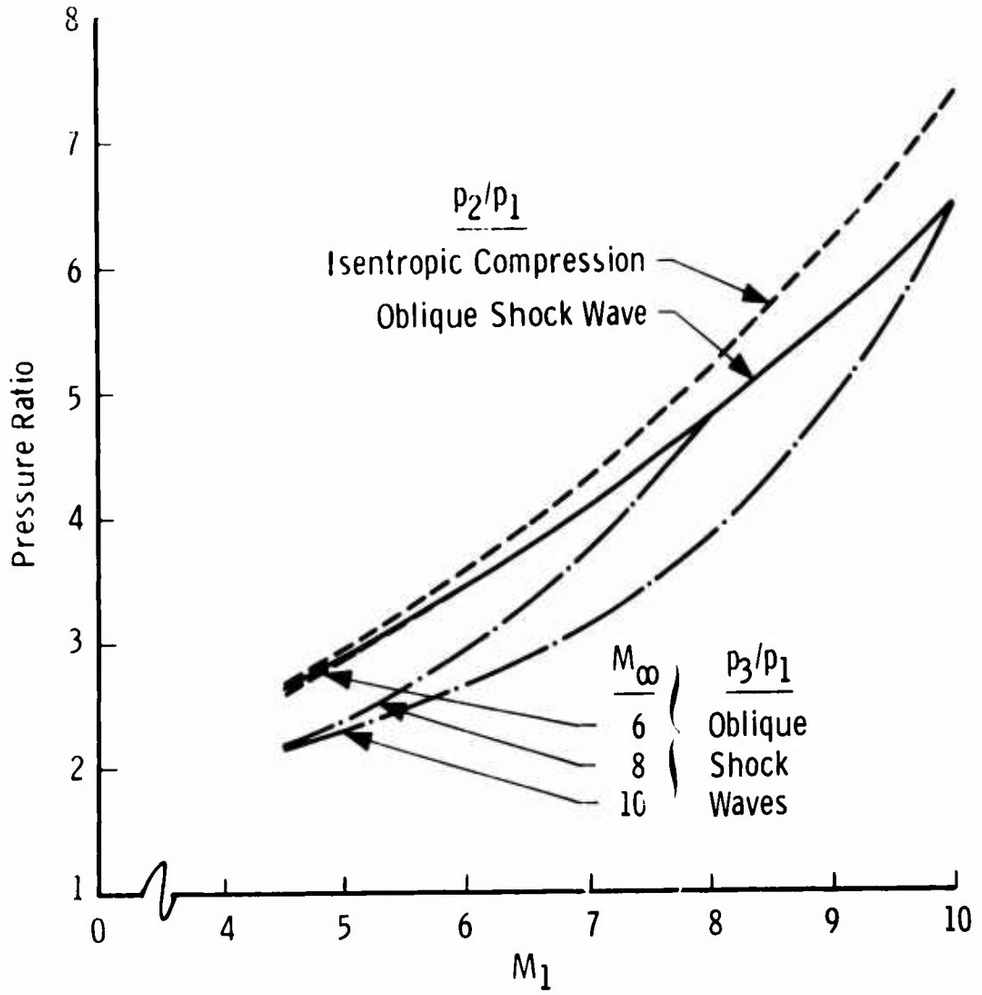

Fig. 17 Effects of Pitch on the Theoretical Isentropic and Oblique Shock Pressure Rises on a 9.5-deg Ramp

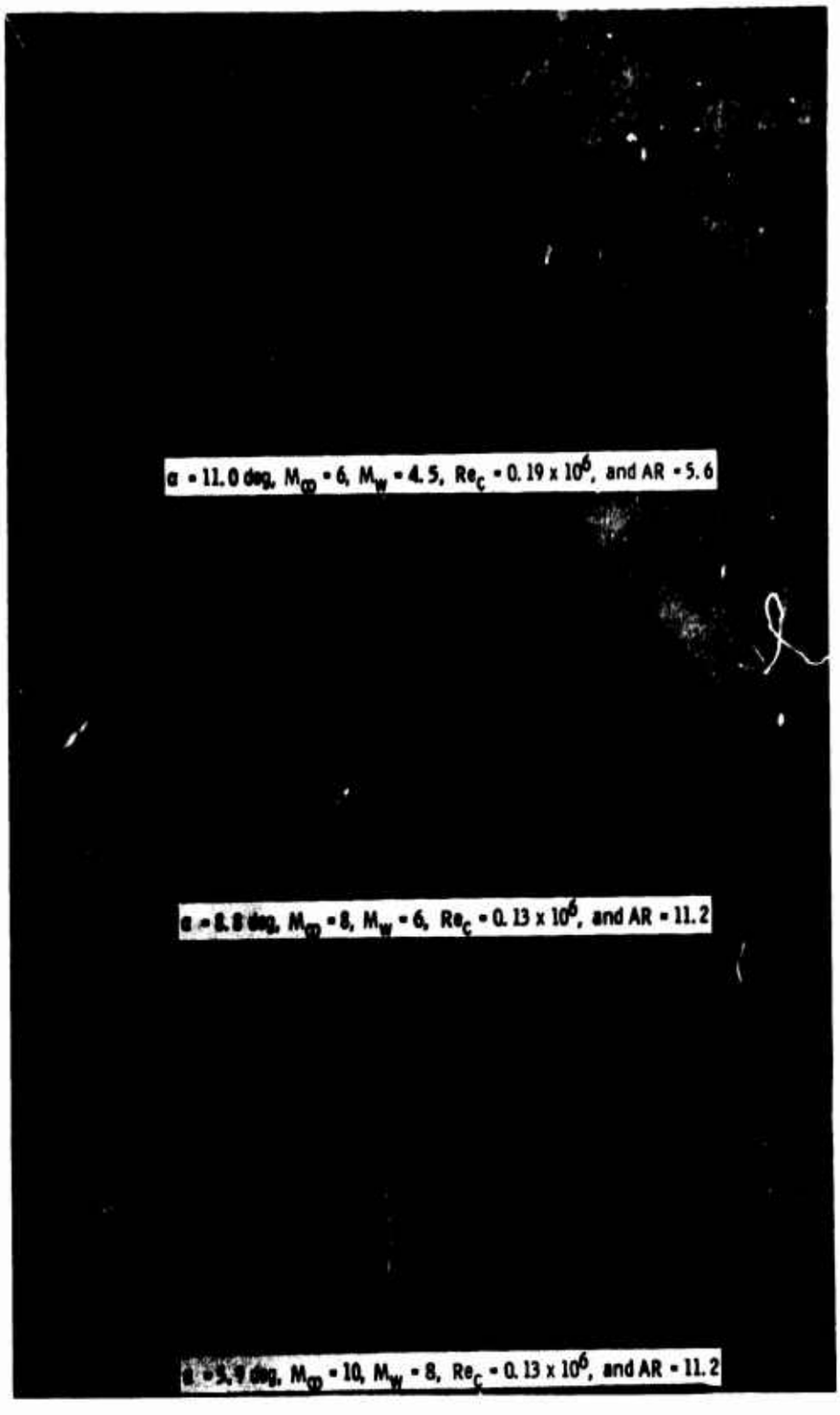

Fig. 18 Shadowgraph Pictures Showing the Effects of Pitch and Mach Number on Shock Wave Patterns on Laminar Model

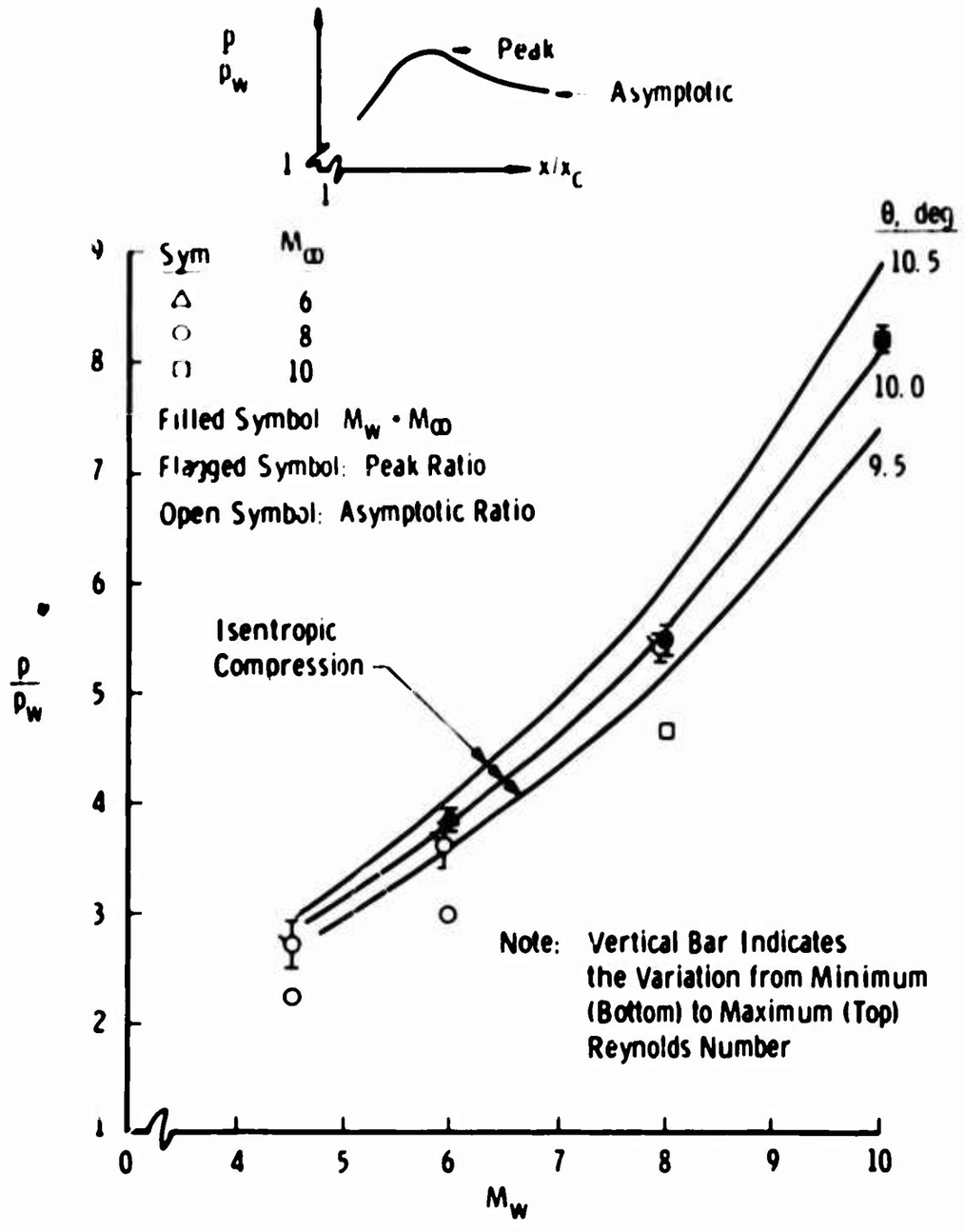

Fig. 19 Comparison of Measured and Theoretical Isentropic Ramp Pressure Ratios

4.1.3 Influence of Aspect Ratio

As stated previously, the primary objective of this investigation was to determine the aspect ratio ($2b/x_c$) required to obtain two-dimensional flow on a model which had a boundary-layer separation that was laminar through reattachment. This was accomplished by reducing the span of the model several times and testing over the same range of Mach numbers and Reynolds numbers with each model. Typical effects of aspect ratio on the longitudinal and spanwise pressure distributions at Mach numbers 6, 8, and 10 are illustrated by the data shown in Figs. 20 through 22.

The centerline pressure distributions for the two aspect ratios investigated at $M_w = 6$ and $Re_c = 0.19$ million (Fig. 20a) were not changed when the aspect ratio was reduced from 11.2 to 5.6. In addition, the spanwise pressure distributions, at several chordwise stations (Figs. 20b and c) show nearly uniform pressure ratio on both models to within about three inches of the outboard edge. Data obtained for four aspect ratios at $M_w = 8$ and $Re_c = 0.19$ million (Fig. 21a) indicate that the changes were perhaps the greatest and most consistent on the flat plate in the separation region when the aspect ratio was reduced to 1.4. Comparison of the off-centerline chordwise pressure distributions for the 11.2 and 1.4 aspect ratio models, Fig. 21b, indicate a large span of two-dimensional flow on the 11.2 model since the data for $z/b = 0.66$ are essentially the same as $z = 0$ (Fig. 21a). A similar chordwise location on the AR = 1.4 model ($z/b = 0.59$) shows, however, a distinct disagreement with the reference curve in the region upstream of the hinge line ($x < x_c$). This spanwise variation of the surface pressure on the 1.4 aspect ratio model is more clearly shown in Figs. 21c and d. These figures show that with the data plotted versus spanwise location at constant x/x_c values the effects of the tip proximity were, as in the $M_w = 6$ case, restricted to a region approximately 3 to 4 in. inboard. These data also show that for $AR \leq 2.8$ there was essentially no region of uniform pressure in the spanwise direction. The centerline and spanwise pressure distributions for $M_w = 10$ and $Re_c = 0.25$ million (Fig. 22) indicate the same lack of a finite span of two-dimensional flow when the aspect ratio was reduced to 2.8.

The spanwise variations in the relative extent of the upstream interaction with aspect ratio at each Mach number and $Re_c = 0.19$ million are shown in Fig. 23 as a function of both the relative spanwise location, $|z - b|/b$, and the absolute spanwise location, $|z - b|$. These data clearly show (especially Fig. 23b) that the edge effect, i.e., decrease in interaction length because of outflow, is manifest inboard a constant absolute distance regardless of the aspect ratio and is not a function of the relative

spanwise location. The data for all three Mach numbers indicate that the minimum semispan for a model with a flat-plate chord of 2.5 in. should be at least 4 in. From these and other data, it is concluded that the 2.8 aspect ratio model (b = 3.5 in.) was a borderline case for obtaining two-dimensional, laminar separation. Further evidence for the above conclusion is presented in another form in Figs. 24 and 25. The change in the centerline interaction length with a change in aspect ratio for M_w = 8 and 10, Fig. 24, shows again that the 2.8 aspect ratio model was a marginal configuration. In fact, the data at M_∞ = 8 show quite unexpectedly that at $Re_c \sim 0.25$ million the interaction length on the 5.6 aspect ratio model was greater than on the 11.2 aspect ratio model. When the centerline interaction lengths for these two aspect ratios are presented as a function of Re_c, as in Fig. 25 for M_w = 6, 8, and 10, the data indicate that the problem of obtaining two-dimensional flow is not only a function of aspect ratio, but is also dependent on Mach number and/or Reynolds number. Note the divergence of the extent of the interaction for the 5.6 aspect ratio model from that of the 11.2 model with either an increase in Re_c at M_w = 6 and 8 or for a decrease in M_w at a constant Reynolds number ($Re_c \sim 0.1$ million).

In order to investigate further the factors influencing uniform, two-dimensional flow, selected test conditions for all aspect ratios were repeated with a set of upper surface side plates installed at the outboard edges. Typical results from this investigation are shown in Figs. 26 and 27 for aspect ratios of 11.2, 2.8, and 1.4 at M_w = 8 and Re_c = 0.19 million. The chordwise pressure distributions, Fig. 26, show that when the model was wide enough to obtain two-dimensional flow on centerline without side plates (aspect ratio of 11.2, Fig. 26a), the only measurable effect of the side plates was to increase the pressure level on the outboard row. It is noted that the pressure level of the outboard row with the side plates installed was generally above even that of the centerline row with or without side plates. In the case of the 1.4 aspect ratio model, which had no two-dimensional flow without side plates, the effect of the side plates was to increase the pressure level and the extent of the interaction on the entire flat plate even beyond that measured on the centerline of the 11.2 aspect ratio model. The spanwise pressure distributions at several values of x/x_c are shown in Fig. 27, and indicate the same general trends as did the chordwise data. It is therefore evident from this investigation that the narrowest semispan model, with a flat-plate chord of 2.5 in., on which two-dimensional, laminar, separated flow can be obtained is about 4 in. It is also concluded that, although the installation of upper surface side plates helps to determine if the flow is two dimensional on the centerline without them, they cannot be used to obtain two-dimensional flow on a model that is otherwise too narrow.

A special model was fabricated to study the influence of the flat-plate length on the capability of obtaining two-dimensional laminar separation. This model had a flat-plate chord of 14 in. and a span of 28 in. which results in an aspect ratio less than that needed for two-dimensional flow on the 2.5-in.-chord model; it must be remembered that it was concluded that the edge effects were manifest inboard a fixed amount (4 in.) and were therefore not directly scaled by the aspect ratio. Because of the longer chord length, the data at Re_c = 0.5 million was the minimum that could be obtained on this model. The centerline pressure distributions obtained with this model at M_w = 6, Re_c = 0.5 and 0.75 million (with the model pitched at M_∞ = 8) are compared in Fig. 28 with the data from the 2.5-in.-chord model for aspect ratios of 1.4 and 2.8. These data show that the 14-in.-chord model had a much steeper pressure gradient on the ramp than either the 2.8 or the 1.4 aspect ratio models, and that the flat-plate pressure distribution closely approximated that of the 1.4 aspect ratio model. Because of the much longer flat plate, the location of boundary-layer transition, as shown in Fig. 28a, was much farther upstream, relative to flat-plate length, than on the 2.5-in.-chord models. Shadowgraph pictures of the flow during reattachment on the 14-in.-chord model and the 2.5-in.-chord model at M_w = 8 which are presented in Fig. 29d also illustrate the substantial differences in transition location. As with the 2.5-in. model, the actual transition location indicated for θ = 9.5 deg is shown to have been upstream of that for θ = 0. It is commonly accepted that a transitional reattaching boundary layer will cause the length of the interaction on the flat plate to decrease from that obtained with a laminar reattaching boundary layer at the same Reynolds number. The inference then is, that the reduced interaction length obtained on the 14-in. chord was not necessarily caused by the non-two-dimensional flow but was, more probably caused by boundary-layer transition during reattachment.

The centerline pressure distributions for the same three models described above but at $M_w = M_\infty$ = 8 and Re_c = 0.5 million, Fig. 29a, show the same trends as the M_w = 6 data. The spanwise data at several chordwise stations (Figs. 29b and c), contrary to the previous conclusions, indicate that the distance over which the edge effects are manifest was not the same as for the shorter models. In fact, within the interaction pressure rise (x/x_c = 0.8) the edge effects appear to have extended all the way to the model centerline. This spanwise variation on the 14-in. chord model may well be in part a result of nonuniform spanwise transitional reattachment.

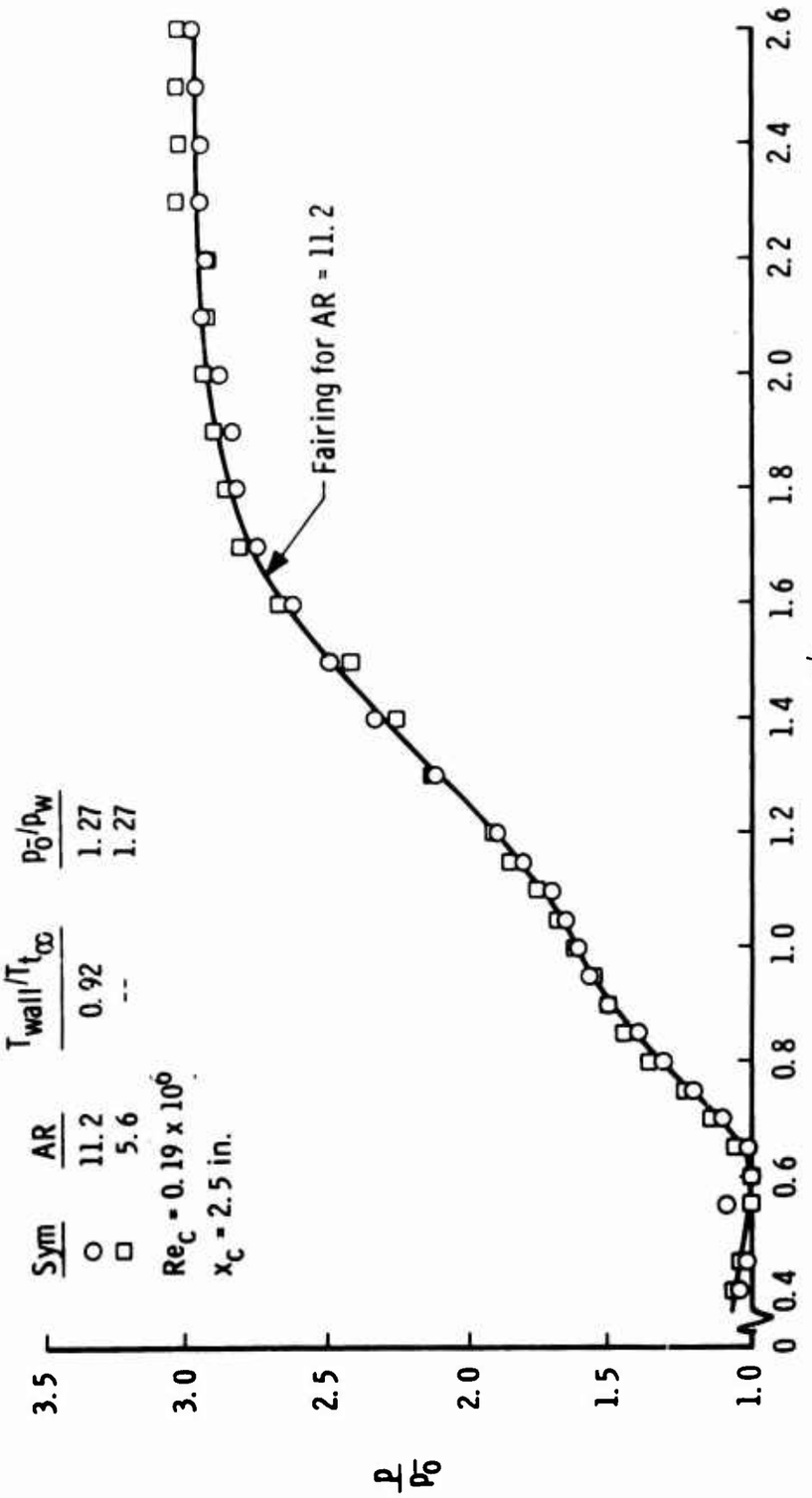

a. Longitudinal Centerline Distribution

Fig. 20 Effect of Aspect Ratio on Pressure Distributions at $M_w = M_\infty = 6$

Sym	AR	T_{wall}/T_{t_∞}	$p_{\bar{o}}/p_w$
○	11.2	0.92	1.27
□	5.6	--	1.27

$Re_c = 0.19 \times 10^6$

$x_c = 2.5$ in.

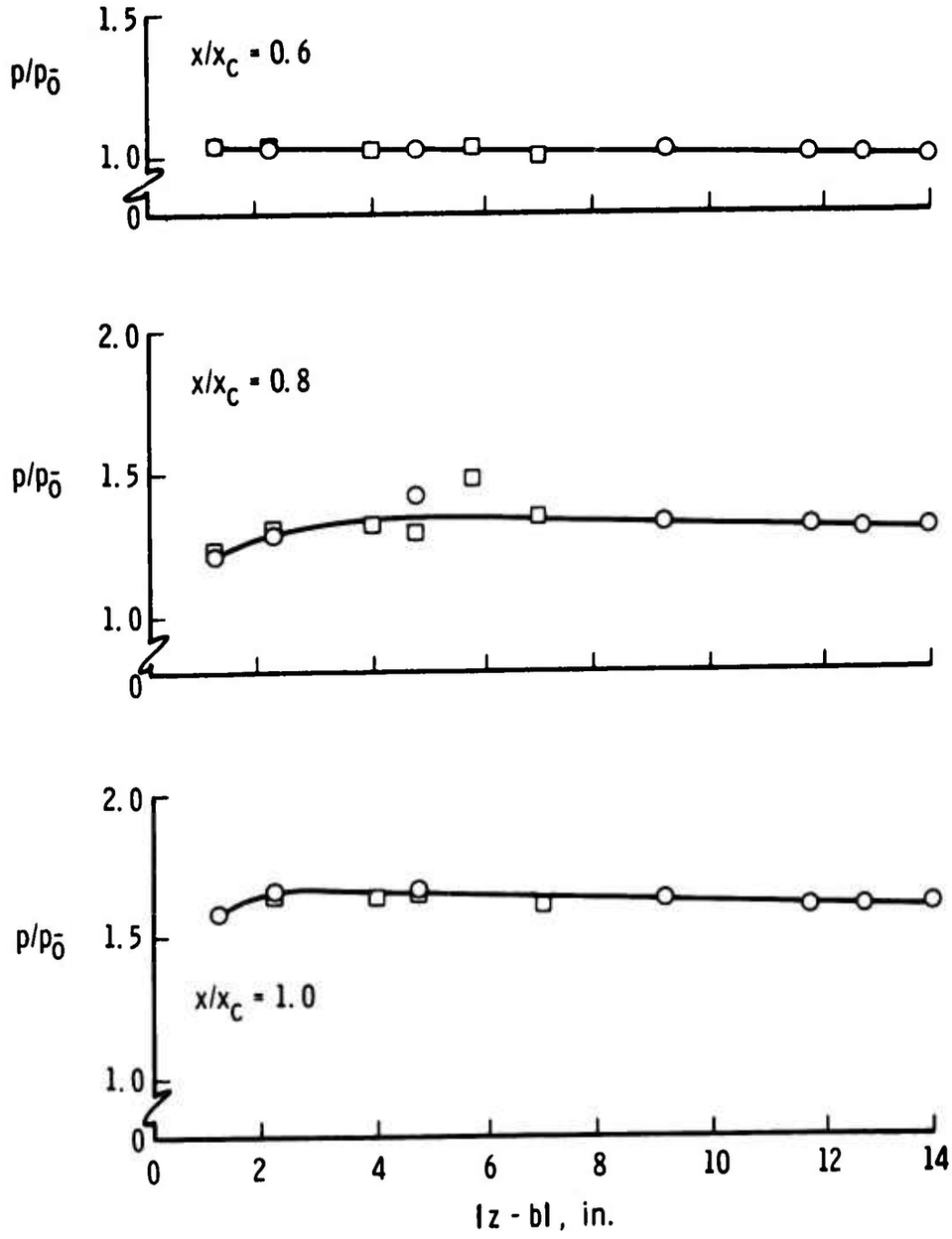

b. Spanwise Distribution on Flat Plate

Fig. 20 Continued

Sym	AR	T_{wall}/T_{t_∞}	$p_{\bar{0}}/p_w$
○	11.2	0.92	1.27
□	5.6	--	1.27

$Re_c = 0.19 \times 10^6$

$x_c = 2.5$ in.

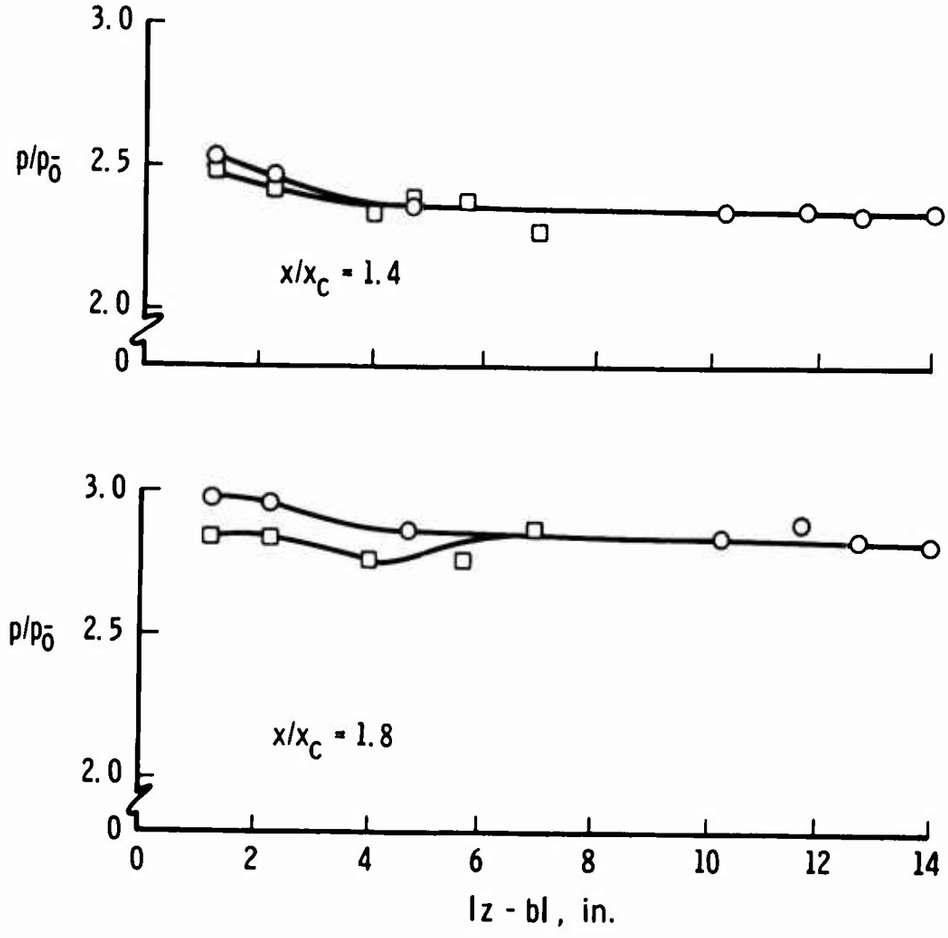

c. Spanwise Distribution on Ramp
Fig. 20 Concluded

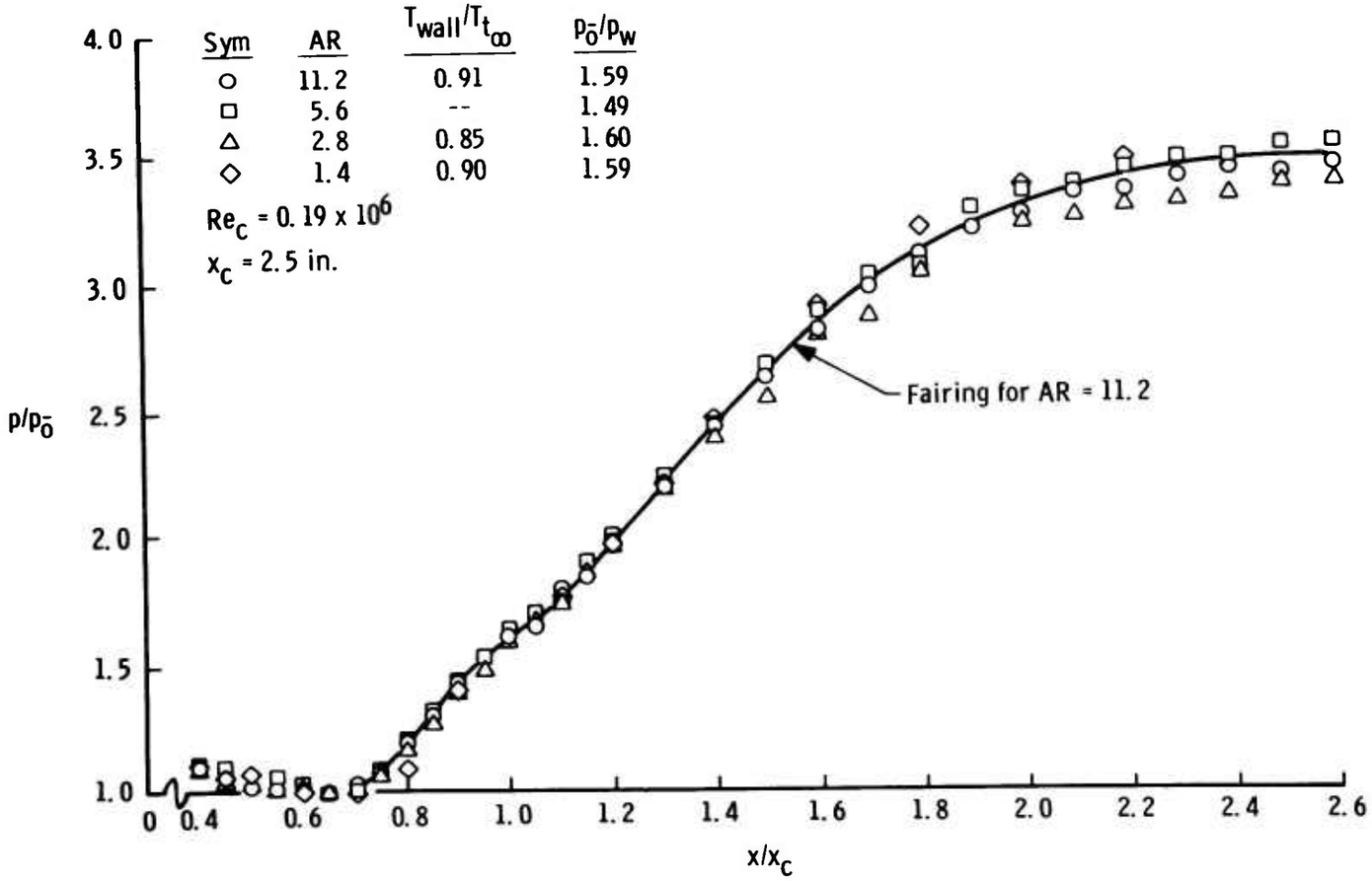

a. Longitudinal Centerline Distributions

Fig. 21 Effect of Aspect Ratio on Pressure Distributions at $M_w = M_\infty = 8$

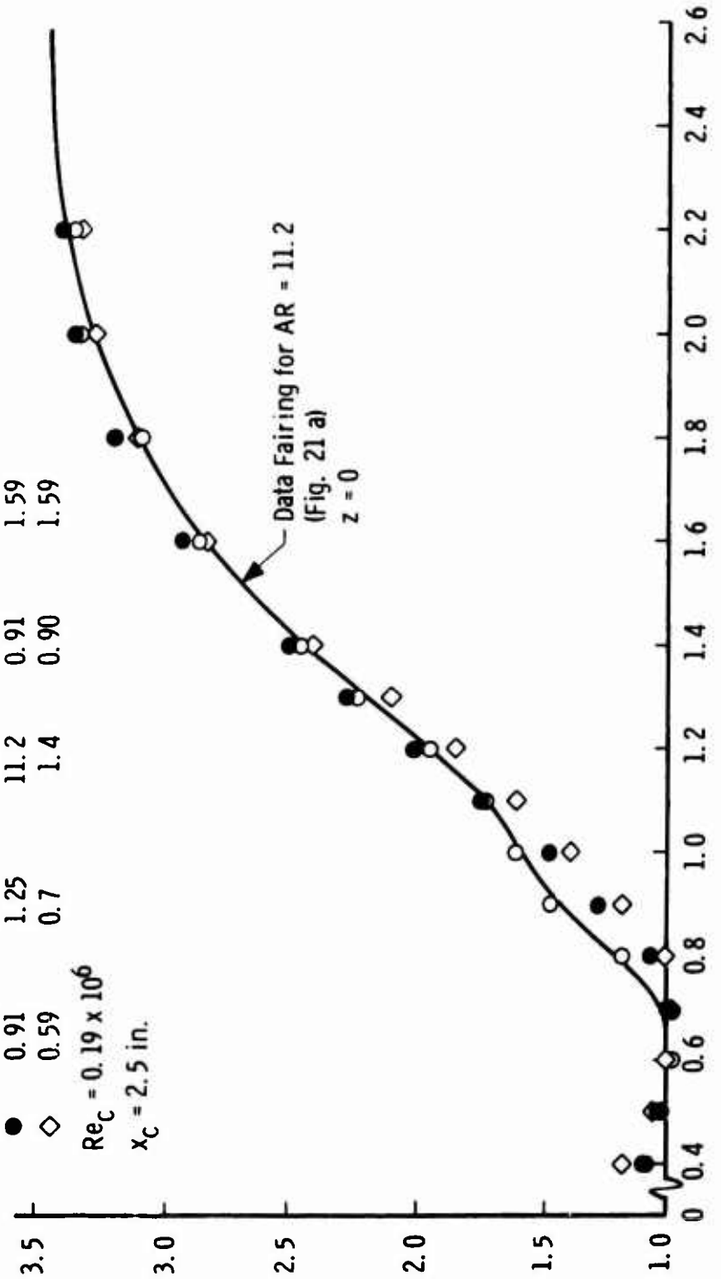

b. Longitudinal Distributions off Centerline
Fig. 21 Continued

Sym	AR	T_{wall}/T_{t_∞}	$p_{\bar{o}}/p_w$
○	11.2	0.91	1.59
□	5.6	--	1.49
△	2.8	0.85	1.60
◇	1.4	0.90	1.59

$Re_c = 0.19 \times 10^6$

$x_c = 2.5$ in.

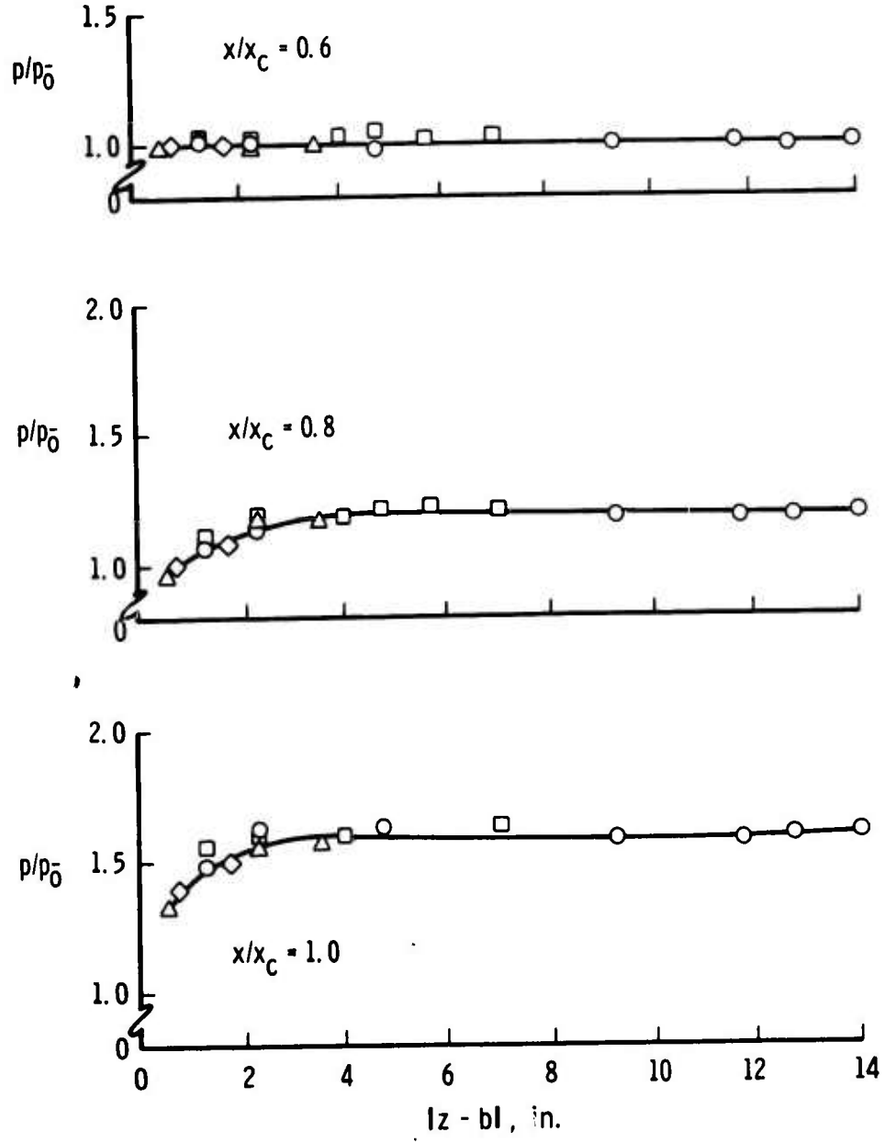

c. Spanwise Distribution on Flat Plate

Fig. 21 Continued

Sym	$\dot{A}R$	T_{wall}/T_{t_∞}	$p_{\bar{0}}/p_w$
○	11.2	0.91	1.59
□	5.6	--	1.49
△	2.8	0.85	1.60
◇	1.4	0.90	1.59

$Re_c = 0.19 \times 10^6$

$x_c = 2.5$ in.

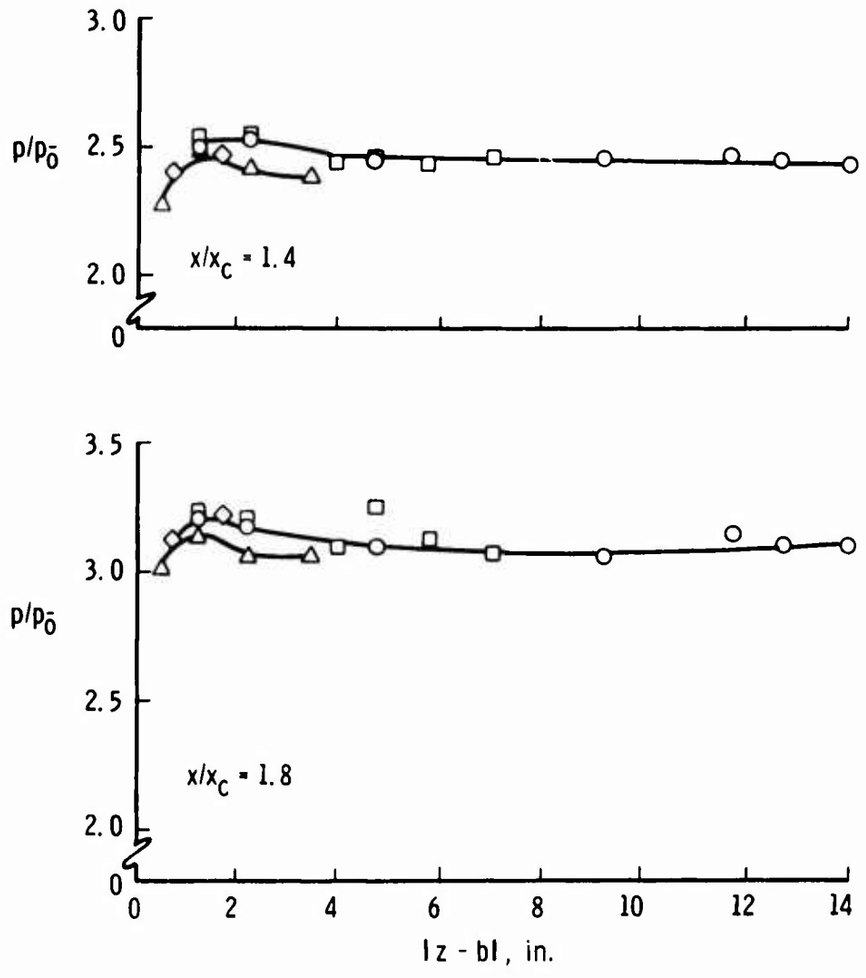

d. Spanwise Distribution on Ramp

Fig. 21 Concluded

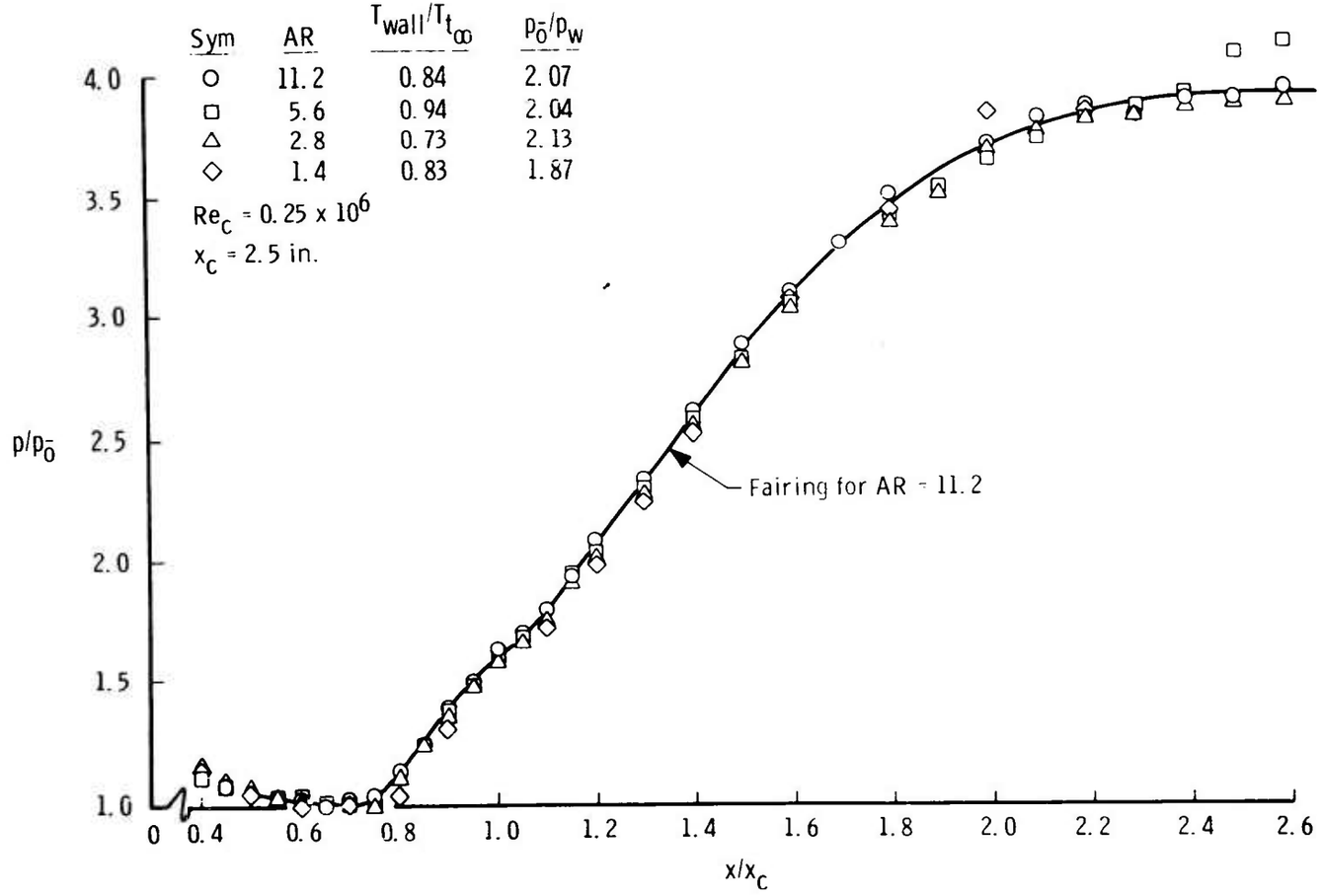

a. Longitudinal Centerline Distribution

Fig. 22 Effect of Aspect Ratio on Pressure Distribution at $M_w = M_\infty = 10$

Sym	AR	T_{wall}/T_{t_∞}	$p_{\bar{o}}/p_w$
○	11.2	0.84	2.07
□	5.6	0.94	2.04
△	2.8	0.73	2.13
◇	1.4	0.83	1.87

$Re_c = 0.25 \times 10^6$

$x_c = 2.5$ in.

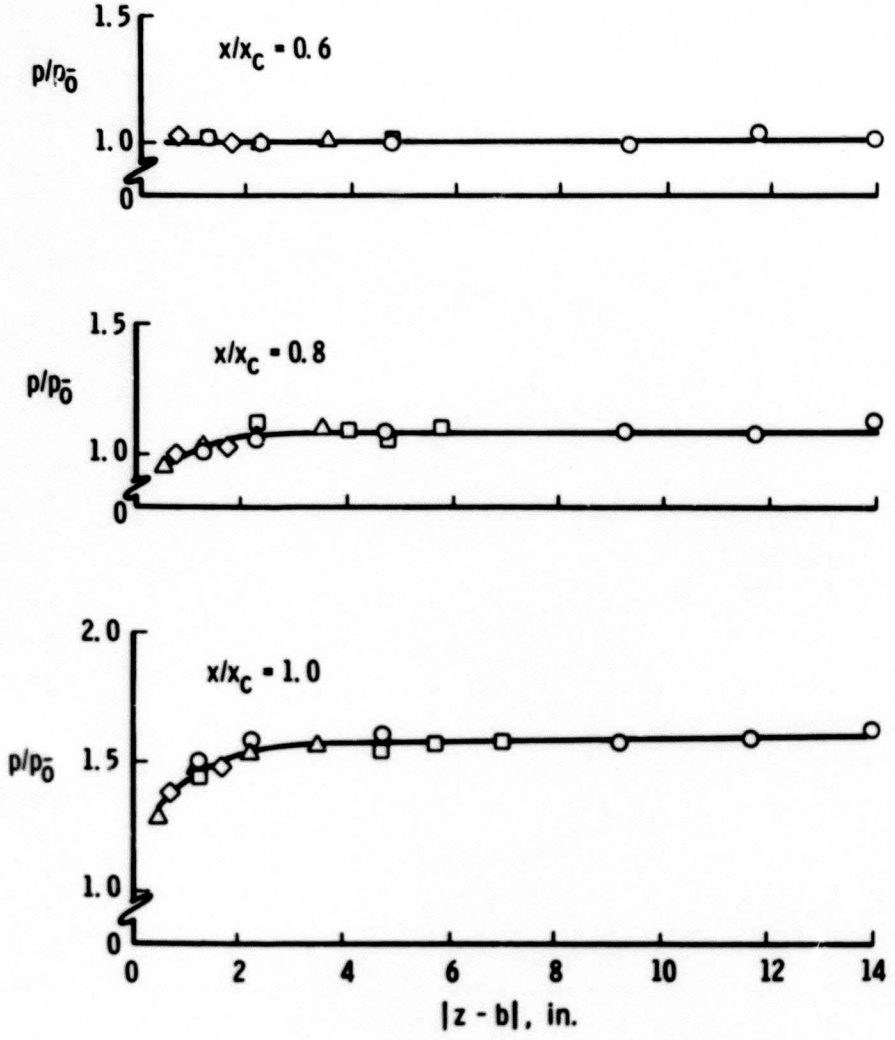

b. Spanwise Distribution on Flat Plate

Fig. 22 Continued

Sym	AR	T_{wall}/T_{t_∞}	$\bar{p_0}/p_w$
○	11.2	0.84	2.07
□	5.6	0.94	2.04
△	2.8	0.73	2.13
◇	1.4	0.83	1.87

$Re_c = 0.25 \times 10^6$

$x_c = 2.5$ in.

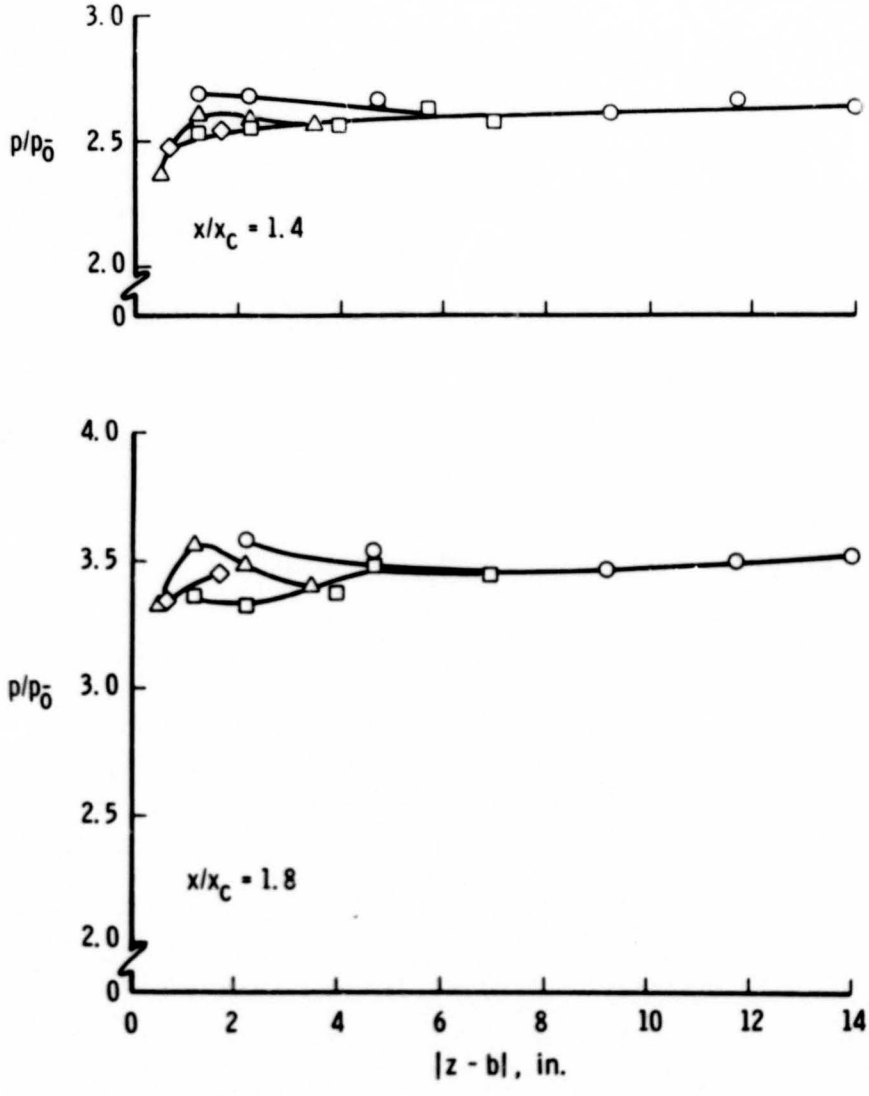

c. Spanwise Distribution on Ramp

Fig. 22 Concluded

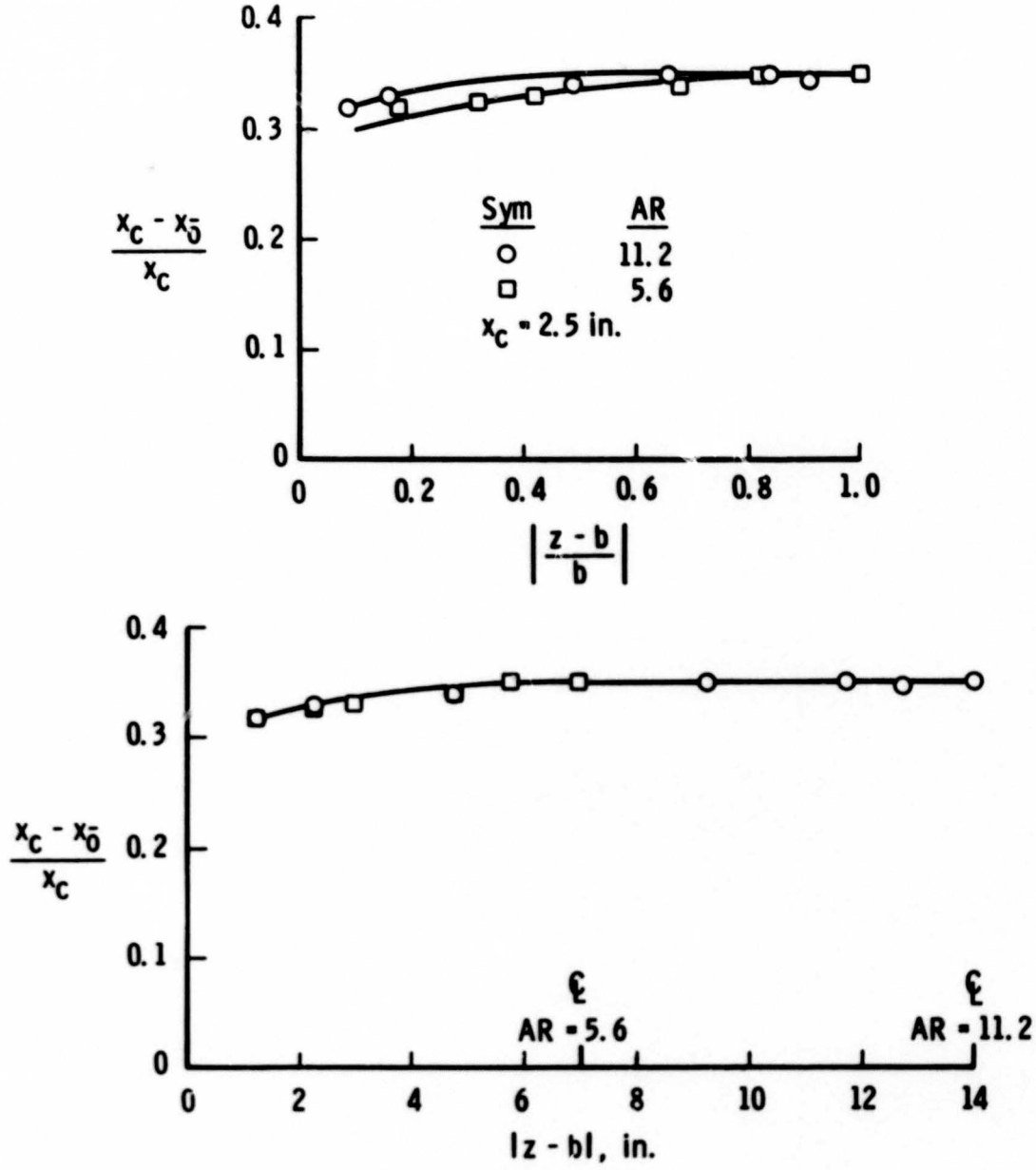

a. $M_w = M_\infty = 6$

Fig. 23 Effect of Aspect Ratio on the Extent of the Separation Region at $Re_c = 0.19 \times 10^6$

Sym	AR
○	11.2
□	5.6
◇	2.8
△	1.4

x_c = 2.5 in.

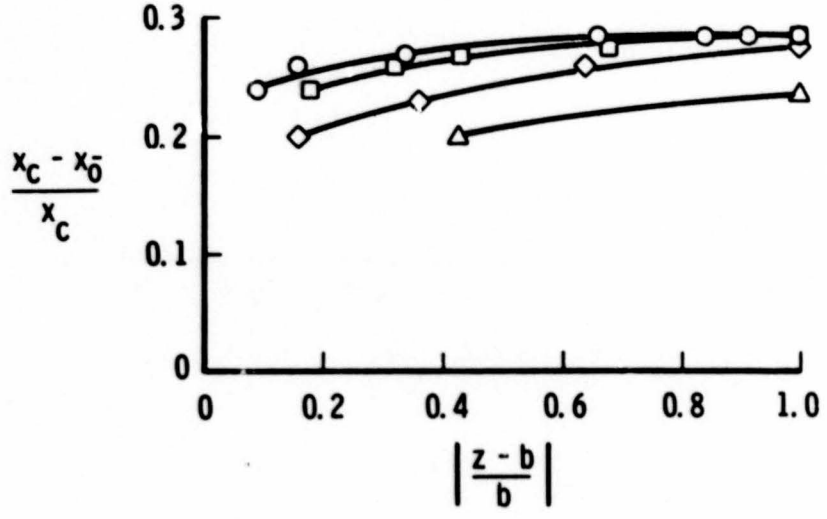

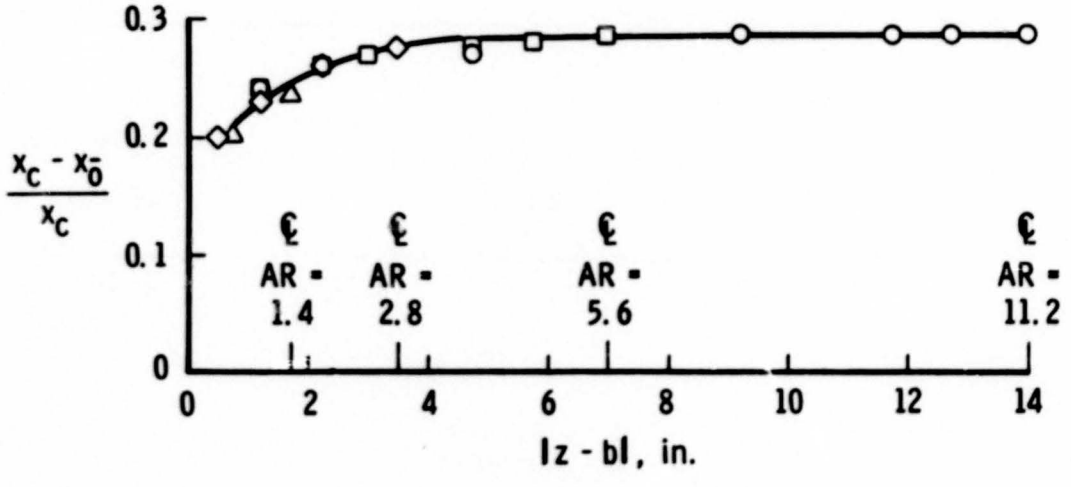

b. $M_w = M_\infty = 8$

Fig. 23 Continued

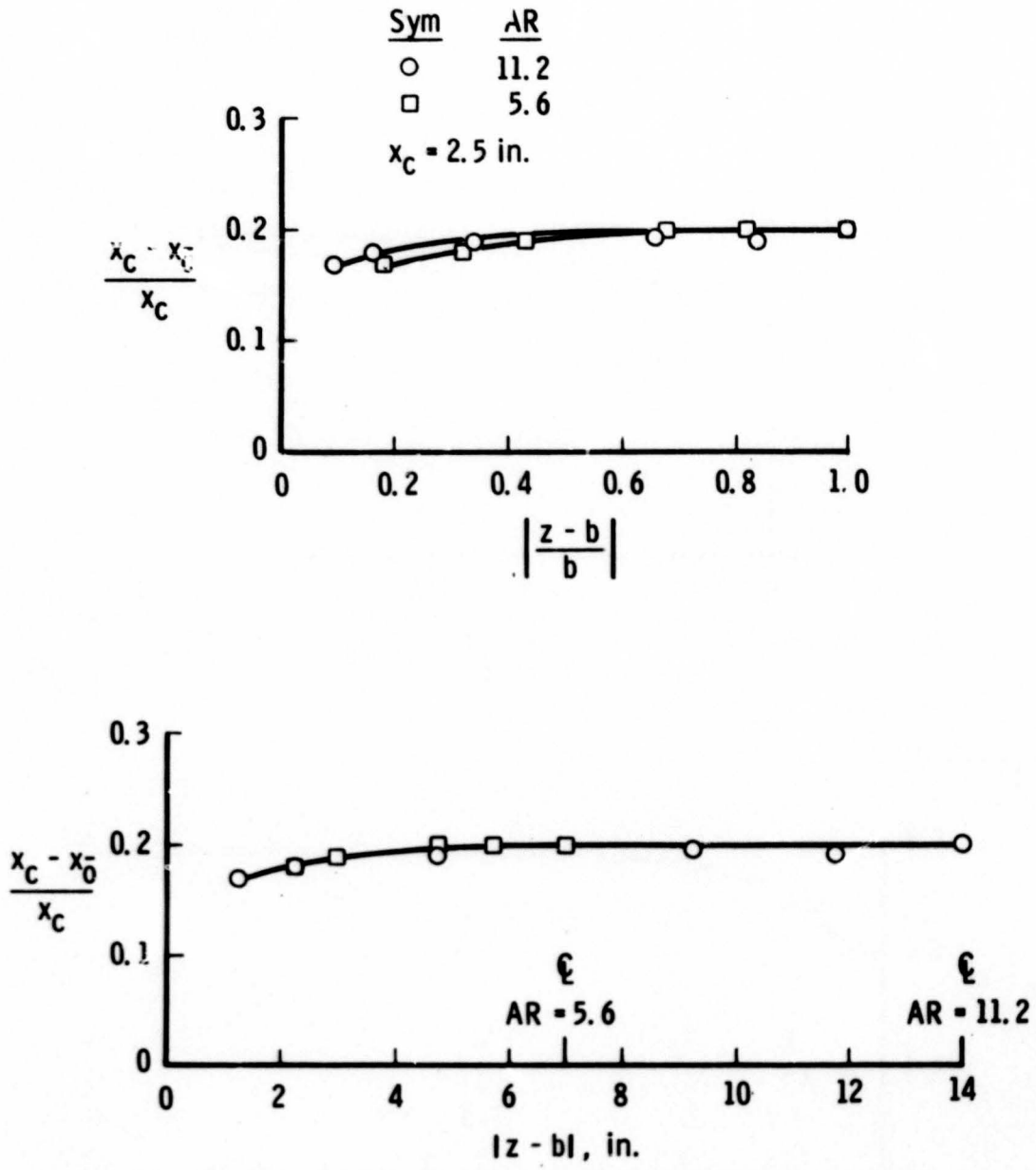

c. $M_w = M_\infty = 10$
Fig. 23 Concluded

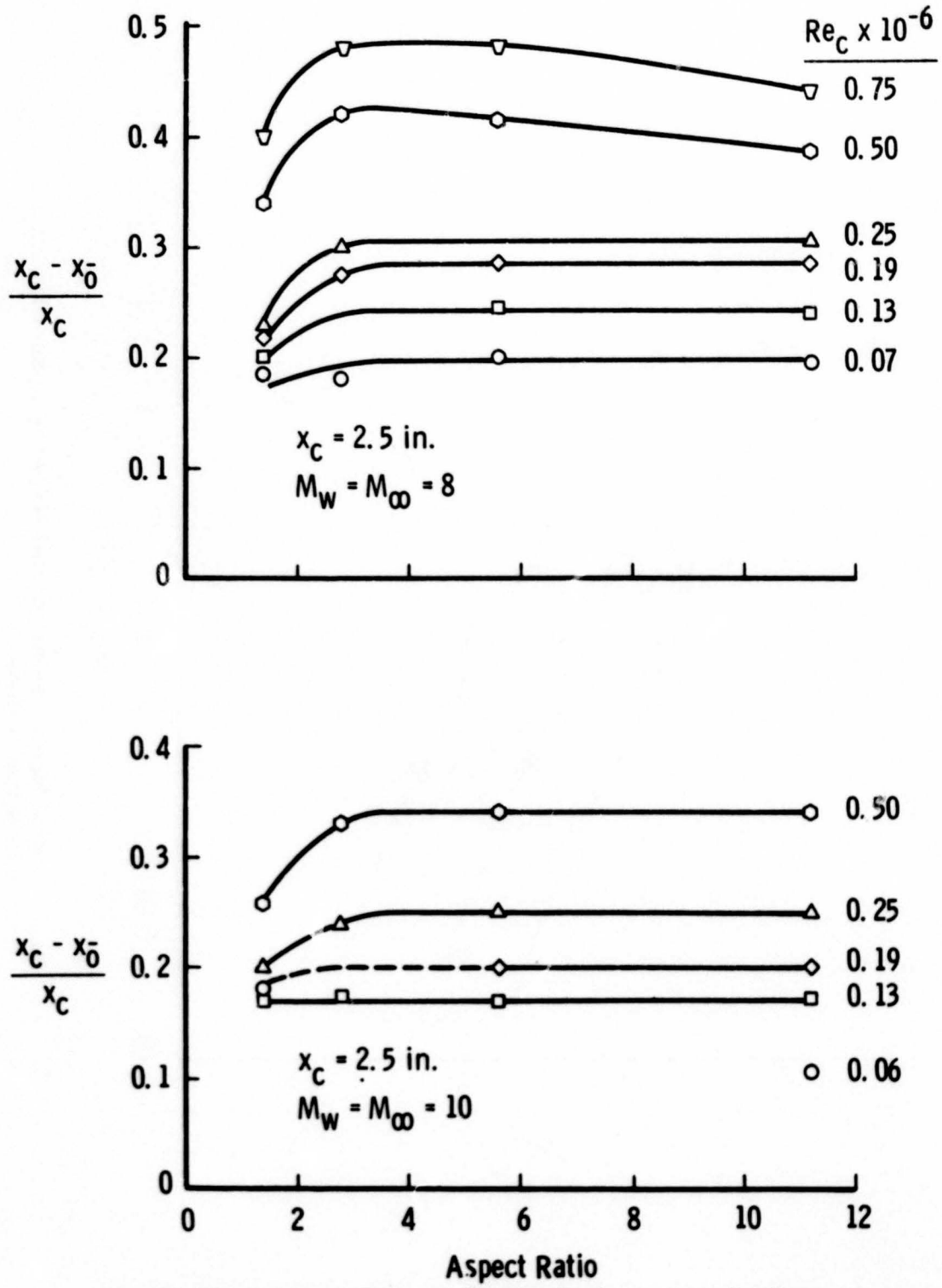

Fig. 24 Effect of Aspect Ratio and Reynolds Number on Centerline Extent of the Separation Region

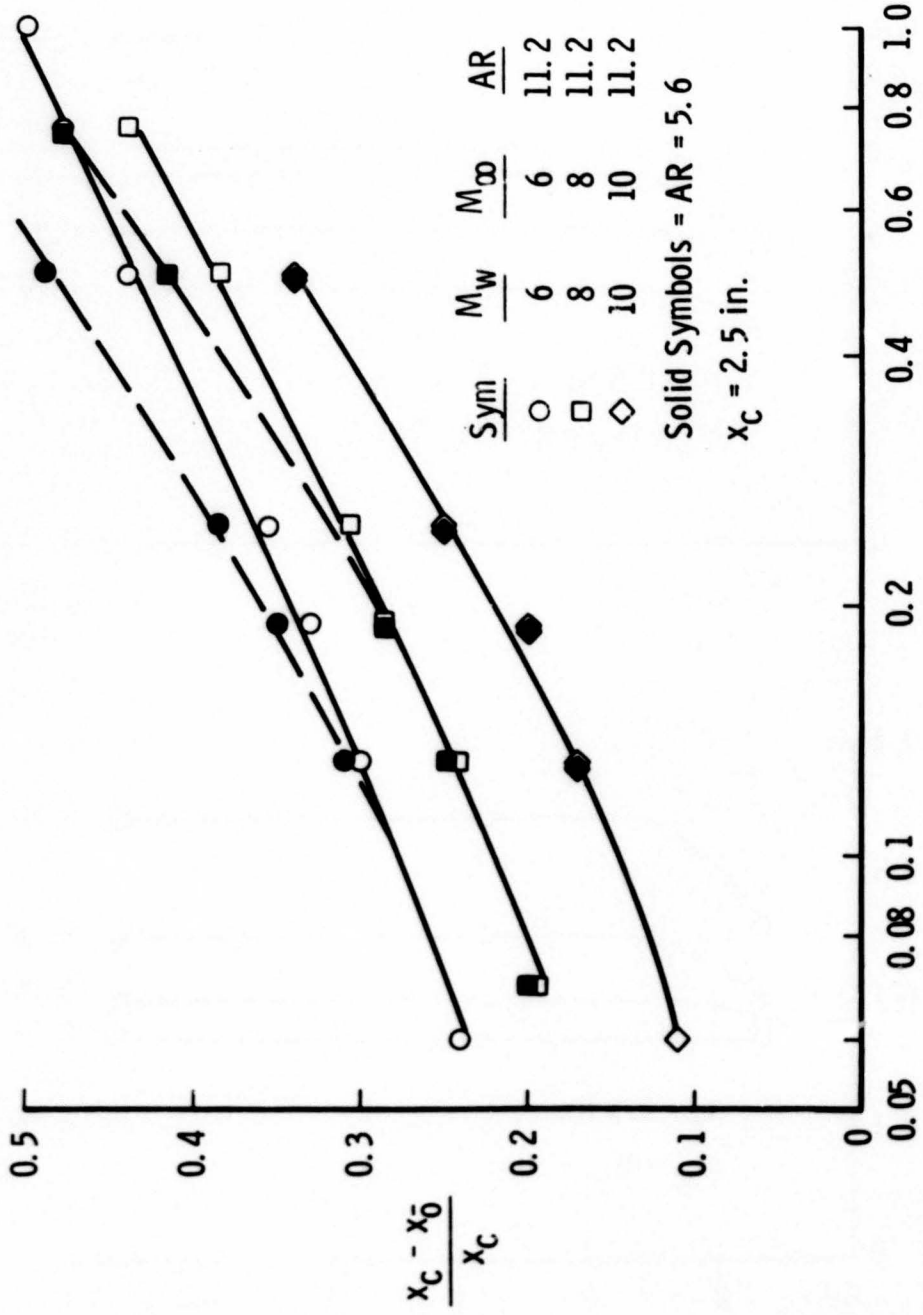

Fig. 25 Effect of Reynolds Number and Mach Number on Centerline Extent of the Separation Region

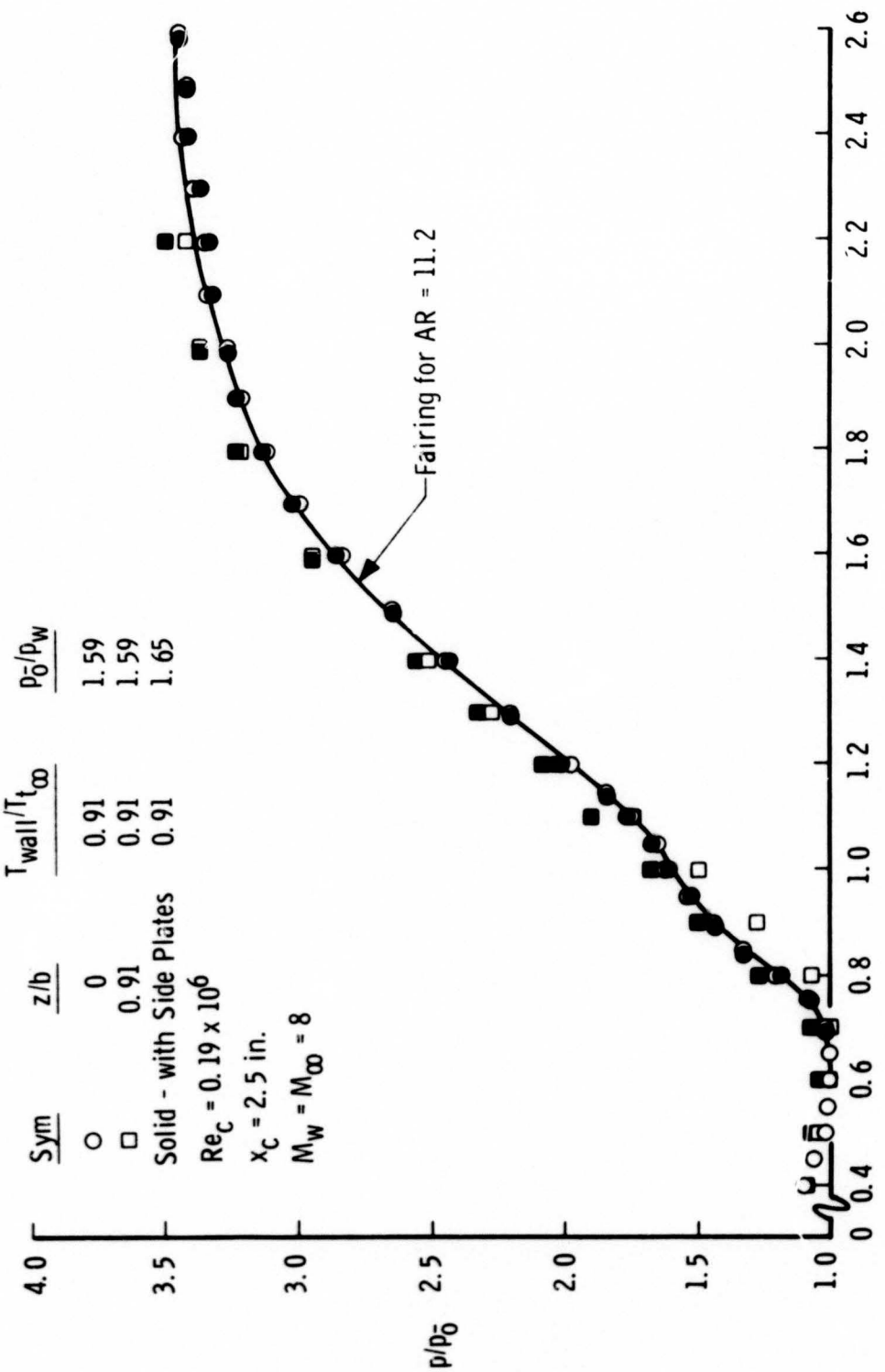

a. AR = 11.2

Fig. 26 Effect of Upper Surface Side Plates on Longitudinal Pressure Distributions

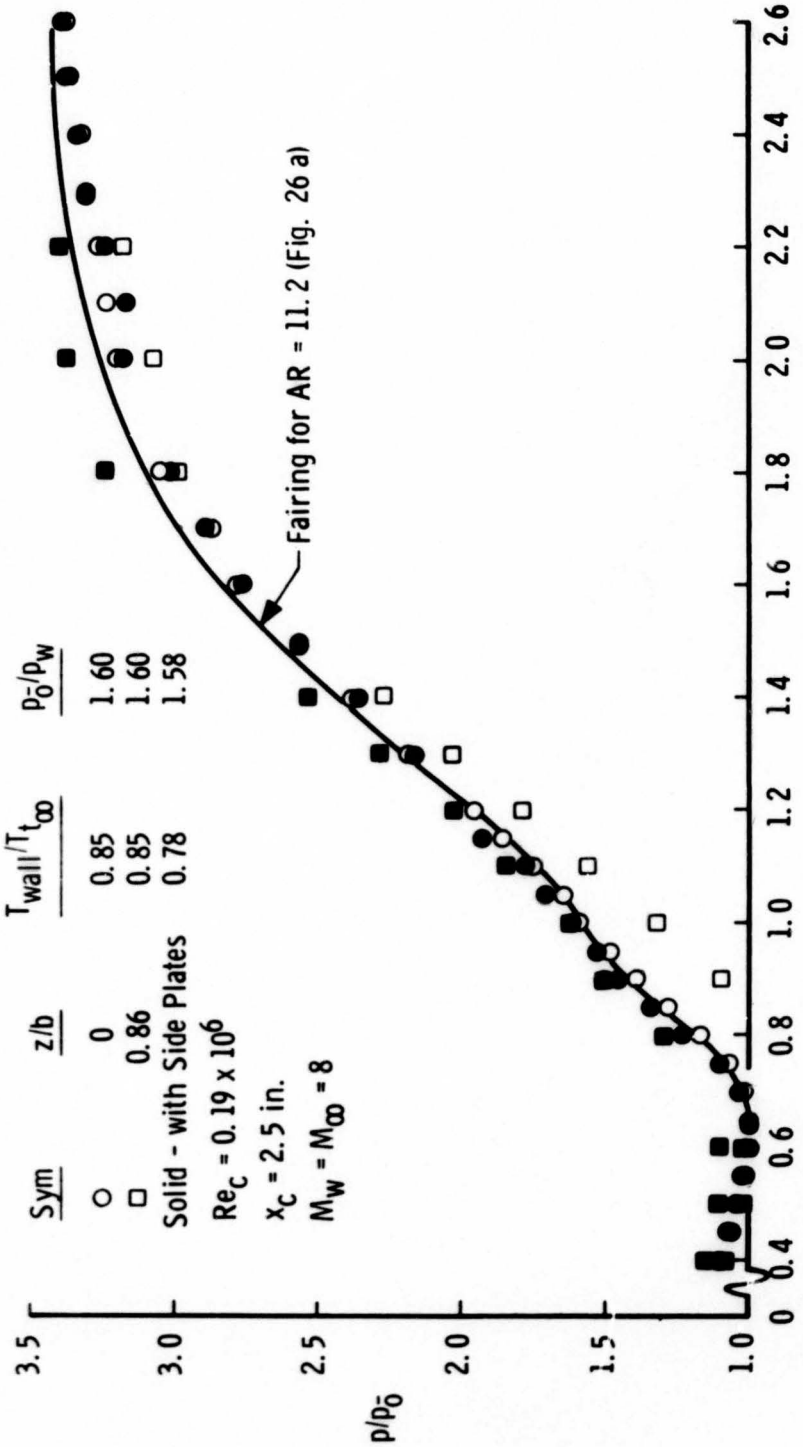

b. AR = 2.8
Fig. 26 Continued

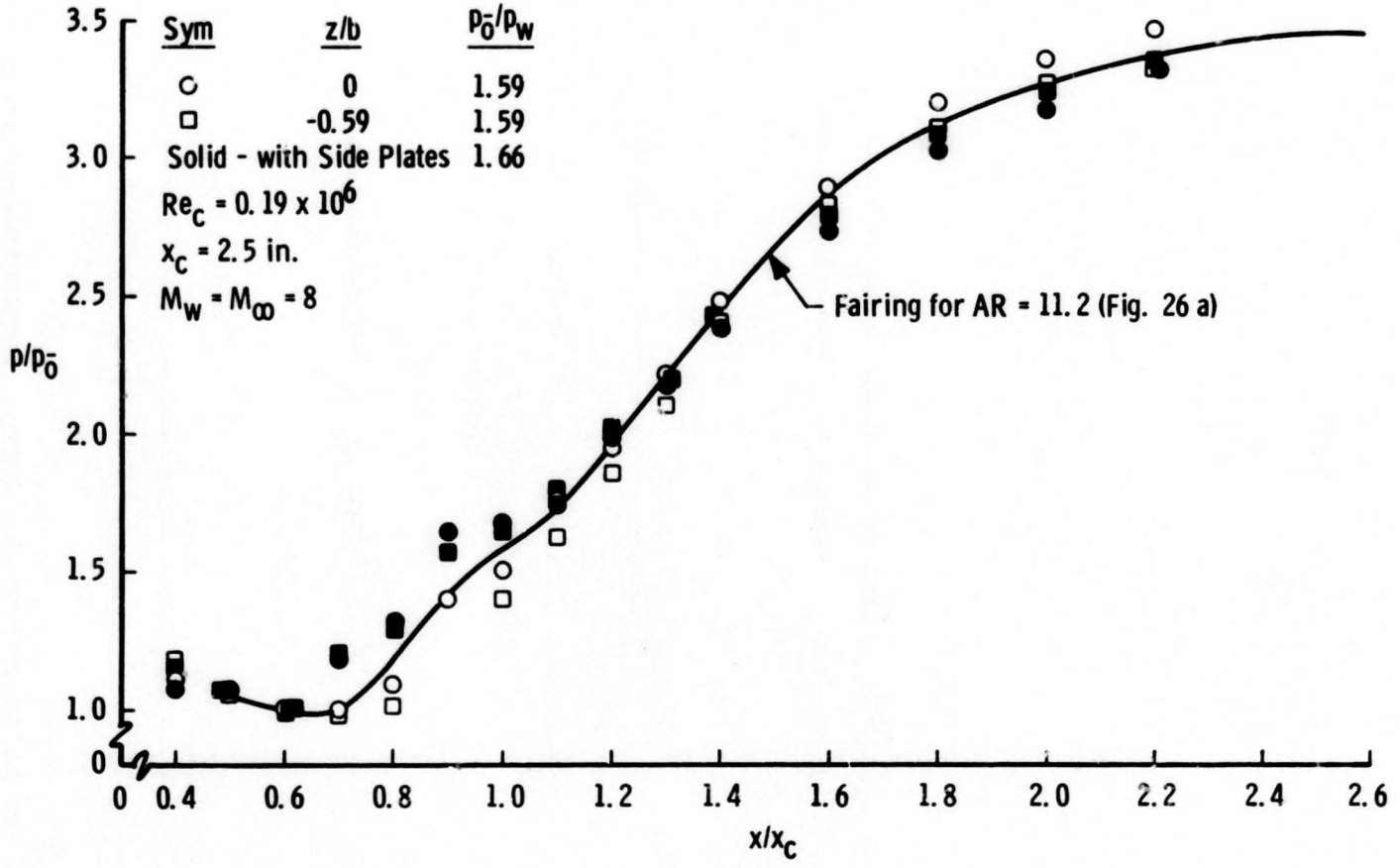

c. AR = 1.4

Fig. 26 Concluded

		Side Plates On		Side Plates Off	
Sym	AR	T_{wall}/T_{t_∞}	$p_{\bar{0}}/p_w$	T_{wall}/T_{t_∞}	$p_{\bar{0}}/p_w$
○	11.2	0.91	1.59	0.91	1.65
□	2.3	0.95	1.60	0.78	1.58
◇	1.4	--	1.59	--	1.66

Solid with Side Plates

$Re_c = 0.19 \times 10^6$

$M_w = M_\infty = 8$

$x_c = 2.5$ in.

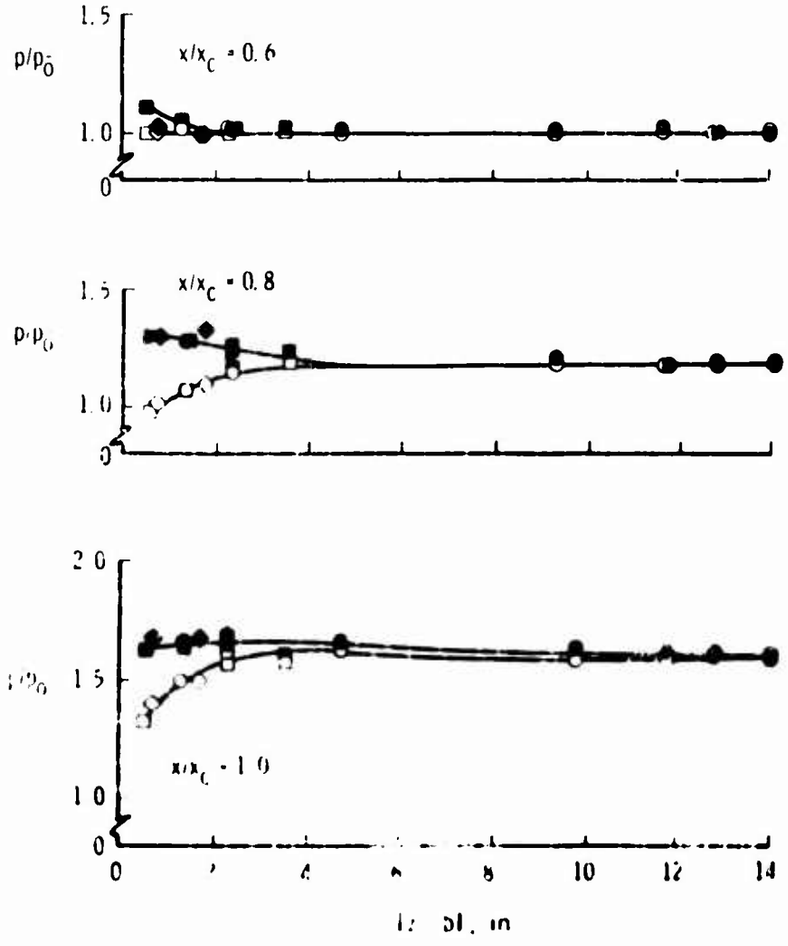

Flat Plate Distributions

Fig. 27 Effect of Upper Surface Side Plates on Spanwise Pressure Distributions

Sym	AR	T_{wall}/T_{t_∞}	$p_{\dot{0}}/p_{\cdot}$	T_{wall}/T_{t_∞}	$p_{\dot{0}}/p_{w}$
○	11.2	0.91	1 59	0 91	1 65
□	2.8	0.85	1 60	0 78	1 58
◇	1.4	--	1 59		1 66

Solid - with Side Plates

$Re_c = 0.19 \times 10^6$

$M_w = M_\infty = 8$

$x_c = 2.5$ in.

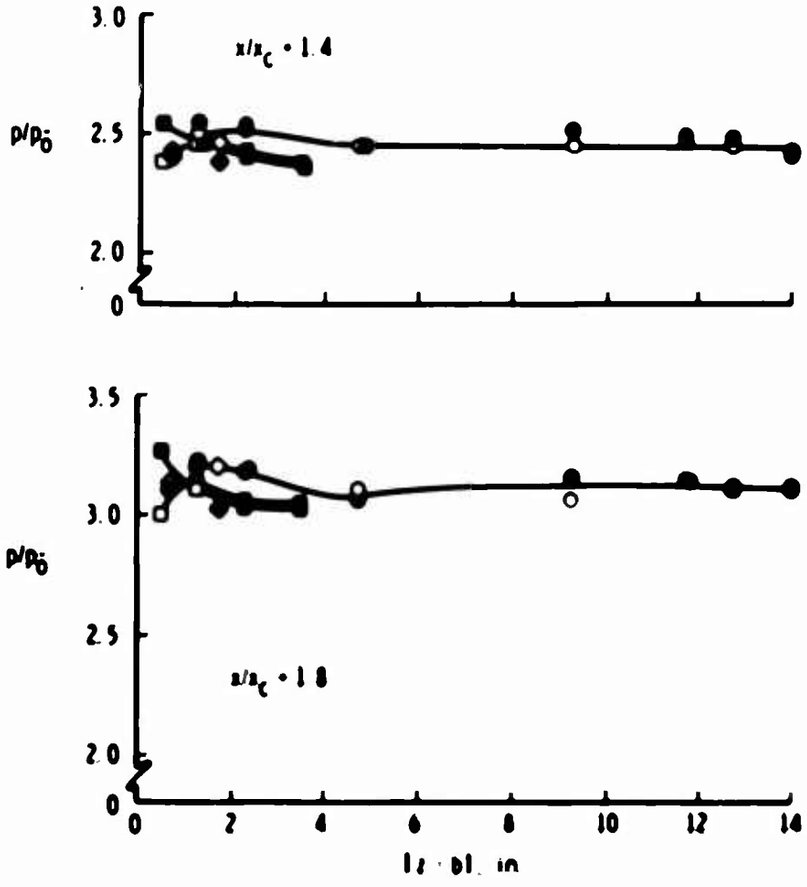

b Ramp Distributions
Fig 27 Concluded

Sym	AR	x_c, in.	$(u/\nu)_\infty \times 10^{-6}$, in.$^{-1}$	T_{wall}/T_{t_∞}	$p_{\bar{o}}/p_w$
○	2.8	2.5	0.13	0.86	1.17
□	2.0	14.0	0.026	0.71	1.11
△	1.4	2.5	0.13	0.89	1.21

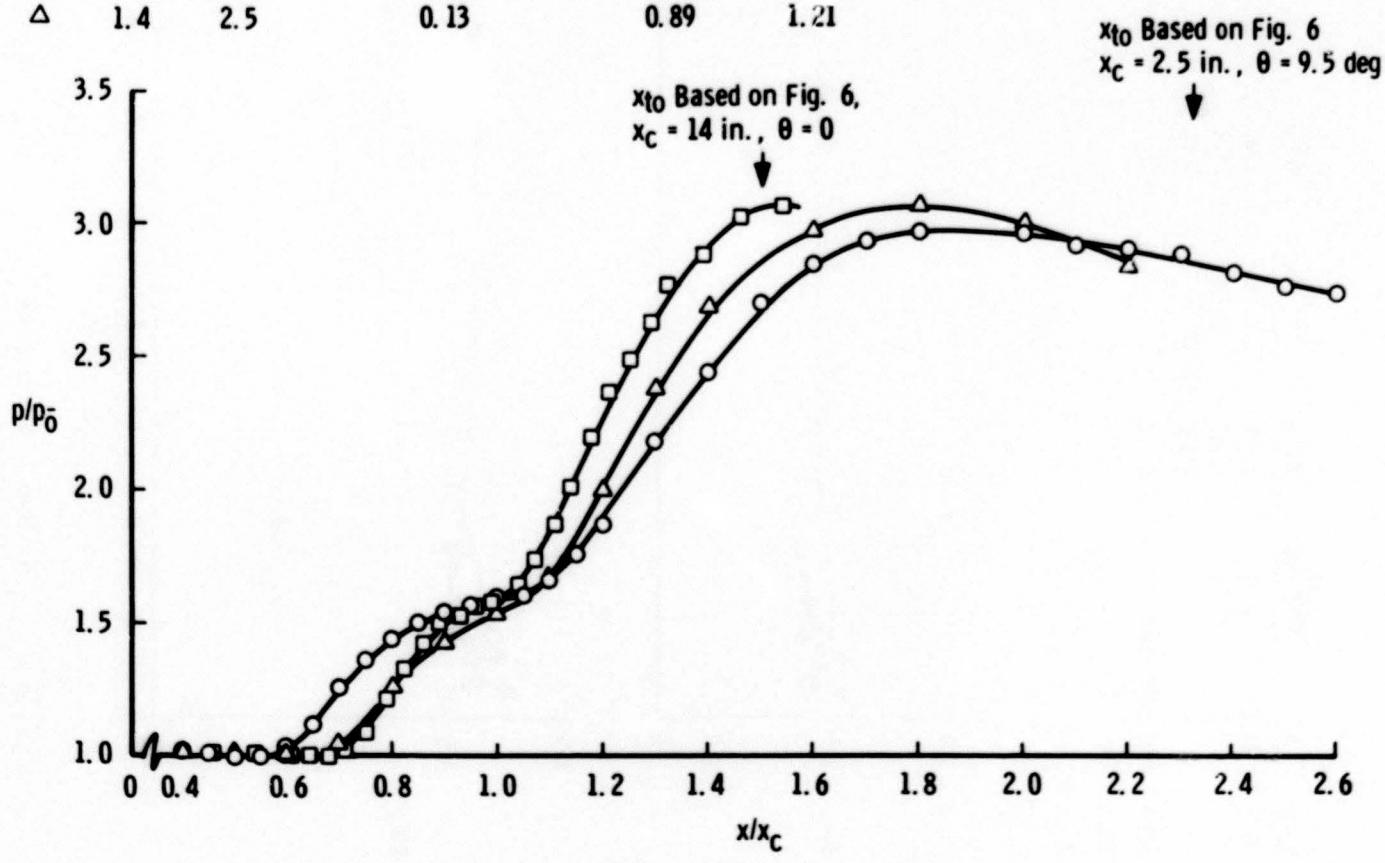

a. $Re_c = 0.50 \times 10^6$

Fig. 28 Effect of Flat-Plate Length on Centerline Pressure Distributio at $M_w = 6$, $M_\infty = 8$

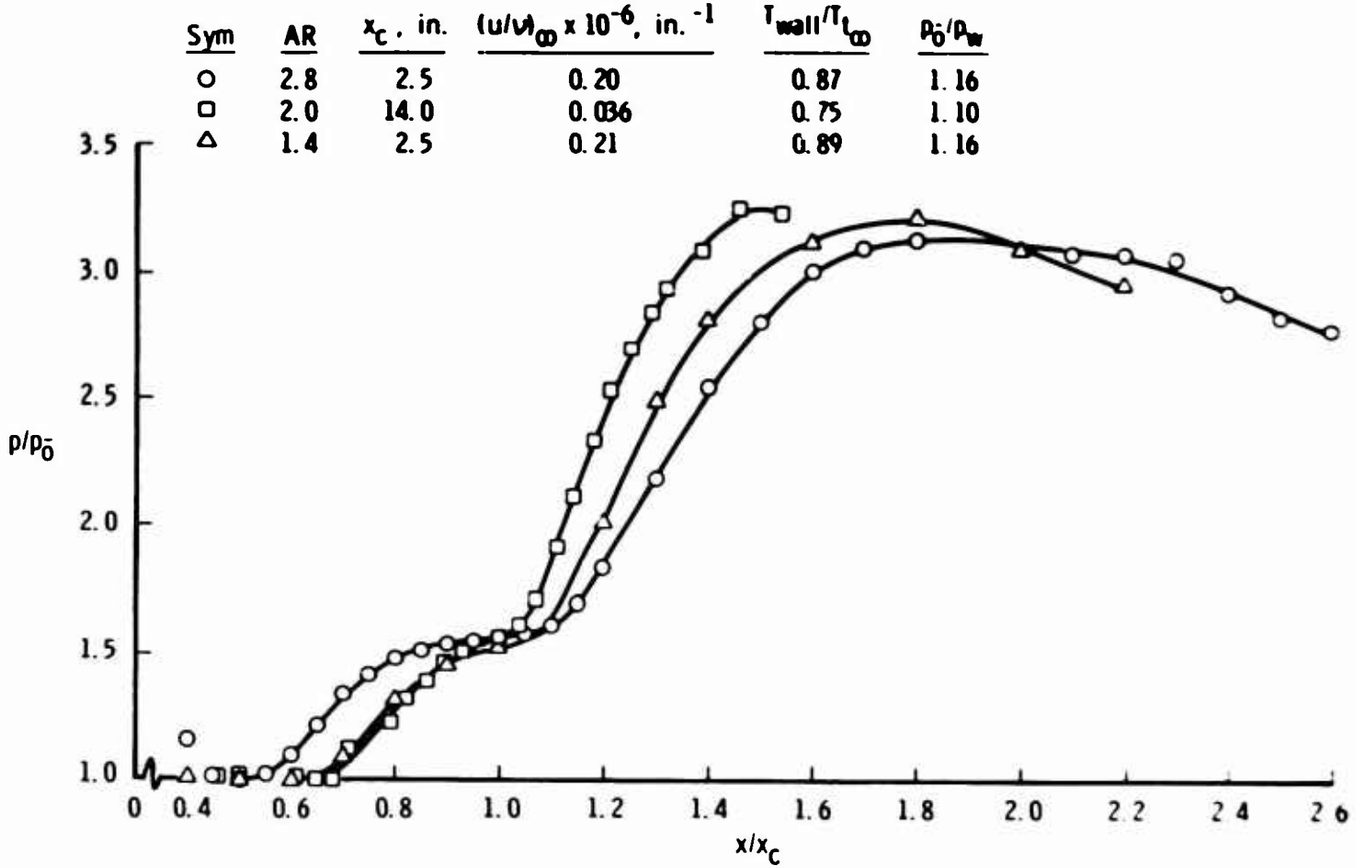

b. $Re_c = 0.75 \times 10^6$

Fig. 28 Concluded

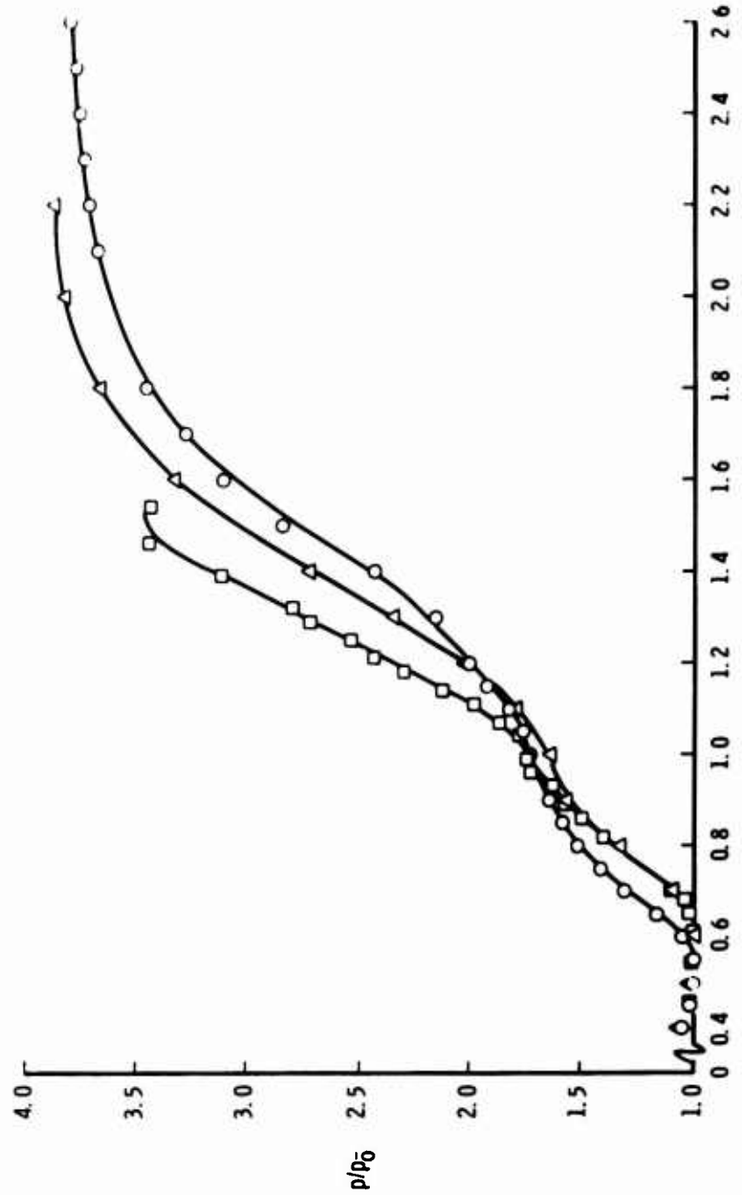

a. Longitudinal Centerline Pressure Distributions

Fig. 29 Effect of Flat-Plate Length on Pressure Distributions and Transition Location, $M_w = M_\infty = 8$

Sym	AR	x_c, in.	$(\rho V)_\infty \times 10^{-6}$, in.$^{-1}$	T_{wall}, °R	p_0/p_∞
○	2.8	2.5	0.20	0.85	1.81
□	2.0	14.0	0.036	0.75	1.78
△	1.4	2.5	0.20	0.91	1.8[illegible]

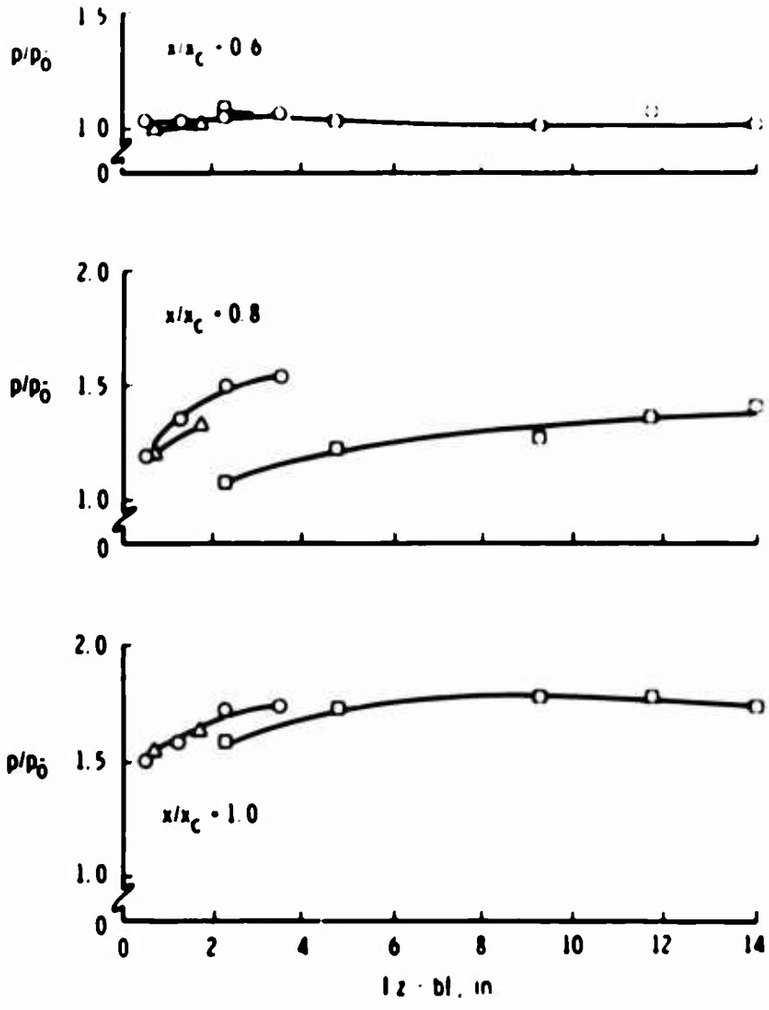

b. Spanwise Pressure Distributions on Flat Plate

Fig. 29 Continued

	2.8	2.5	0.20	0.37	1.41
	2.0	14.0	0.036	0.75	1.28
	1.4	2.5	0.20	0.91	1.42

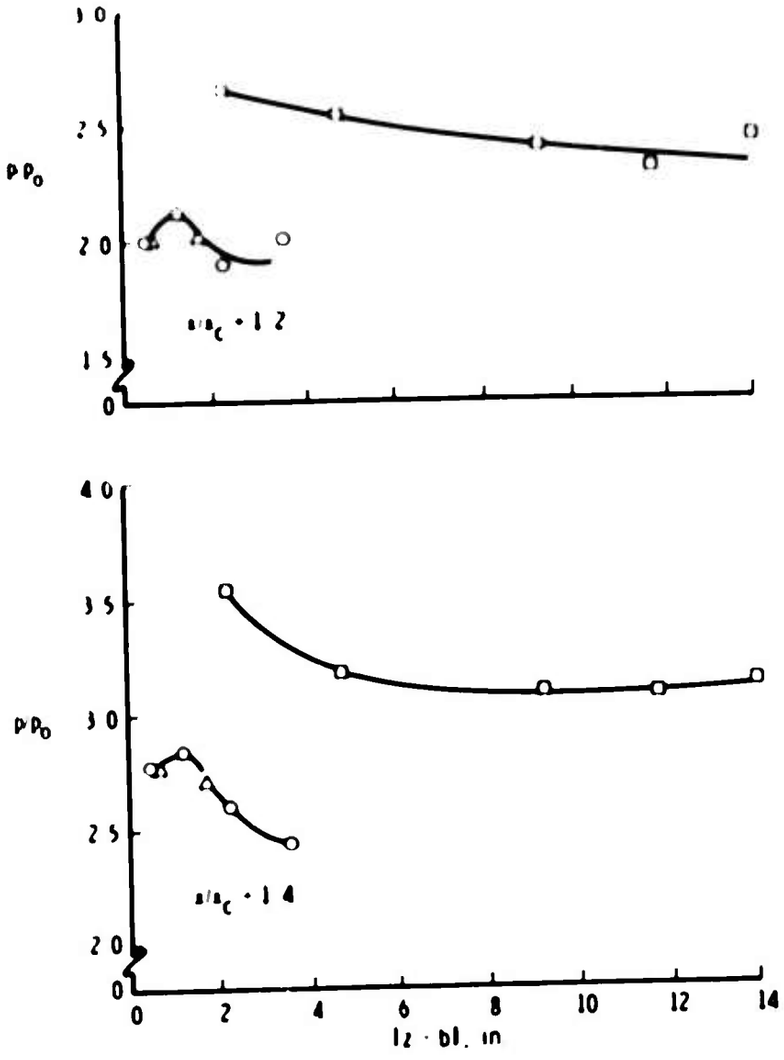

c. Spanwise Pressure Distribution on Ramp
Fig. 29 Continued

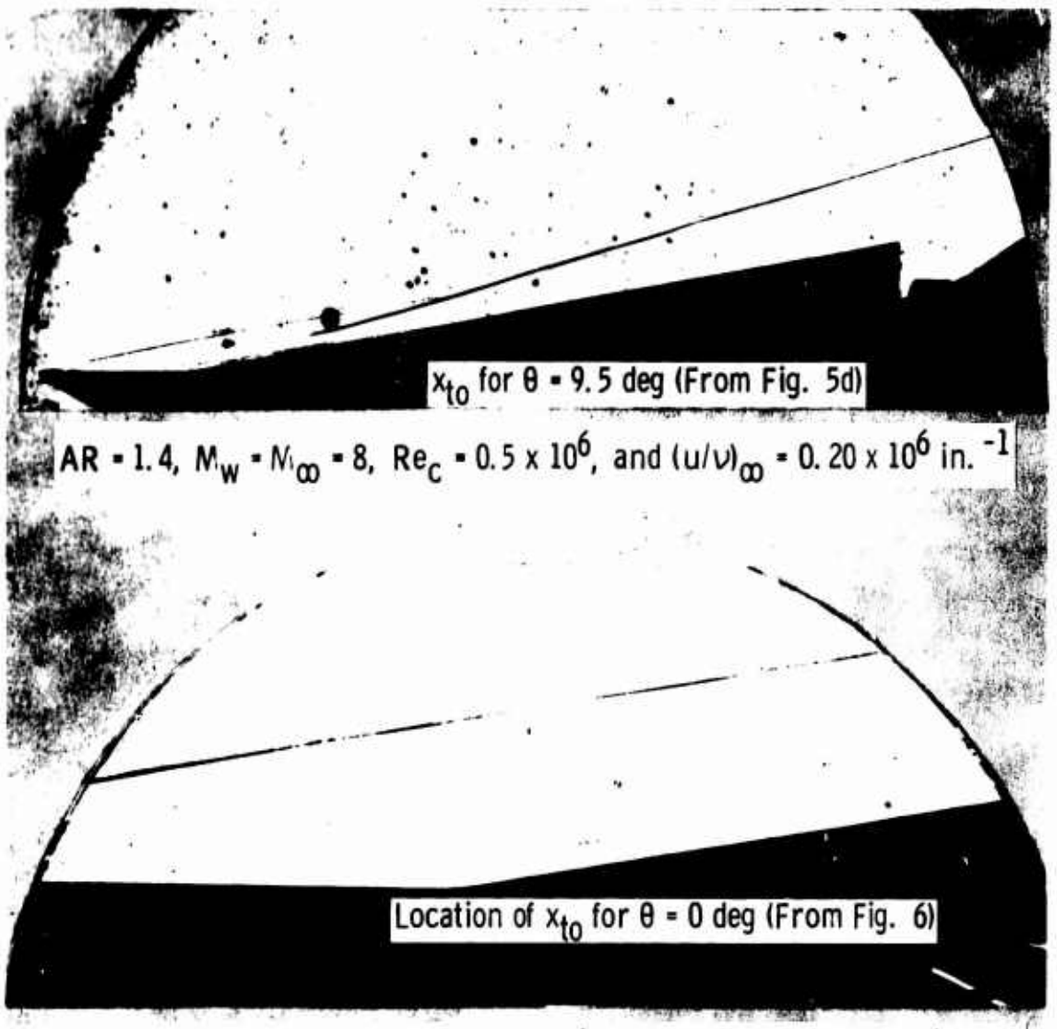

d. Shadowgraph Pictures for x_c = 2.5 and 14.0 in.
Fig. 29 Concluded

4.1.4 Comparisons with Theory and Published Data

4.1.4.1 Correlations of Pressure Data at $x \leq x_c$

The net peak pressure rise, $(p_c - p_{\bar{o}})/p_{\bar{o}}$, measured on the flat plate ($x \leq x_c$) is a parameter of some interest because (1) it is a partial measure of the loading induced by the separation, and (2) of the data obtained during the many investigations of flow separation, it is the only parameter derived from pressure measurements which exhibits reasonable correlation when plotted versus the Reynolds number, $Re_{\bar{o}}$. It was demonstrated first in Ref. 2 that this pressure rise varied inversely with $Re_{\bar{o}}^{1/4}$ for a wide variety of configurations as long as there was a substantial plateau in the pressure distribution upstream of the corner. Moreover, it was also demonstrated that this pressure rise, when expressed as a pressure coefficient varied inversely with the Mach number function, $(M_w^2 - 1)^{1/4}$, in the range $1 \lessapprox M_w \lessapprox 3.6$. Data for a wider range of Mach numbers were examined in Ref. 8 and found to correlate according to

$$C_{p_c} Re_{\bar{o}}^{1/4} = 1.56(M_w^2 - 1)^{-0.262} \qquad (1)$$

The plateau pressure coefficient (C_{p_p}) of Ref. 8 has been redefined herein to be C_{p_c} (pressure coefficient at the corner) because of the absence of a substantial plateau in the present data. In the presence of a true plateau, the two values would be identical ($C_{p_c} = C_{p_p}$).

Data obtained during this investigation are compared with Eq. (1) in Fig. 30, and it is obvious that the present data do not correlate with previous results at $M_w > 6$ and/or $Re_{\bar{o}} \lessapprox 0.2$ million. This is undoubtedly related to the absence of a pressure plateau under such conditions (for example, the longitudinal pressure distribution obtained at $M_w = 6$, $Re_c = 0.13 \times 10^6$ and shown on the lower half of Fig. 30). Since the only data of this investigation which fit the pressure plateau correlation (Eq. (1)) are those which are most likely transitional during flow reattachment, and since essentially none of the previously published data meet the accepted criteria for laminar flow reattachment, it must therefore be concluded that the present data support the conjecture of Ref. 9 that a pressure plateau is characteristic of transitional reattaching adiabatic flows at supersonic and hypersonic speeds.

It is interesting to note that for these data the ratio of the pressure at the corner to the inviscid wedge pressure (p_c/p_w) was found to be pri-

marily dependent on the local inviscid Mach number (M_w) and insensitive to an increase in local Reynolds number.

Because the flow in the neighborhood of separation is governed by a coupled interaction between the boundary layer and the external supersonic flow, the surface pressure distribution in this so-called "free-interaction" region follows a law of similarity deduced first in Ref. 2 for adiabatic flows, then extended to the variable wall temperature case by Curle (Ref. 10). Data from this investigation for the full Mach number range, both pitched and unpitched are compared in Fig. 31 with the results of Ref. 3. Although it is evident that the present results are quite effectively correlated using the Chapman-Curle coordinates, there is a discrepancy noted between them and those of Lewis et al. It is observed that the present results show less tendency to approach a plateau, but this is probably of minor significance since the domain of similarity should not extend very far beyond separation ($X \approx 1.2$). However, the reason for differences at $X < 1.2$ is not understood.

4.1.4.2 Comparisons with the Lees-Reeves Integral-Moment Theory

One of the best available theoretical methods for analyzing a shock wave and boundary-layer interaction in adiabatic flow is the integral-moment theory developed by Lees and Reeves (Ref. 11). A computer program to solve these equations was developed in the VKF, and was modified to account for the effects of the weak viscous interaction upstream of the main one using the equations given in Ref. 7. A unique solution is obtained by specifying only M_w, Re_c, and θ. The beginning of the interaction is then found by iteration as a two-point-boundary value problem where it is required that (1) the local Mach number gradient be zero at the start of the interaction and (2) the Mach number on the ramp be convergent to that corresponding to an isentropic compression through an angle, θ, starting at M_w. Without any loss of generality (Ref. 7), it was assumed that the viscosity constant, C, was equal to one for the calculations presented herein. Although the value of C was found to affect the scale of the overall interaction, the pressure gradients were noted to be essentially unchanged.

A comparison of theory with selected data at $M_w = 6$ is provided in Fig. 32 for Reynolds numbers ranging from near the incipient separation condition ($Re_c = 0.06$ million) to that corresponding to a significant separation ($Re_c = 0.50$ million). The agreement upstream of the hinge line is considered quite satisfactory although it may be observed that the pressure rise measured begins farther downstream than indicated by the theory. There appears to be a more notable discrepancy in both the maximum pressure gradient on the ramp ($x/x_c > 1$) and the overall pressure rise, although the two are obviously related one to the other. The agreement on the ramp is best at the highest Reynolds number because

the pressure gradient predicted by theory changed more with Reynolds number than did the data.

Another comparison of theory and experiment is provided in Fig. 33 where the relative upstream extent of the interaction is shown as a function of Reynolds number. Since other published data are included in this comparison, it was necessary to include additional theoretical estimates at ramp angles corresponding to the range covered in all of the experiments. It is obvious from this figure that the results of this investigation span the broadest range of Reynolds number yet obtained for laminar reattaching flows. Note, for example, the fall off in the results of Ref. 3 at $Re_c > 0.2$ million, an effect which is typical of transition occurring before reattachment. The present data and those of Ref. 5, by their general agreement (especially the trends with Re_c) with respect to theoretical predictions, show that laminar flow reattachment is feasible at low hypersonic speeds for ramps of at least 11 deg at Reynolds numbers up to 1 million with adiabatic wall temperatures.

A crossplot of the theoretical results in Fig. 33 is presented in Fig. 34 to illustrate (1) the influence of ramp deflection angle on the upstream interaction scale as well as to show (2) the general agreement of the present results and those of Refs. 3 and 5. It should be noted that the results from both of these references were obtained with aspect ratios which must be judged as, at least, marginal based on the present results (see Section 4.1.3). It is noted that although the data for θ = 10 deg (Ref. 5) show closer agreement with the theory, they are unexpectedly high when compared to the present results.

Another comparison of the longitudinal pressure distributions derived from theory and experiment are presented in Fig. 35 for the three Mach numbers investigated (unpitched) at a constant Reynolds number. It is evident again that the theory gives the most discrepant results on the ramp and that the magnitude increases with Mach number increase. Nevertheless, as also noted previously in Ref. 5, the scale of the upstream interaction measured is remarkably well predicted by the theory. An alternate presentation of the effect of Mach number on the interaction scale at various Reynolds numbers is presented in Fig. 36, and it is apparent here that (1) the differences between theory and experiment and (2) the general variation with Mach number are both essentially independent of the value of Reynolds number.

A final comparison of theory with experiment is given in Fig. 37 where data obtained with the model pitched are also included. The data obtained with the model pitched are, as expected from the discussions in Section 4.1.2, in further disagreement with theory than the results obtained at α = 0.

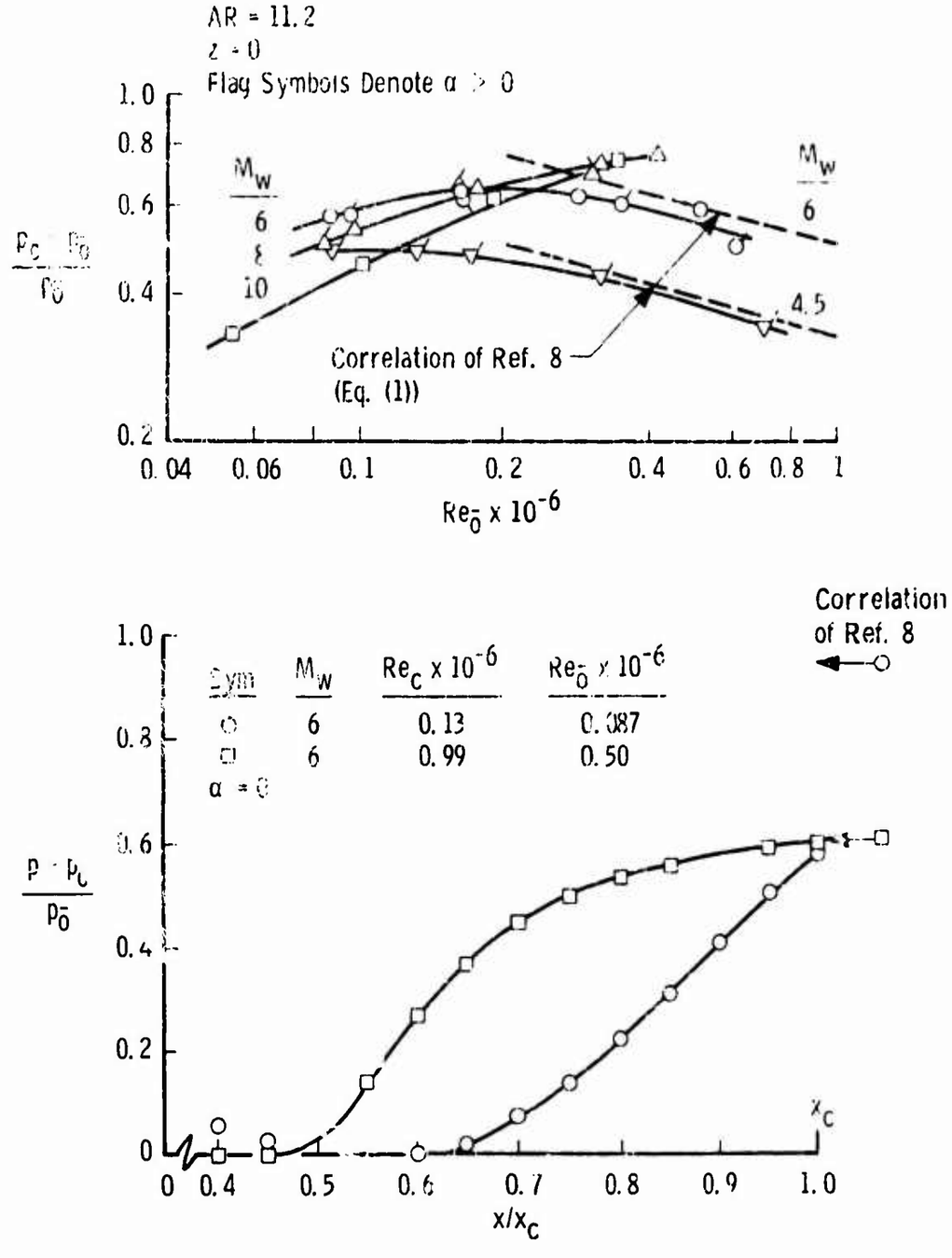

Fig. 30 Variation of the Laminar Peak Pressure Ratio on the Flat Plate with Reynolds Number and Mach Number

Sym	M_∞	M_w	$Re_c \times 10^6$	T_{wall}/T_w
	6	4.5	0.19	4.5
	6	6	0.19	7.5
	6	6	0.50	7.7
	8	6	0.19	7.2
	8	8	0.19	12.3
	10	8	0.19	11.1
	10	10	0.19	17.1

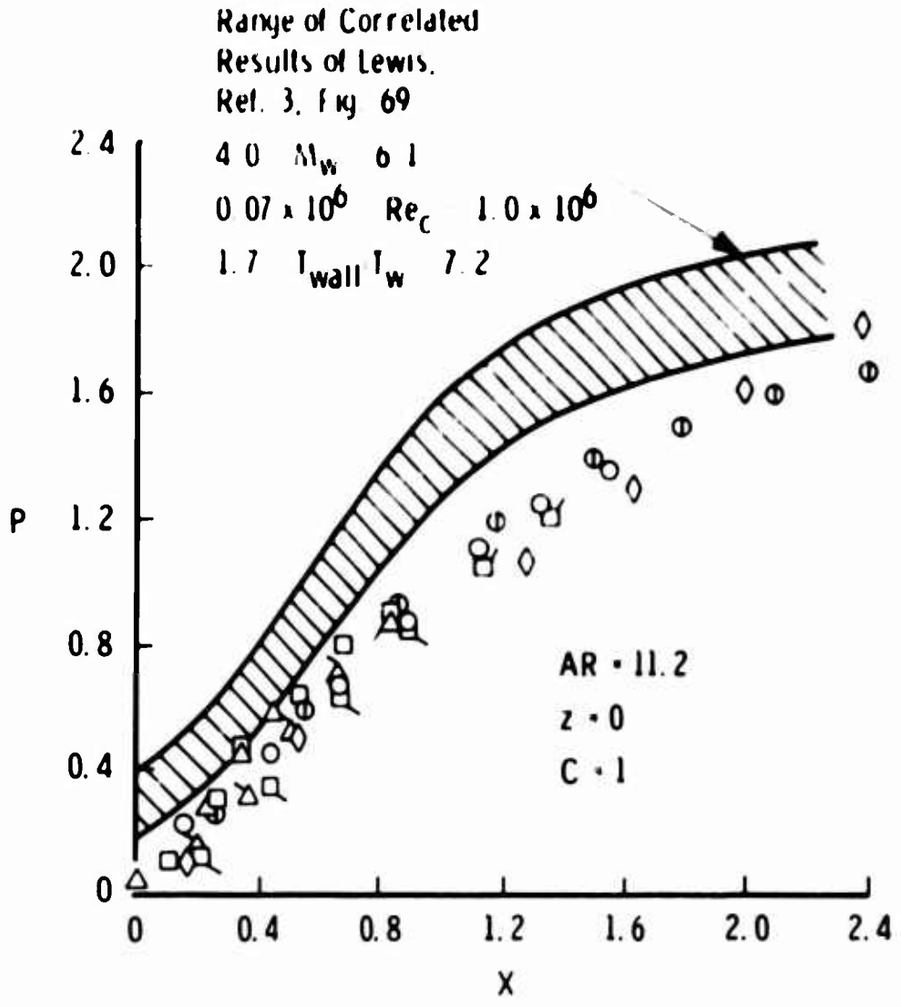

Fig. 31 Comparison of Present Data with Published Data in Chapman-Curle Coordinates

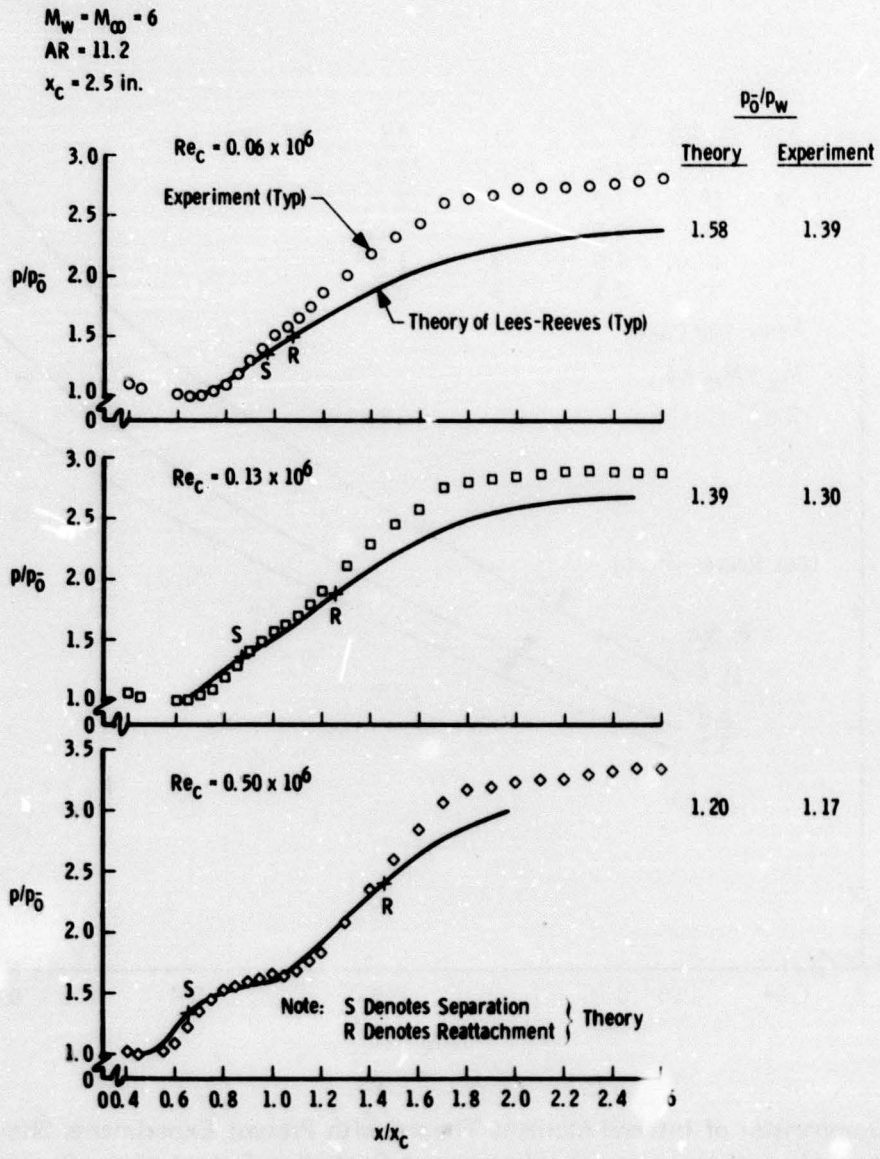

Fig. 32 Comparison of Integral-Moment Theory with Present Experiments Showing the Effect of Reynolds Number on Centerline Pressure Distributions

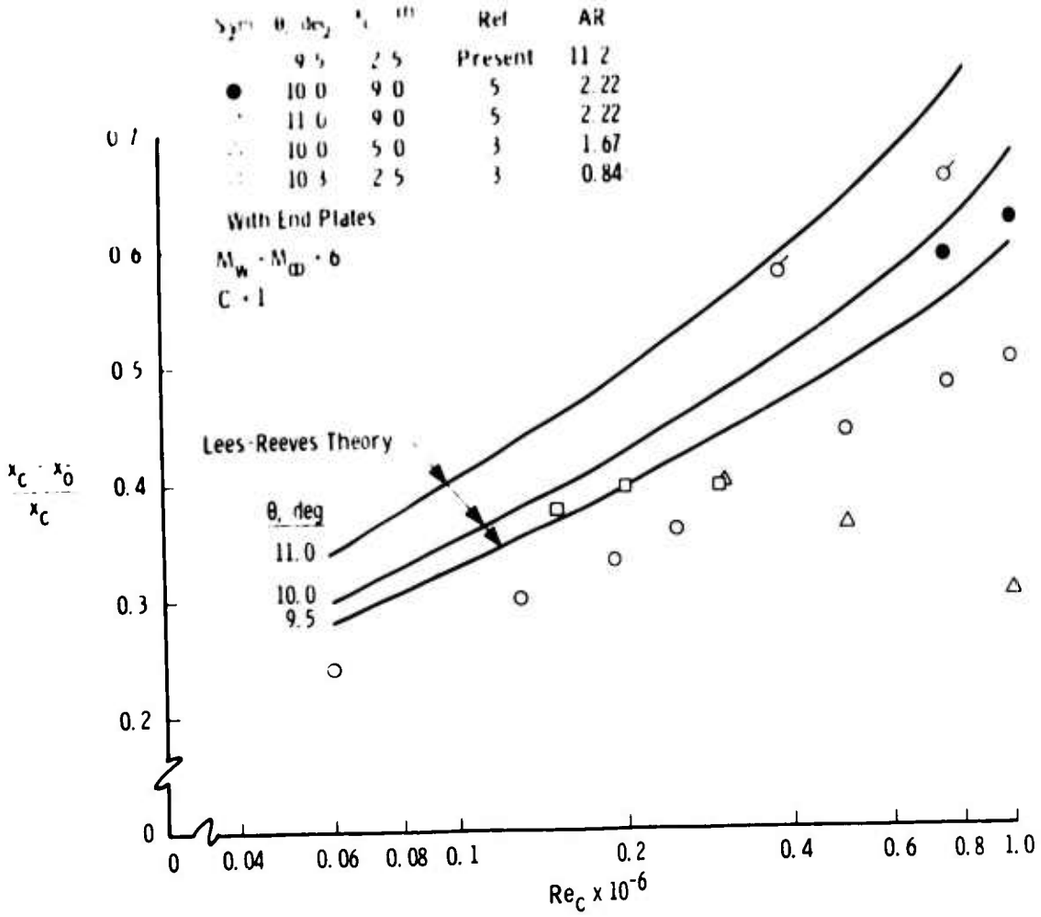

Fig. 33 Comparison of Integral-Moment Theory with Present Experiments Showing the Effect of Reynolds Number on the Centerline Extent of the Separation Region

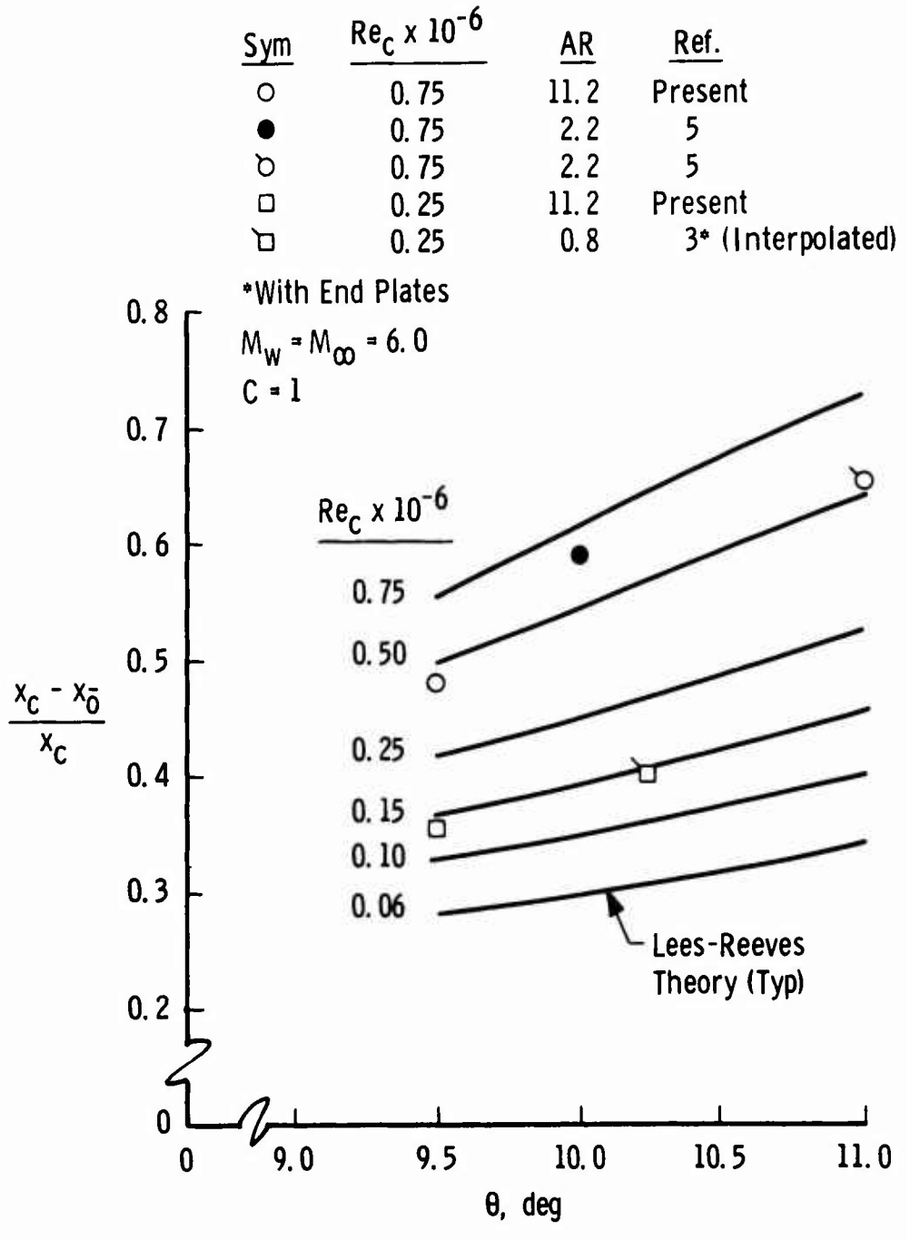

Fig. 34 Comparison of Integral-Moment Theory to Present Experiments Showing the Effect of Ramp Angle on the Centerline Extent of the Separation Region

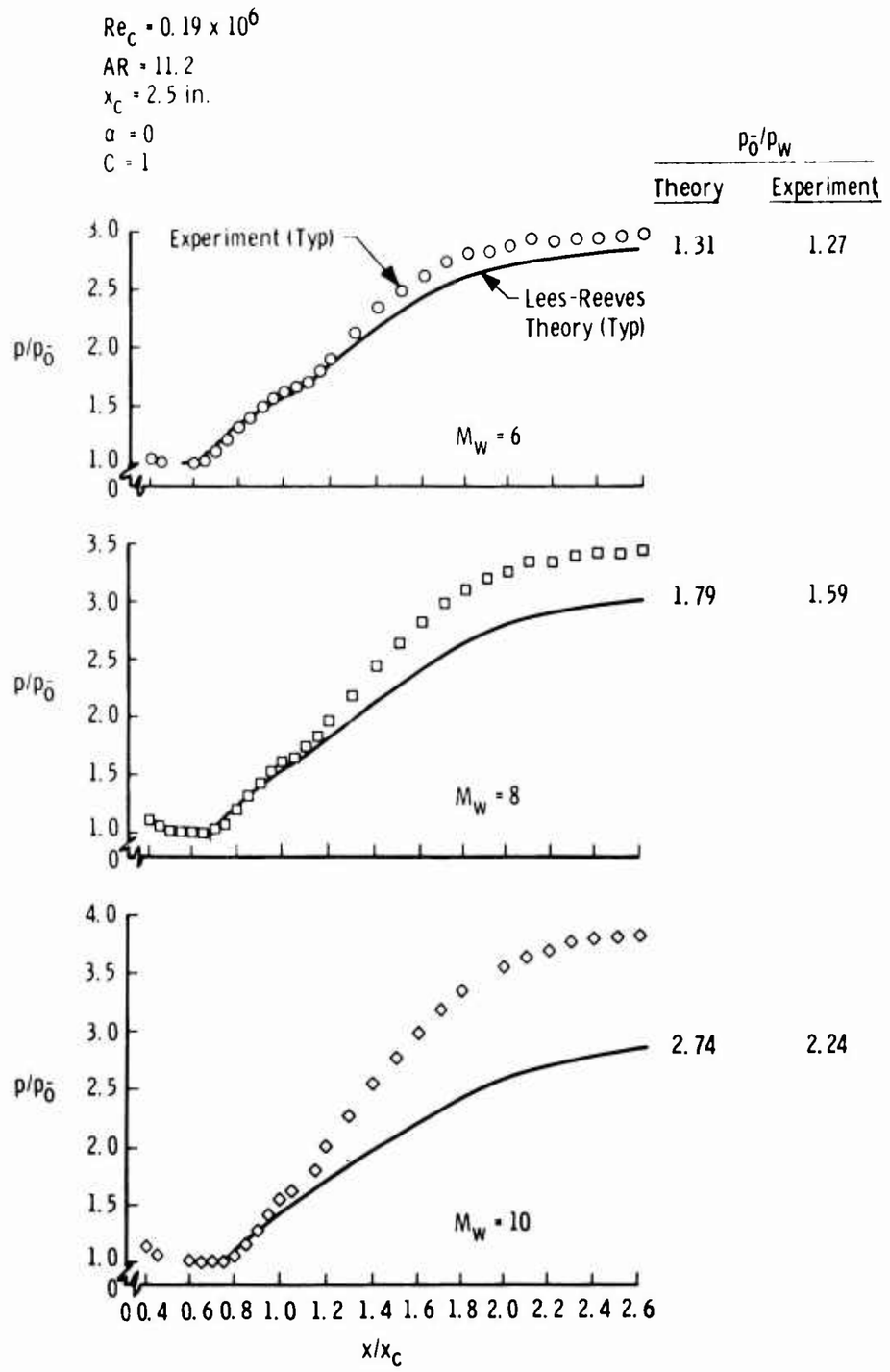

Fig. 35 Comparison of Integral-Moment Theory to Present Experiments Showing the Effect of Mach Number on the Centerline Pressure Distribution

Sym	$Re_c \times 10^{-6}$	AR	x_c, in.
△	0.13	11.2	2.5
○	0.25	11.2	2.5
◇	0.50	11.2	2.5

Solid Symbols, $M_\infty = 6$
All Others, $M_w = M_\infty$
$C = 1$

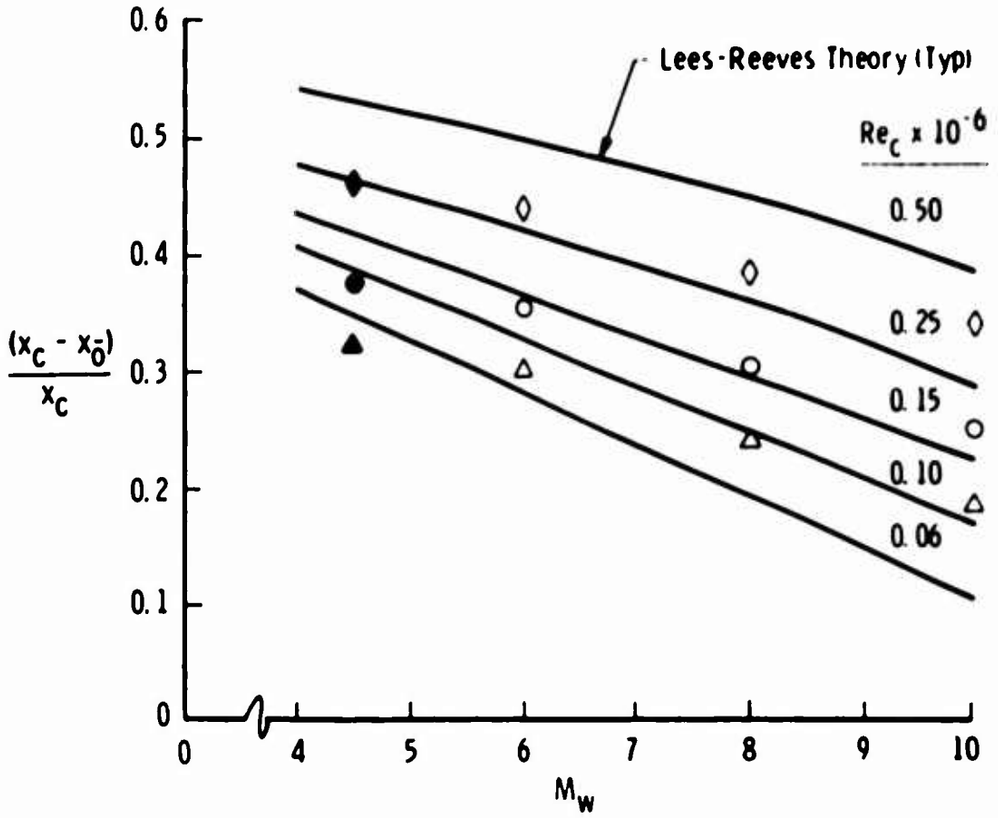

Fig. 36 Comparison of Integral-Moment Theory to Present Experiments Showing the Effect of Mach Number on the Centerline Extent of the Separation Region

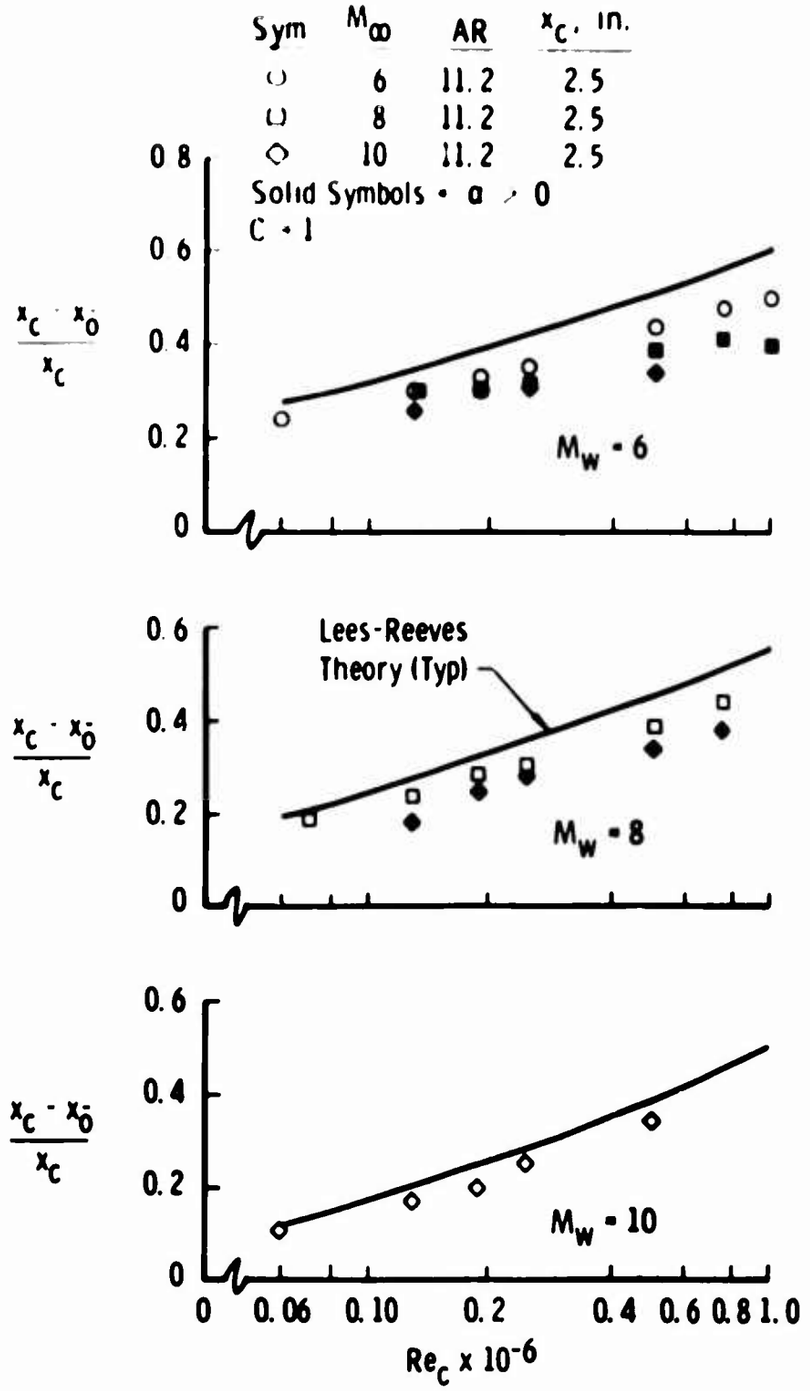

Fig. 37 Comparison of Integral-Moment Theory to Present Experiments Showing the Combined Effects of Reynolds Number and Pitch on the Centerline Extent of the Separation Region

4.2 TURBULENT FLOW MODEL

4.2.1 Boundary-Layer Pitot Pressure Surveys

In order to establish the conditions at which the boundary layer would be turbulent sufficiently far upstream of the hinge line, pitot surveys were made on the model at $M_\infty = 8$ with the ramp removed. The boundary-layer profiles shown in Fig. 38a, which were obtained with the model pitched to provide $M_w = 6$, indicate that the boundary layer was turbulent over the downstream half of the plate. However, with the model unpitched, $M_w = M_\infty = 8$, the profiles in Fig. 38b indicate that the boundary layer was more nearly transitional, particularly at $x/x_c = 0.571$ which was near the expected start of the interaction. Because of this indication of a marginal turbulent flow at $M_\infty = 8$, all subsequent tests were conducted at $M_\infty = 6$. The Mach number profiles shown in the above and succeeding figures were calculated by assuming the static pressure was constant through the boundary layer and equal to the value at $y = \delta$, consistent with the Mach number derived from normal shock tables and isentropic external flow. The value of δ used to calculate y/δ is indicated on the pitot pressure profiles.

A check was made at $M_w = M_\infty = 6$ to determine the effectiveness of the boundary-layer trips. While these boundary-layer surveys were made with the 30-deg ramp installed, they were taken upstream of the ramp-induced interaction. Surveys taken at the same Reynolds number and station, Fig. 39, show that the trips were quite effective in obtaining a turbulent boundary layer. Pitot surveys, which were taken with the 1.0 aspect ratio model pitched to obtain $M_w = 4.5$ (Fig. 40), show that with the boundary-layer trips installed a turbulent boundary layer was obtained at the two test Reynolds numbers ($Re_c = 6.04$ million and 9.06 million). While these data were obtained with the 35-deg ramp installed, the surveys were made upstream of the interaction region. Several surveys which were made at $M_w = M_\infty = 6$ (unpitched) are shown in Fig. 41. These data show very little difference in the Mach number profiles for the different aspect ratios at $Re_c = 6$ million, even though one of the surveys was taken relatively far upstream ($x/x_c = 0.428$). The data, for even the lower Reynolds numbers indicate that the boundary layer was still turbulent.

Sym	$Re_C \times 10^6$	x/x_C	$Re \times 10^6$	AR	θ, deg
○	6.30	0.571	3.60	2	0
□	6.26	0.714	4.48	2	0
△	6.23	0.950	5.92	2	0

Solid Symbols = Estimate of δ

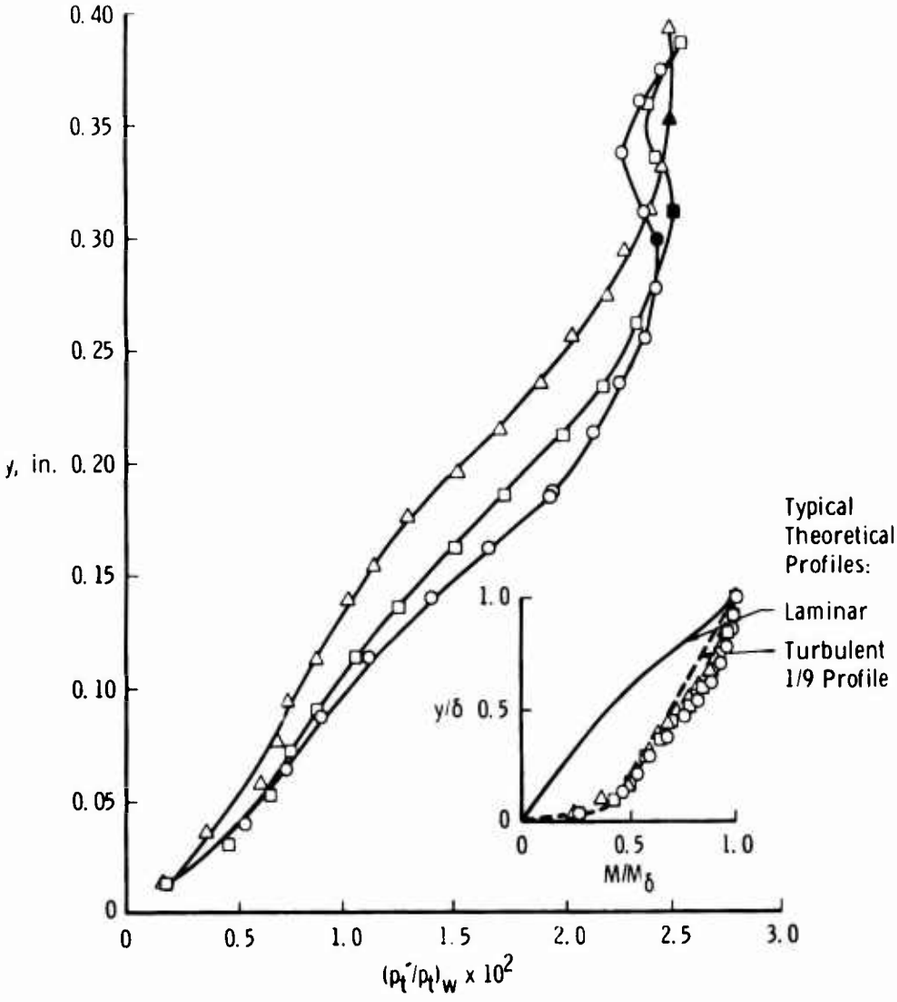

a. $M_w = 6$

Fig. 38 Boundary-Layer Profiles on Flat Plate at $M_\infty = 8$

Sym	$Re_c \times 10^6$	x/x_c	$Re \times 10^{-6}$	AR	θ, deg
○	4.11	0.571	2.35	2	0
□	4.15	0.714	2.96	2	0
△	4.15	0.950	3.94	2	0

Solid Symbols = Estimate of δ

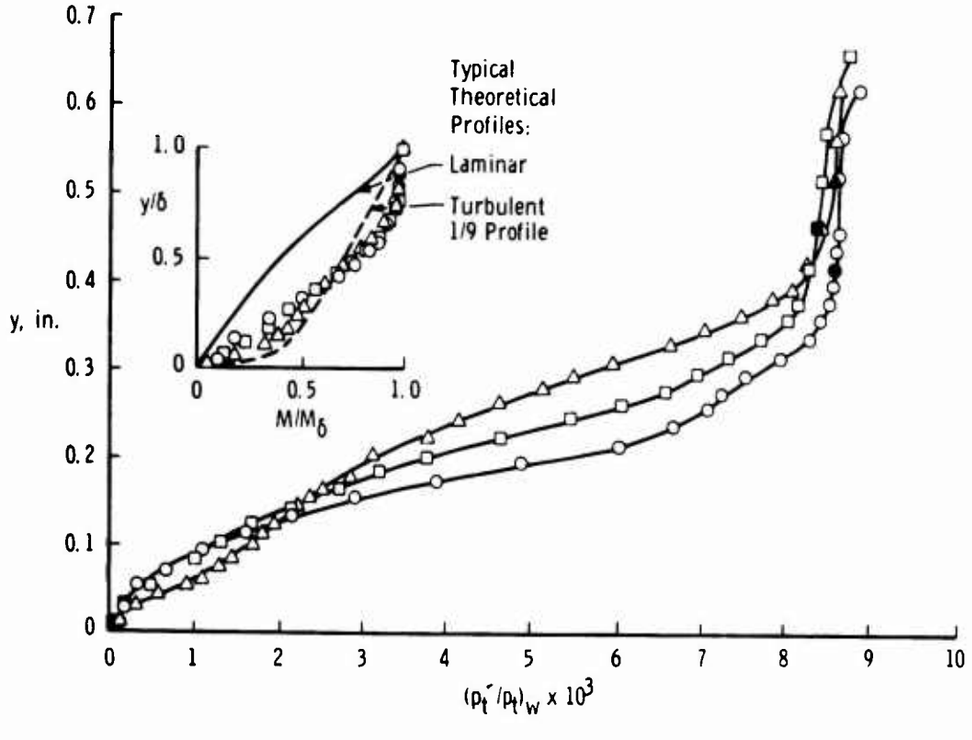

b. $M_w = 8$

Fig. 38 Concluded

Sym	$Re_c \times 10^{-6}$	x/x_c	$Re \times 10^{-6}$	AR	θ, deg	Trips
○	6.03	0.714	4.31	2	30	On
□	6.00	0.714	4.28	2	30	Off

Solid Symbols = Value at δ

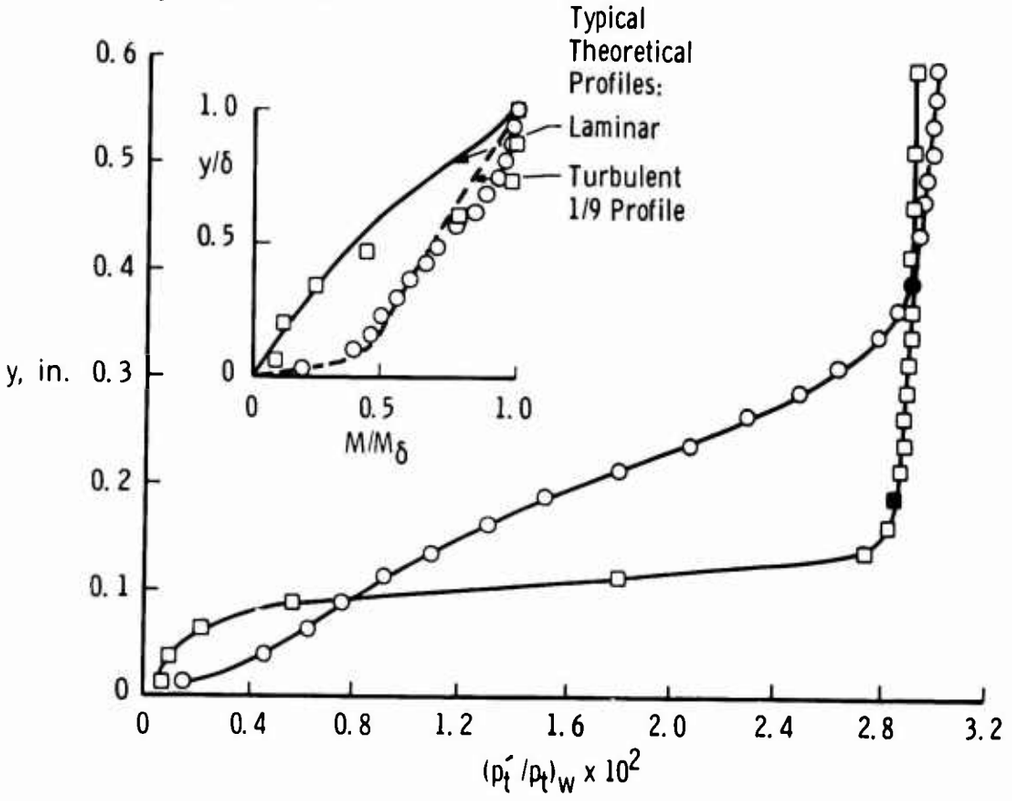

Fig. 39 Effect of Trips on Boundary-Layer Profiles

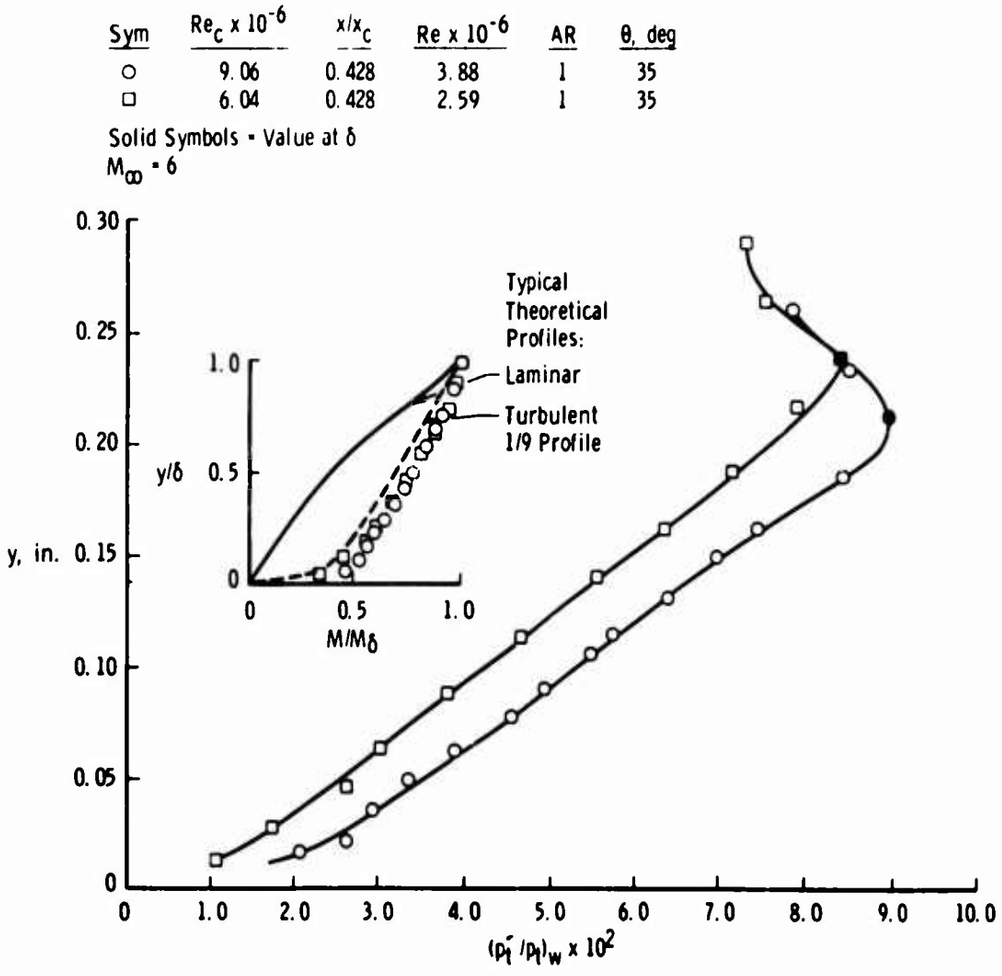

Fig. 40 Effect of Reynolds Number on Boundary-Layer Profiles at M_w = 4.5

Sym	$Re_c \times 10^{6}$	x/x_c	$Re \times 10^{-6}$	AR	θ, deg
○	6.03	0.714	4.31	2	30
□	6.04	0.714	4.32	1	35
◇	6.06	0.428	2.60	1	35
△	4.08	0 714	2.92	1	35

$M_\infty = 6$

Solid Symbols = Estimate of δ

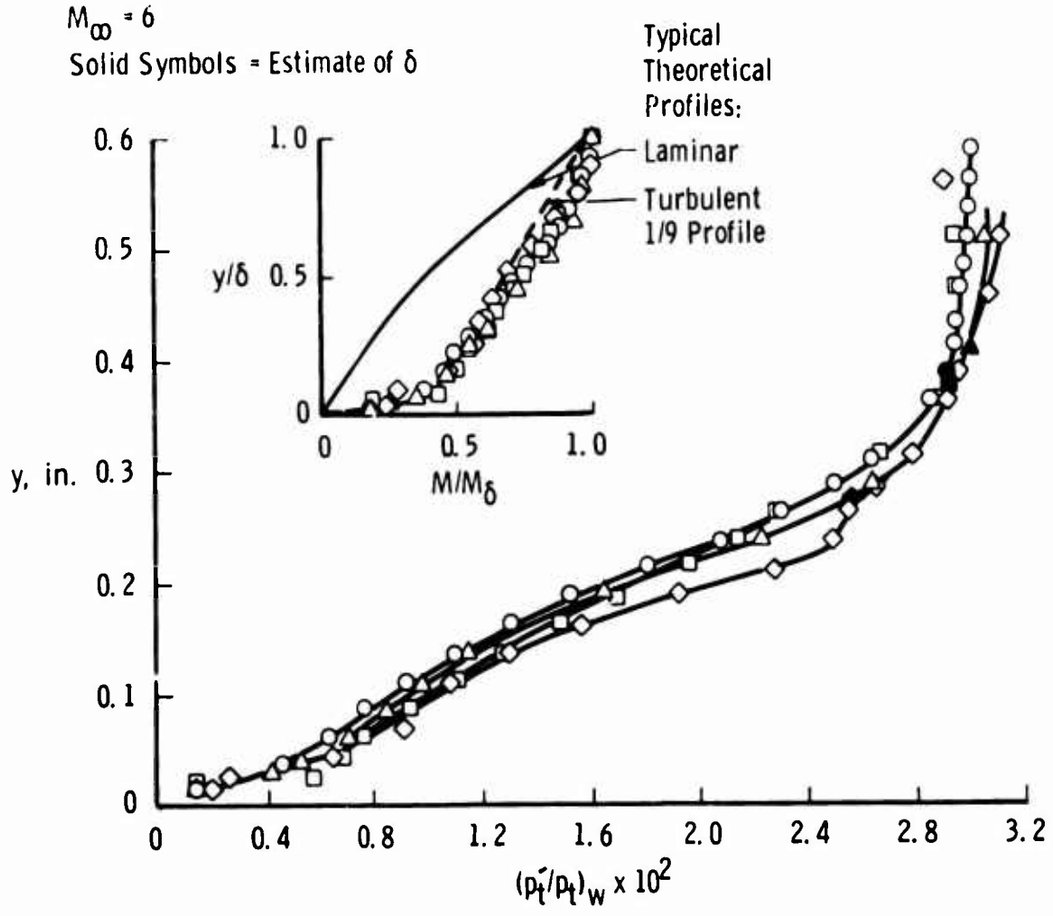

Fig. 41 Effect of Reynolds Number on Boundary-Layer Profiles at M_w = 6.0

4.2.2 Influence of Model Geometry and Local Conditions

Because the maximum width model that can be injected into the tunnel is approximately 28 in., and because it was considered that the flat-plate length (to obtain turbulent flow sufficiently far upstream of the interaction) was required to be at least 14 in., the maximum aspect ratio was essentially limited to a value of 2. As a result, the test matrix was limited by the model geometry and the maximum available free-stream Reynolds number. On the basis of the laminar investigation, it was known that this aspect ratio would be, at best, marginal for obtaining two-dimensional flow, especially when considering the larger pressure differential between the interaction region and free stream.

Longitudinal pressure distributions at several spanwise stations are presented in Fig. 42 for the two aspect ratios. Data for AR = 2, which are presented in Fig. 42a, indicate that a small span of two-dimensional flow was present on each side of the centerline because the longitudinal pressure distribution at $z/b = 0.161$ agrees with that on the centerline. However, when the aspect ratio was reduced to 1 (Fig. 42b), the first longitudinal row off centerline again was in very close agreement with the centerline, but the extent of the interaction upstream of the 35-deg ramp was greatly reduced. These data indicate that there must have been spanwise outflow in both cases, although there was an area near the model centerline where the spanwise pressure was uniform. An oil-flow photograph obtained by applying small dots of a mixture of silicon oil and titanium dioxide before injection of the AR = 1 model, Fig. 42b, also shows the nonuniform spanwise separation obtained with a 35-deg ramp. Further evidence that the flow was not two dimensional, even when the aspect ratio was 2, was obtained when upper surface side plates were installed. Figure 43 shows that the centerline pressure distributions were markedly changed, with side plates installed for both aspect ratios, thus indicating that the extent of the interaction was reduced because of edge effects. Longitudinal pressure distributions at three spanwise stations are shown in Fig. 44 with the model pitched to achieve a lower local Mach number, $M_w = 4.5$. It is noted that the first off-centerline distribution shows less agreement with the centerline, both on the flat plate and on the ramp, than did the data at $M_w = 6$ in Fig. 42b. This result suggests that the spanwise outflow effects increased with Mach number decrease; however, it must be remembered that the overall pressure level was much higher relative to the free stream when the model was pitched. The effect of a change in ramp angle on the turbulent separation is shown in Fig. 45. These data show that an increase in ramp angle of only 5 deg, from 30 to 35 deg, caused a very large increase in the extent of the interaction. The data also indicate that the 30-deg ramp caused very little, if any, boundary-layer separation at these conditions.

A supplemental measurement was made to determine the cause of the slight increase in pressure ratio just ahead of the hinge line at θ = 35 deg (note data at x/x_c = 0.99 in Figs. 42a, 43, and 44). A full span vertical "fence" made of 0.005-in. shim stock was installed at the hinge line. The data at Re_c = 6.0 million, θ = 35 deg, and AR = 1.0 were repeated with a fence height of 0.1 in. and 0.25 in. The only effect of the fence was found to be a slight increase in the pressure ratio just downstream of the hinge line (x/x_c = 1.04) and a slight decrease in the pressure ratio at x/x_c = 0.99. Thus, it is reasoned that the original perturbation in pressure may be associated with some secondary separation within the primary recirculation region near the hinge line.

The effect of a change in Reynolds number on the centerline pressure distribution for a 35-deg ramp is shown in Fig. 46. These data show that the upstream extent increased when the Reynolds number was increased. However this trend is opposite to that found by Thomke and Roshko (Ref. 12) for smaller ramp angles at $M_w \approx 4$. On the other hand, data of Sterrett and Emery (Ref. 13), which were obtained by varying the plate length at M_w = 5.8, show a negligible change in the relative extent of the upstream interaction when the Reynolds number, Re_c, was changed from 7.4 to 12.7 million. More measurements are required to resolve this question because so very few data are available in the literature.

It is indicated in Figs. 42 through 46 that the peak pressure ratio on the ramp never reached that predicted by an isentropic compression, but the "asymptotic" pressure ratio (as defined in Fig. 19) was very close to that predicted by the oblique shock relations.

A summary plot of the spanwise variation of the extent of the upstream interaction for the 35-deg ramp (both aspect ratios) and for the 30-deg ramp (aspect ratio of 2) is shown in Fig. 47. In the same way as for the laminar data, the relative extent of the interaction is presented both as a function of (1) the relative spanwise location and (2) the absolute distance from the outboard edge of the model. These data show that, unlike the laminar models, the absolute spanwise distance to achieve a uniform interaction was not a constant for different span models. However, even though the spanwise extent of the interaction was constant for a small distance off centerline, with the aspect ratio 2 model, the data presented previously with side plates installed indicated that there may still be some outflow effects. It is therefore tentatively concluded that an aspect ratio greater than 2 is required to obtain turbulent boundary-layer separations which are unaffected (near the centerline of symmetry) by spanwise outflow effects.

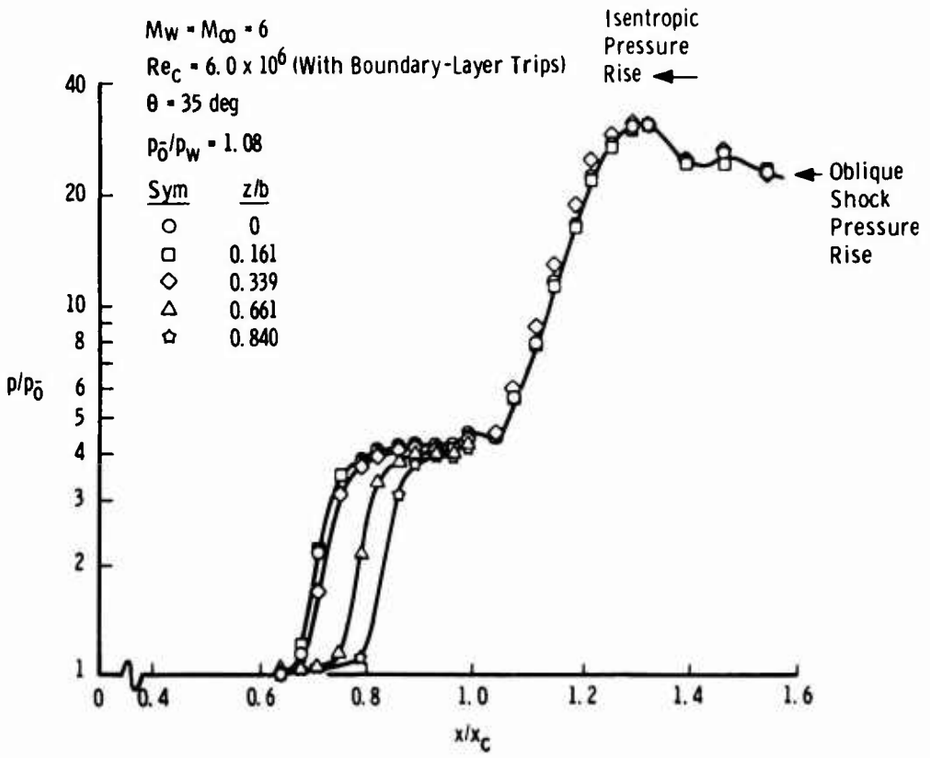

a. AR = 2

Fig. 42 Effect of Spanwise Location on Longitudinal Pressure Distribution

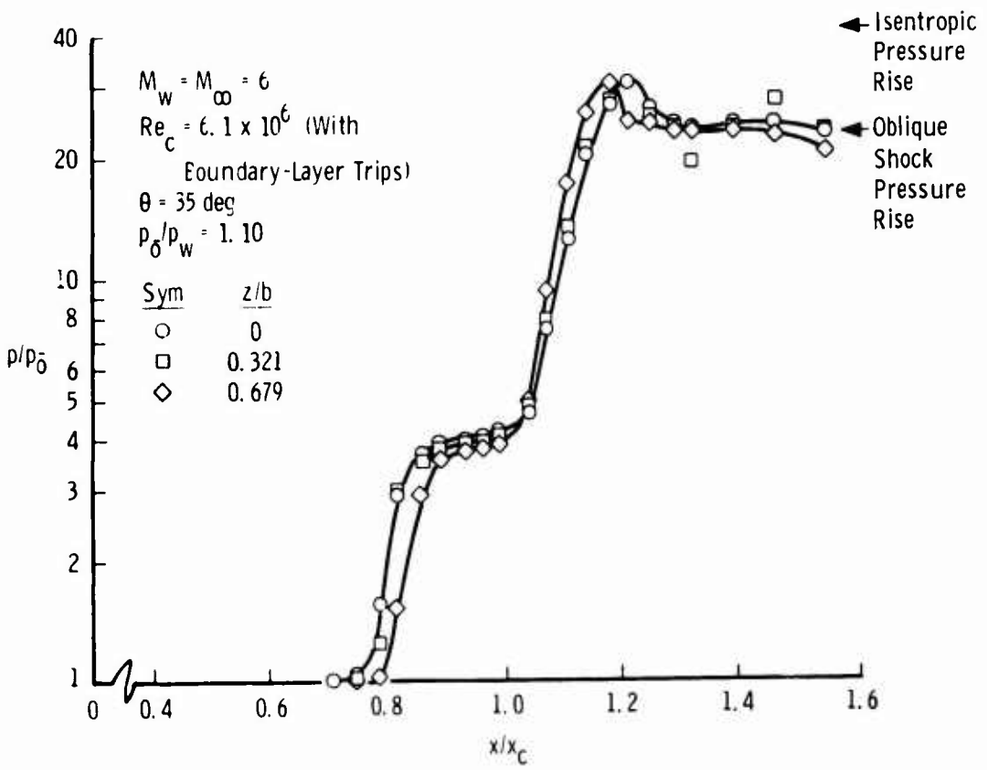

b. AR = 1

Fig. 42 Concluded

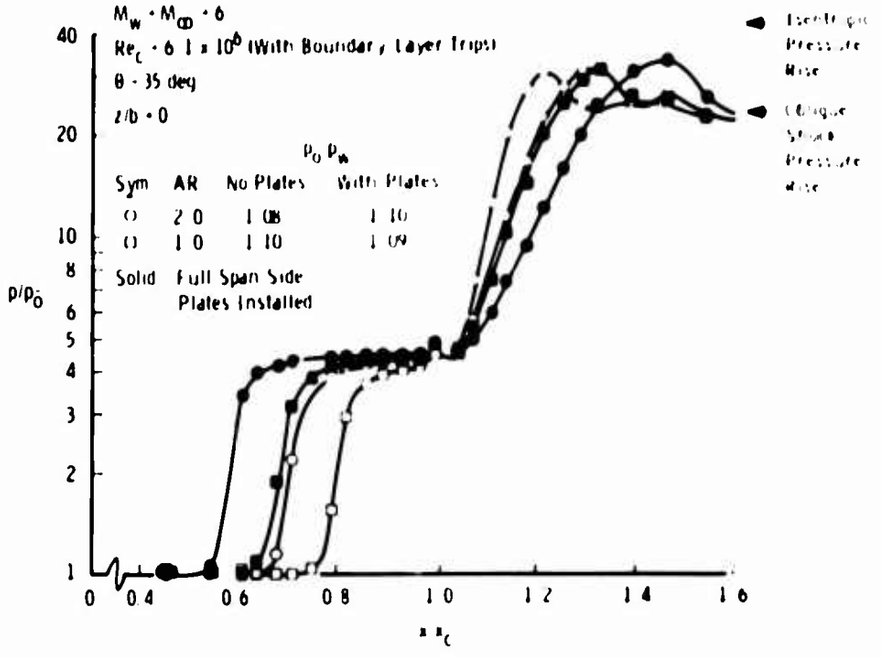

Fig. 43 Effect of Side Plates on Longitudinal Pressure Distributions

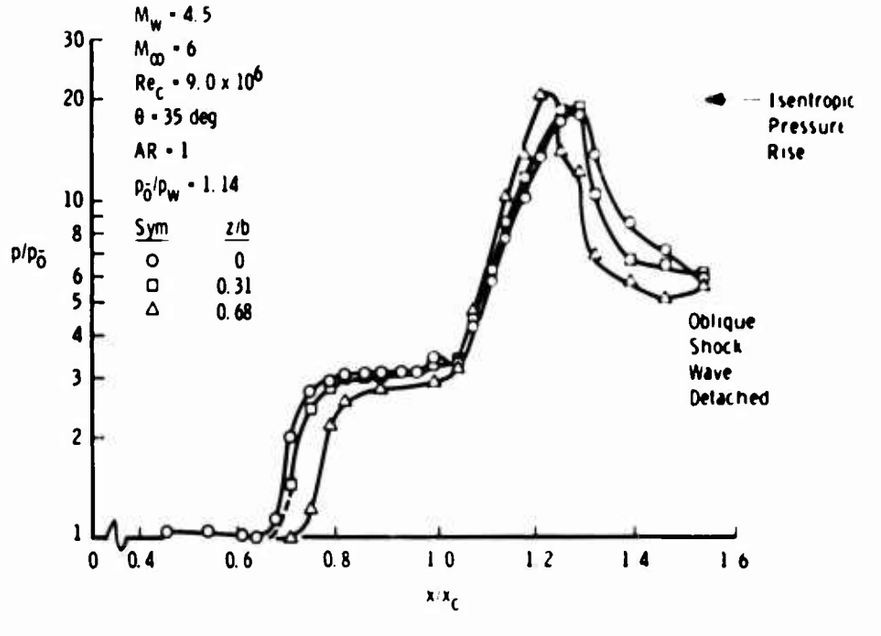

Fig. 44 Effect of Pitch on Longitudinal Pressure Distributions

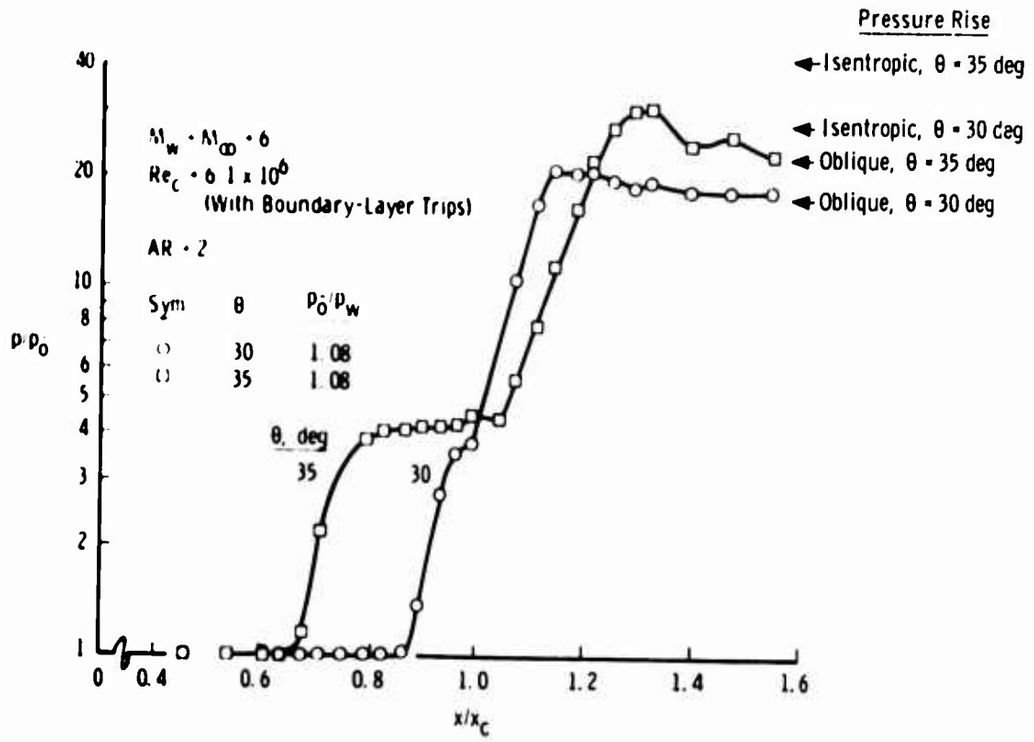

a. Centerline Pressure Distribution

Fig. 45 Effect of Ramp Angle on Longitudinal Pressure Distributions

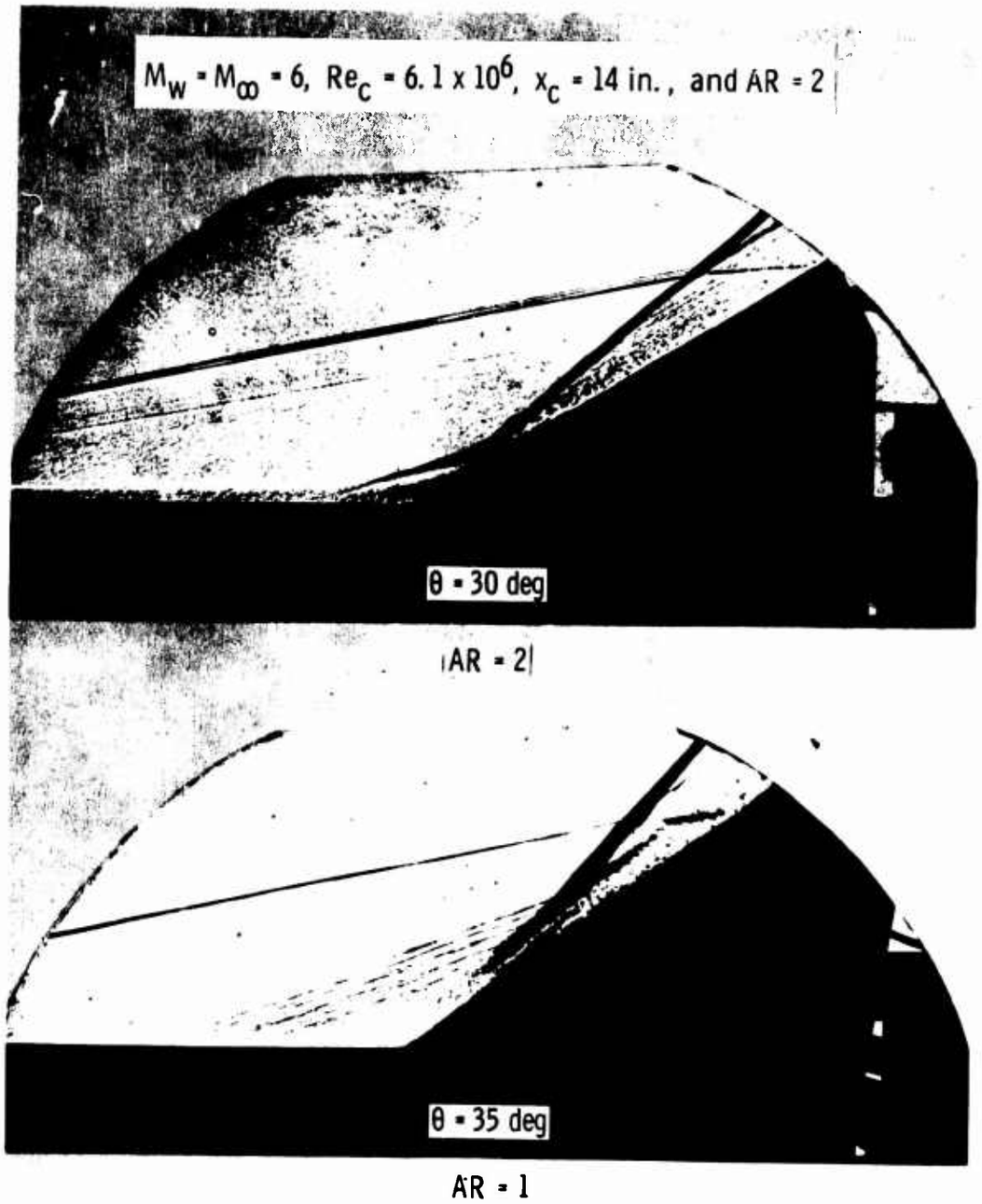

b. Shadowgraph Pictures
Fig. 45 Concluded

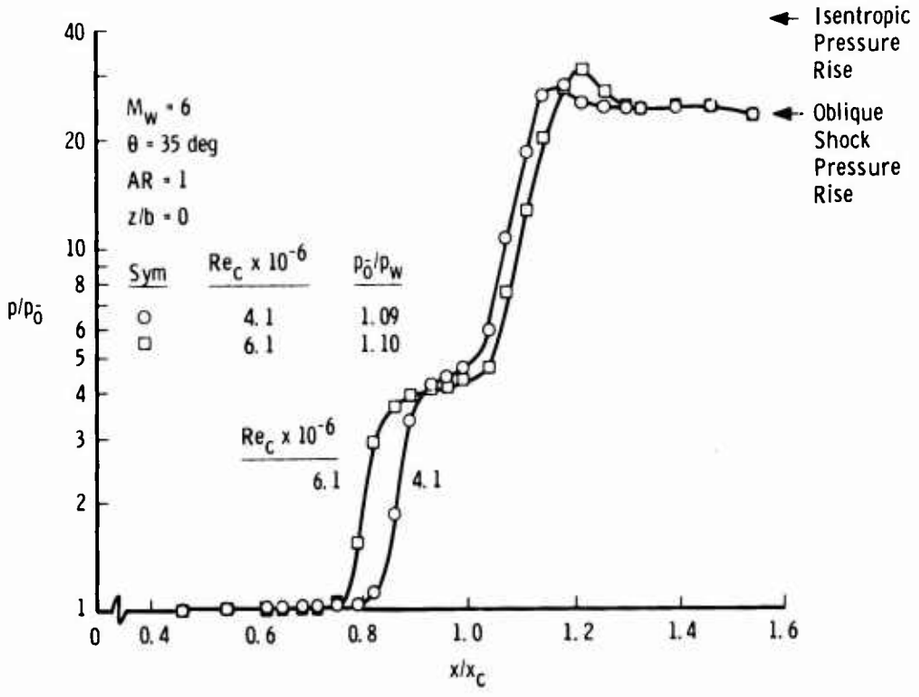

Fig. 46 Effect of Reynolds Number on Centerline Pressure Distribution

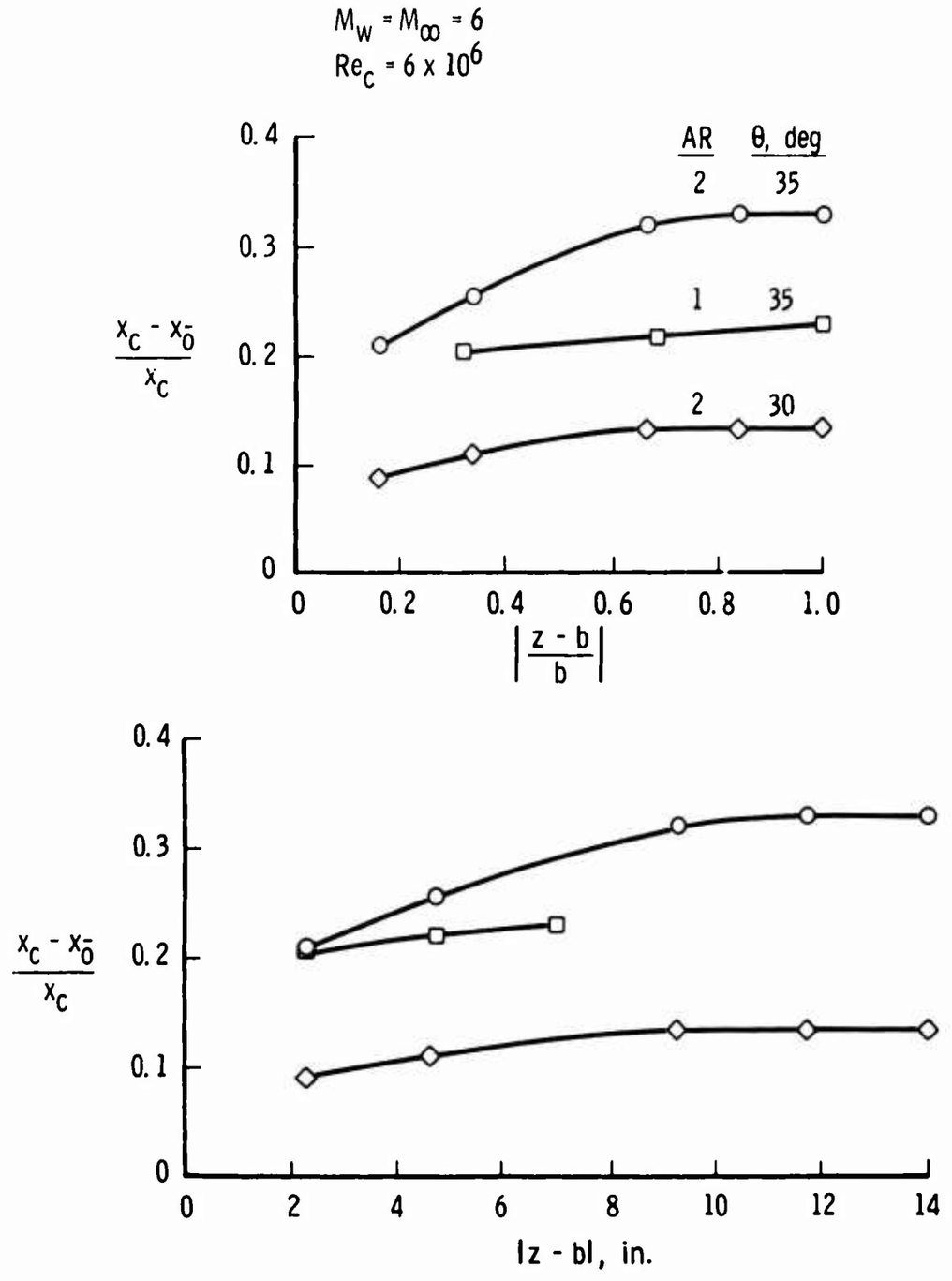

Fig. 47 Effect of Aspect Ratio on Centerline Extent of the Turbulent Separation Region

4.2.3 Comparisons with Other Experiments

The peak pressure rise ratio, $(p_c - p_{\bar{0}})/p_{\bar{0}}$, in turbulent flow, like that for laminar flow separations, is a parameter of general interest in the literature on supersonic flow separations induced by either steps or ramps. The present data are presented in Fig. 48 in two forms plotted versus the Reynolds number at the start of the interaction on the flat plate, $Re_{\bar{0}}$. Included in this figure are data (obtained with forward-facing steps) which are provided to verify the $M_w = 4.5$ data obtained in this investigation. It is noted that, generally, the pressure rise ratio increased with Mach number increase. However, the comparison of the correlation of the plateau pressure coefficient from Ref. 8 with these data shows rather appreciable differences with the Mach number 3 data of Refs. 14 and 15. It is noted, however, that these data, particularly at $M_w = 6$, show a variation with Reynolds number in substantial agreement with the correlation (Ref. 8).

The data from Fig. 48 are compared in Fig. 49 with the two most widely referenced correlations of the plateau pressure coefficient as a function of Mach number. These correlations acknowledge no definable effect of Reynolds number, but the data presented are shown to fall within the range between these correlations at the Mach number where the differences are the largest. The agreement of the present test data with the correlation of Ref. 13 is excellent.

In an attempt to provide a better correlation of turbulent separation data in the ranges just considered, the peak pressure ratio was plotted in the form shown in Fig. 50. The basic difference in this form and that of Ref. 8 is noted to be in the Mach number function which is considered a relationship more appropriate to the pressure rise dependence.

Finally, a comparison of the present results with the published data for the upstream extent of the turbulent separation induced by ramps is shown in Fig. 51. The upstream extent $(x_c - x_{\bar{0}})$ for the present results has been nondimensionalized by the value of boundary-layer thickness at $x_{\bar{0}}$, which was derived from the survey data presented in Fig. 41.

The data of Ref. 16 were originally presented in this same nondimensional form, whereas the data of Refs. 12 and 13 have been normalized using the boundary-layer survey data contained in each report. The data of Refs. 12 and 16, which are remarkably consistent considering the vast difference in Reynolds number, show that the upstream extent increases with ramp angle increase but decreases with Mach number increase (up to about $M_w = 4$). The results of Ref. 13 are especially interesting because they show that the upstream extent decreased when

aspect ratio was increased (decrease in flat-plate length), whereas the present data (which were obtained by increasing the flat-plate span) show an opposite trend. It will be noted, however, that the present data for a Reynolds number decrease (AR = 1.0) show the same trend as the data of Ref. 13 which also correspond to a Reynolds number decrease. These data, in particular, therefore indicate that the upstream extent $(x_c - x_{\bar{0}})$ is not directly scaled by $\delta_{\bar{0}}$ alone. In addition, the present data for AR = 2.0 indicate that the upstream extent may be much larger than anticipated from the trends and magnitude previously obtained.

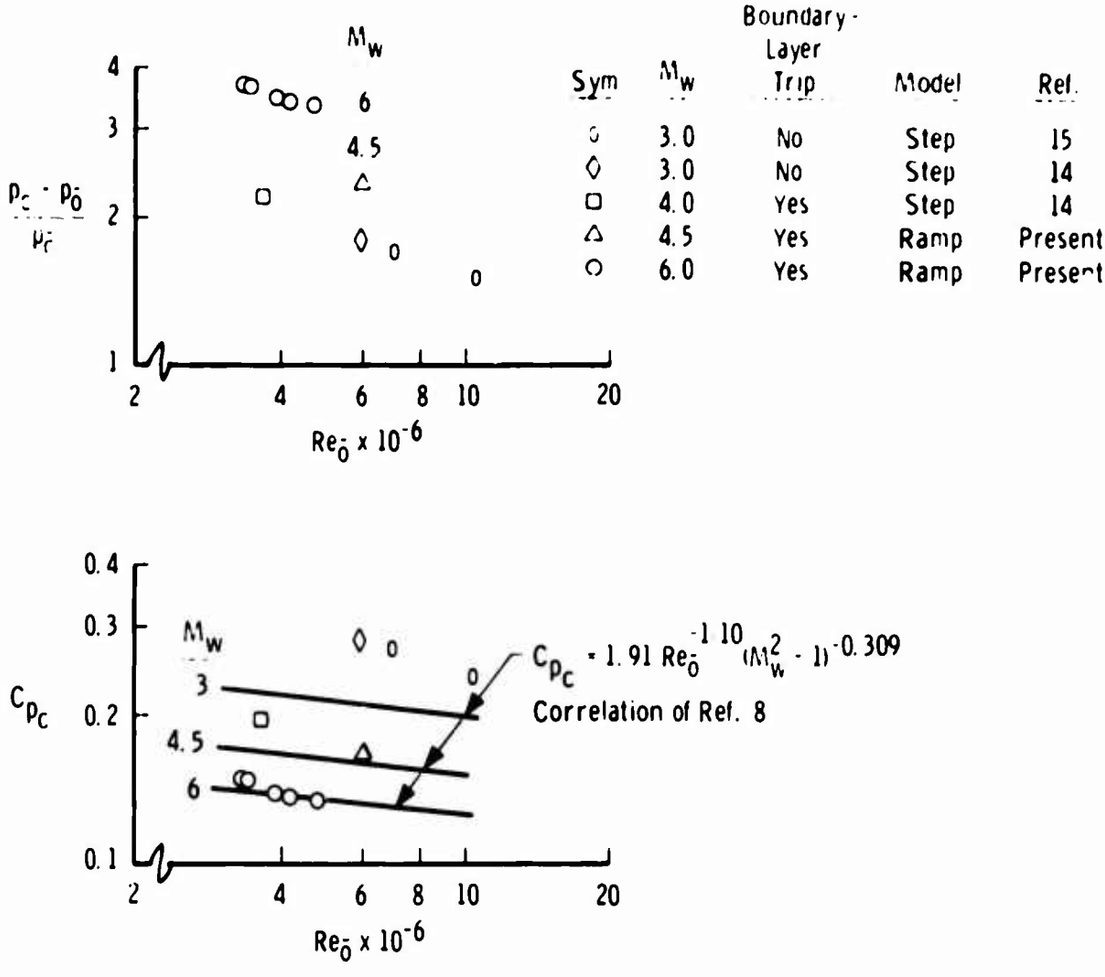

Fig. 48 Comparisons of Present Turbulent Peak Pressure Ratio on the Flat Plate with Published Data

Sym	M_w	Boundary Layer Trip	Model	Ref.
○	3	No	Step	15
◇	3	No	Step	14
□	4	Yes	Step	14
△	4.5	Yes	Ramp	Present
○	6	Yes	Ramp	Present

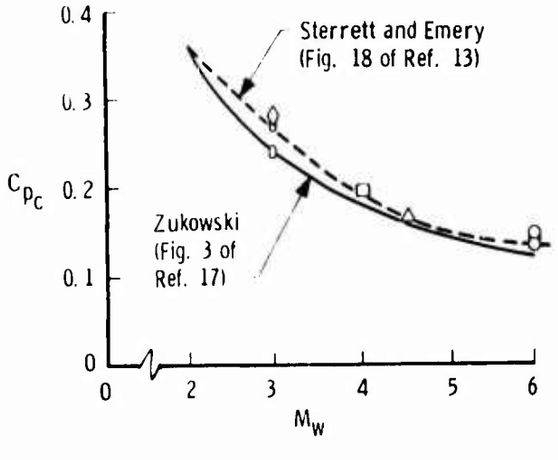

Fig. 49 Comparison of Present Turbulent Peak Flat Plate Pressure Coefficient with Published Data Showing the Effect of Mach Number

Sym	M_w	Ref.
△	3.0	14 and 15
◇	4.0	14
○	4.5	Present
BOI	6.0	Present

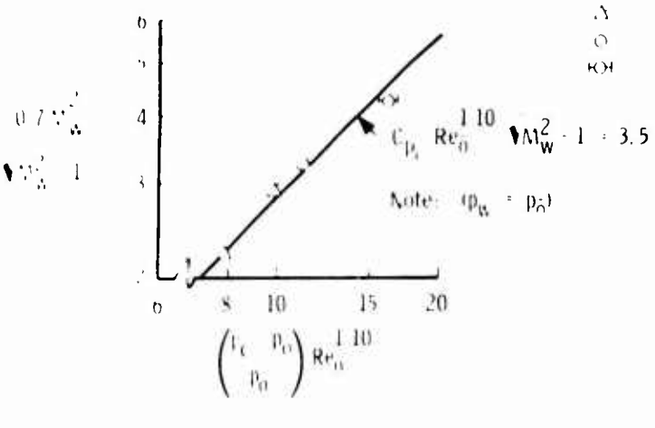

Fig. 50 Suggested Correlation of the Turbulent Peak Flat Plate Pressure Data

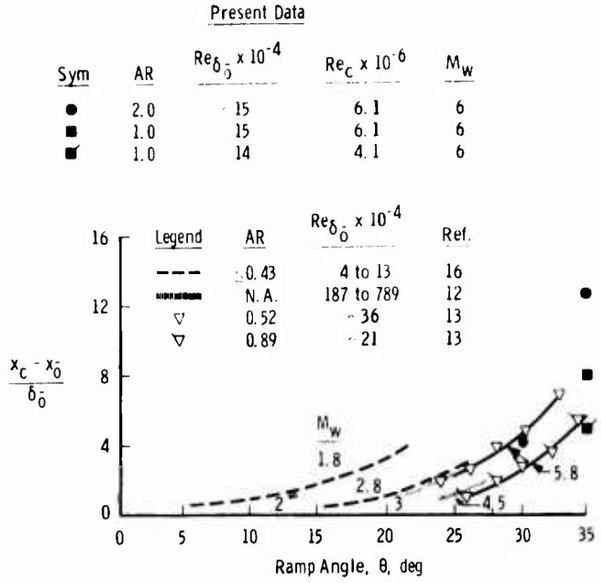

Fig. 51 Comparison of Present Data for the Centerline Extent of the Separation Region with Published Data Showing the Effect of Ramp Angle in Turbulent Flow

SECTION V
SUMMARY

The conclusions and results of particular significance derived from this experimental investigation, which was concerned mainly with defining the influence of flat-plate aspect ratio on ramp-induced separations in supersonic adiabatic flows, may be summarized as follows:

1. The region of nonzero spanwise pressure gradients inboard of the tips of a 2.5-in. flat plate (chord) was found to be (a) essentially independent of span variations and (b) equal to about 4 in. for laminar reattaching flows at $4.4 \leq M_w \leq 10$. It is concluded, therefore, that a flat-plate aspect ratio of the order of 3 is required to be assured of negligible effects induced by the finite span.

2. For turbulent boundary layers before the separation on a 14-in. (chord) flat plate, the region of nonzero spanwise pressure gradients is shown to have extended almost three times the distance (1b above) inboard of the tips at $M_w = 6$. It is indicated by the results that even the widest turbulent model (28 in.) was probably not free of finite span effects.

3. Pitching the laminar flow model (2.5-in. chord) to vary the inviscid Mach number approaching the ramp was ascertained to have no defineable influence on the spanwise pressure gradient, although it did produce small, yet measurable, decreases in the relative extent of the separation region.

4. Whenever vertical side plates were added (to restrict the outflow), it was noted that the relative extent of separation region increased all the way to the centerline of symmetry whenever the spanwise pressure gradient on the centerline was nonzero before the addition of the side plates.

5. Comparisons of calculations made using the Lees-Reeves integral-moment theory with longitudinal surface pressure measurements on the laminar flow model indicated the following points of difference and agreement:

   a. The extent of the separation region increased with Reynolds number at essentially the same rate as predicted, in the Reynolds number range from about 0.06 million to 1.0 million (based on flat-plate length).

   b. The extent of the separation region decreased with Mach number increase in the local Mach number range from about $4.4 < M_w$ to 10, in general agreement with predictions.

   c. The extent of the separation region was always less (no more than about 20 percent) than that predicted by theory.

   d. Although the separation pressure gradient was generally in agreement with theory, the reattachment (ramp) pressure gradient was appreciably greater than was predicted. This discrepancy was noted to increase as the extent of the separation region decreased.

REFERENCES

1. Gadd, G. E., Holder, D. W., and Regan, J. D. "An Experimental Investigation of the Interaction between Shock Waves and Boundary Layers." Proc. of the Royal Society of London, Series A, Vol. 226, 1954.

2. Chapman, D. R., Kuehn, D. M., and Larson, H. K. "Investigation of Separated Flows in Supersonic and Subsonic Streams with Emphasis on the Effects of Transition." NACA TN 3869, March 1957.

3. Lewis, J. E. "Experimental Investigation of Supersonic Laminar, Two-Dimensional Boundary-Layer Separation on a Compression Corner with and without Cooling." California Institute of Technology, Ph. D. Thesis, 1967.

4. Holden, M. S. "Leading-Edge Bluntness and Boundary Layer Displacement Effects on Attached and Separated Laminar Boundary Layers in a Compression Corner." AIAA 6th Aerospace Sciences Meeting, Paper No. 68-68, January 1968.

5. Rhudy, R. W. "Investigation of Laminar Boundary-Layer Separation on a Flat-Plate-Ramp Combination with and without Mass Removal at Mach Numbers 6, 8, and 10." AEDC-TR-69-199 (AD702078), March 1970.

6. Pate, S. R. and Schueler, C. J. "An Investigation of Radiated Aerodynamic Noise Effects on Boundary-Layer Transition in Supersonic and Hypersonic Wind Tunnels." AIAA 3rd Aerodynamic Testing Conference, Paper No. 68-375, April 1968.

7. Klineberg, J. M. "Theory of Laminar Viscous-Inviscid Interactions in Supersonic Flow." California Institute of Technology, Ph. D. Thesis, 1968.

8. Popinski, Z. and Ehrlich, C. F. "Development Design Methods for Predicting Hypersonic Aerodynamic Control Characteristics." AFFDL-TR-66-85, September 1966.

9. Gray, J. D. "On the Existence of a Pressure Plateau in Pure Laminar Separated Flows." AIAA Journal, Vol. 4, August 1966.

10. Curle, N. "The Effects of Heat Transfer on Laminar Boundary Layer Separation in Supersonic Flow." Aero. Quarterly, Vol. XII, November 1961.

11. Lees, L. and Reeves, B. L. "Supersonic Separated and Reattaching Laminar Flows: Part I. General Theory and Application to Adiabatic Boundary Layer/Shock Wave Interactions." AIAA Journal, November 1964.

12. Thomke, G. J. and Roshko, A. "Incipient Separation of a Turbulent Boundary Layer at High Reynolds Number in Two-Dimensional Supersonic Flow over a Compression Corner." DAC-59819, January 1969.

13. Sterrett, J. R. and Emery, J. C. "Experimental Separation Studies for Two-Dimensional Wedges and Curved Surfaces at Mach Numbers of 4.8 to 6.2." NASA TND-1014, February 1962.

14. Hahn, J. S. "Experimental Investigation of Turbulent Step-Induced Boundary-Layer Separation at Mach Numbers 2.5, 3 and 4." AEDC-TR-69-1 (AD683767), March 1969.

15. Wilson, R. E. "An Experimental Investigation of Separated Turbulent Supersonic Flow at $M_\infty = 3.0$." The University of Tennessee Space Institute Master's Thesis, June 1966.

16. Drougge, G. "An Experimental Investigation of the Influence of Strong Adverse Pressure Gradients on Turbulent Layers at Supersonic Speeds." FFA Aeronautical Research Institute of Sweden, Report 46, 1953.

17. Zukowski, E. F. "Turbulent Boundary-Layer Separation in Front of a Forward-Facing Step." AIAA Journal, October 1967.

APPENDIX I
TABLES

TABLE I
INSTRUMENTATION LOCATIONS
a. Laminar Models (Except for Aspect Ratio 2.0), x_c = 2.5 in.

		Spanwise Pressure Tap Location, z, in.								
x, in.	x/x_c	0	1.25	2.25	3.00	4.35	5.35	7.35	11.35	12.35
0.50	0.20	x	x	x	x	x	x	x	x	x
0.75	0.30	x								
1.00	0.40	x	x	x	x	x	x	x	x	x
1.125	0.45	x(a)								
1.25	0.50	x(b)	x	x	x	x	x	x	x	x
1.375	0.55	x(a)								
1.50	0.60	x(b)	x	x	x	x	x	x	x	x
1.625	0.65	x(a)								
1.75	0.70	x(b)	x	x	x	x	x	x	x	x
1.875	0.75	x(a)								
2.00	0.80	x(b)	x	x	x	x	x	x	x	x
2.125	0.85	x(a)								
2.25	0.90	x(b)	x	x	x	x	x	x	x	x
2.375	0.95	x(a)								
2.50	1.00	x	x	x	x	x	x	x	x	x
2.625	1.05	x(a)								
2.75	1.10	x	x	x	x	x	x	x	x	x
2.875	1.15	x(a)								
3.00	1.20	x	x	x	x	x	x	x	x	x
3.25	1.30	x	x	x	x	x	x	x	x	x
3.50	1.40	x	x	x	x	x	x	x	x	x
3.75	1.50	x								
4.00	1.60	x	x	x	x	x	x	x	x	x
4.25	1.70	x								
4.50	1.80	x	x	x	x	x	x	x	x	x
4.75	1.90	x								
5.00	2.00	x	x	x	x	x	x	x	x	x
5.25	2.10	x								
5.50	2.20	x	x	x	x	x	x	x	x	x
5.75	2.30	x								
6.00	2.40	x								
6.25	2.50	x								
6.50	2.60	x								
7.00	2.80	x								
7.50	3.00	x								

NOTES: a. These taps are alternately at z = 0.125 and -0.125 in.

b. Five 0.030-in.-ID taps at z = 0.25 in.
Five 0.062-in.-ID taps at z = -0.25 in.
All other taps are 0.015-in. ID.

Thermocouples were located at z = 0.875, 4.35, and 11.35 in. at x = 1.50, 8.50, and 12.50 in. (total of nine).

TABLE I (Continued)
b. Turbulent Models and Laminar Model of Aspect Ratio 2.0 (x_c = 14.0 in.)

Longitudinal Pressure Tap Locations

x, in.	x/x_c
[illegible]	0.464
[illegible]	[illegible]
[illegible]	0.604
[illegible]	0.643
[illegible]	[illegible]
10.0	0.714
10.5	0.750
11.0	0.786
11.5	0.821
12.0	0.857
12.5	0.893
13.0	0.929
13.5	0.964
14.0	1.000
14.5	1.036
15.0	1.071
15.5	1.107
16.0	1.143
16.5	1.179
17.0	1.214
17.5	1.250
18.0	1.286
18.5	1.321
19.5	1.393
20.5	1.464
21.5	1.536

NOTES:

1. [illegible] in. ID.
2. [illegible]
3. Typical for all spanwise rows

TABLE I (Concluded)
c. Relative Locations of Instrumentation for Each Configuration

Aspect Ratio	x_c, in.	z/b — Spanwise Location, z, in. 0	1.25	2.25	[illegible]	4.75	5.75	9.25	11.75	12.75
[illegible]	[illegible]			0.161		0.339		0.661	0.839	0.911
[illegible]			[illegible]	0.321	0.429	0.679	0.821			-
[illegible]		0	[illegible]	[illegible]	0.857					
[illegible]*								-	-0.588	0

Aspect Ratio	x_c, in.	z/b — Spanwise Location, z, in. 0	2.25	4.75	9.25	11.75
[illegible]	14.0	0	0.161	0.339	0.661	0.841
[illegible]	14.0	0	0.321	0.679		-

*[illegible] was constructed using a section cut from the outside [illegible] AR [illegible] model.

TABLE II
TEST SUMMARY FOR LAMINAR INVESTIGATION
θ = 9.5 deg

M_w	M_∞	AR	$Re_c \times 10^{-6}$						
			0.06	0.13	0.19	0.25	0.50	0.75	1.0
4.5	6	11.2	*		* x		*	*	
	8			* x	* x	*	*	*	*
	6	5.6			* x				
	8			* x	* x		*		*
	8	2.8		* x	* x		*		*
	8	1.4		* x	* x		*		*
6.0	6	11.2	*	* x	*	*	*	*	*
	8			*	* x	*	*	*	*
	10			* x	* x	*	*		
	6	5.6		* x	* x	* x	*		
	8			* x	* x		*		*
	10			* x	x	*	*		
	8	2.8		* x	* x	*	*	*	*
	10			* x		*	*		
	8	2.0					* x	* x	
	8	1.4		* x	* x	*	*	*	*
	10			* x		* x	* x		
8.0	8	11.2	*	* x	* x	*	*	*	
	10			*	* x	*	*	*	
	8	5.6	*	* x	* x		*	*	
	10			*	* x	*	*	*	
	8	2.8	*	* x	* x	* x	*	*	
	10			* x			*		
	8	2.0				*(0.35)x	* x	* x	
	8	1.4	*	* x	* x	*	*	*	
	10			* x	* x	*	* x		
10.0	10	11.2	x	* x	* x	*	*		
		5.6		* x	* x	*	*		
		2.8		* x		*	*		
		1.4	*	* x		* x	* x		

* No Side Plates

x Full Span Side Plates

TABLE III
TEST SUMMARY FOR TURBULENT INVESTIGATION
a. Surface Pressures

M_∞	$M_\bullet$	AR	θ, deg	x, in.	$Re_\infty \times 10^{-6}$ 2.6	4.1	6.1	9.1	Notes
6	8	2	Flat Plate	13.3		*	*		
				10.0			*		
				8.0			*		
8				13.3		*			
				10.0		*			
				8.0		*			
6	6	2	10	12.9	*	*	*		No Trips
				10.0	*				
6	6	2	30	12.9		*	*		No Trips
				10.0		* X	* X		
6	6	2	50	12.9			* X		No Seal at Hinge Line
				10.0			*		
4.5	6	1	35	12.5			*	*	No Trips
				10.0				*	
6	6	1	35	12.5		* X	* X		No Trips
				11.8			*		0.1 in. Fence at Hinge Line
				10.0		*	*		0.25 in. Fence at Hinge Line
				6.0			*		

* No Side Plates
X Full Span Side Plates

TABLE III (Concluded)
b. Boundary-Layer Survey Data

M_∞	$M_\bullet$	AR	θ, deg	x, in.	z, in.	$Re_\infty \times 10^{-6}$ 4.1	6.1	9.1	Notes
6	8	2	Flat Plate	13.3	1.0		*		
				10.0			*		
				8.0			*		
8				13.3		*			
				10.0		*			
				8.0		*			
6	6	2	30	12.9	1.0		*		
				10.0			*		
				10.0			*		No Trips
4.5	6	1	35	12.5	7.25			*	
				11.8	1.0		*	*	
				10.0	1.0		*	*	
				6.0	1.0		*	*	
6	6	1	35	12.5	0.25		*		
					6.76		*		
					7.25		*		
				11.8	1.0	*	*		
						*	*		0.10-in. Fence at Hinge Line
							*		0.25-in. Fence at Hinge Line
					4.25		*		
				10.0	1.0	*	*		
				6.0	1.0		*		

APPENDIX II
TABULATED SURFACE PRESSURE DATA

The results of this investigation, which should be of greatest general interest to specialists in the field of flow separation, are presented in two parts in this Appendix. The first part (I) contains results obtained with the widest laminar model (x_c = 2.5 in.) at zero angle of attack for each Reynolds number and Mach number at which tests were conducted. The second part (II) contains results obtained with the turbulent models (x_c = 14 in.) at the conditions listed in the table below.

M_w	M_∞	AR	θ, deg	$Re_c \times 10^{-6}$ 4.1	6.1	9.1
6	6	2	30	x	x	
		2	35		x	
		1	35	x	x	
4.5		1	35			x

The key linking the computer tabulations presented herein to the nomenclature of the body of this report is as follows:

TABULATION KEY

Printed Out	Nomenclature
ALPHA-M	α
A.R.	$2b/x_c$
FINAL	Value at end of data acquisition
INITIAL	Value at start of data acquisition
M-INF	M_∞
M-W	M_w
P/PEO	$p/p_{\bar{o}}$
P-W/P-INF	p/p_∞
RE-INF	$(u/\nu)_\infty$
RE-XC	Re_c
T/T-O	T_{wall}/T_{t_∞}
X/XC	x/x_c
XC	x_c
Z/B	z/b

A=[illegible]	RE=INF	M=∞	RE=A[illegible]	A.R.	ALPHA=M	RE/FT=[illegible]
[illegible]	[illegible]	5.95	[illegible]	11.20	[illegible]	1.00

P/PT=0

X/XC	Z/H=						
			.089	-.181	.339	.661	.839	.911
.2			1.144	1.220	1.[illegible]	1.177	1.212	[illegible]
.3[illegible]		1.347						
.4		1.104	1.097	1.088	1.[illegible]4	1.090	1.125	1.[illegible]
.45		1.066						
.5[illegible]			1.046	1.037	1.034	1.053	1.071	1.[illegible]
.55		1.29[illegible]						
.6		1.015	1.017	1.030	1.019	1.009	1.044	[illegible]
.65		1.00[illegible]						
.7		1.00[illegible]	1.024	1.023	1.025	1.009	1.03[illegible]	[illegible]
.75		1.044						
.8[illegible]		1.095	1.082	1.081	1.077	1.148	1.081	[illegible]
.85		1.185						
.9[illegible]		1.306	1.295	1.293	1.296	1.338	1.285	1.2[illegible]
.95		1.395						
1.00		1.51[illegible]	1.499	1.490	1.478	1.514	1.541	1.[illegible]
1.[illegible]		1.575						
1.1[illegible]		1.657	1.712	1.751	1.697	1.684		1.73[illegible]
1.15		1.753						
1.2[illegible]		1.86[illegible]	1.890	1.943	1.[illegible]75	1.890	1.970	1.[illegible]7
1.3[illegible]		2.013	2.068	2.107	2.039	2.081	2.120	2.14[illegible]
1.4[illegible]		2.191	2.232	2.299	2.217	2.245	2.312	2.367
1.5		2.32[illegible]						
1.6[illegible]		2.43[illegible]			2.436	2.451	2.517	2.60[illegible]
1.7[illegible]		2.501						
1.8[illegible]		2.64[illegible]	2.615	2.654	2.532	2.574	2.626	2.709
1.9[illegible]		2.670						
2.00		2.725			2.641	2.752	2.722	2.750
2.1[illegible]		2.73[illegible]						
2.2[illegible]		2.73[illegible]	2.711	2.736	2.682	2.793	2.736	2.805
2.3[illegible]		2.75[illegible]						
2.4[illegible]		2.76[illegible]						
2.50		2.791						
2.6[illegible]		2.81[illegible]						
2.8[illegible]		2.79[illegible]						
3.00		2.78[illegible]						

T/T-0

	Z/H= .062			Z/H= .312			Z/H= .812		
X/XC	.60	1.40	5.00	.60	1.40	5.00	.60	1.40	5.00
INITIAL	.869	.745	.77[illegible]	.860	.450	.723	.849	.837	.763
FINAL	.865	.738	.771	.856	.845	.721	.846	.832	.764

LAMINAR MODEL

M-INF	RE-INF	M-W	RE-XC	A.R.	ALPHA-M	P-W/P-INF
6.00	5.003E 05	6.00	1.251E 05	11.20	0	1.00

P/PEO

X/XC	Z/B=	0	.089	-.161	.339	.661	.839	.911
.20			1.173	1.175	1.167	1.192	1.198	1.197
.30		1.124						
.40		1.058	1.064	1.059	1.094	1.068	1.090	1.093
.45		1.031						
.50			1.021	1.024	1.028	1.041	1.066	1.062
.55		1.116						
.60		1.000	1.002	1.001	1.009	1.014	1.024	1.031
.65		1.000						
.70		1.043	1.025	1.016	1.024	1.029	1.039	1.031
.75		1.090						
.80		1.194	1.177	1.164	1.175	1.243	1.167	1.124
.85		1.287						
.90		1.400	1.398	1.389	1.392	1.445	1.396	1.345
.95		1.485						
1.00		1.567	1.569	1.555	1.558	1.592	1.598	1.535
1.05		1.615						
1.10		1.695	1.745	1.744	1.744	1.781		1.766
1.15		1.796						
1.20		1.905	1.934	1.962	1.962	2.014	2.005	2.020
1.30		2.105	2.138	2.180	2.158	2.225	2.230	2.296
1.40		2.291	2.334	2.339	2.354	2.370	2.433	2.499
1.50		2.456						
1.60		2.574			2.631	2.654	2.695	2.761
1.70		2.748						
1.80		2.796	2.756	2.790	2.754	2.785	2.847	2.870
1.90		2.821						
2.00		2.843			2.819	2.901	2.894	2.943
2.10		2.865						
2.20		2.879	2.858	2.877	2.881	2.908	2.927	2.921
2.30		2.886						
2.40		2.879						
2.50		2.877						
2.60		2.877						
2.80		2.879						
3.00		2.879						

T/T-O

	Z/B= .062			Z/B= .312			Z/B= .812		
X/XC	.60	1.40	5.00	.60	1.40	5.00	.60	1.40	5.00
INITIAL	.87.	.778	.741	.859	.440	.732	.846	.825	.735
FINAL	.88	.778	.759	.867	.453	.741	.855	.839	.752

LAMINAR MODEL

M-INF	RE-INF	M-W	RE-XC	A.W.	ALPHA-W	P-W/P-INF
5.98	4.967E 06	5.98	1.869E 05	11.20	.00	1.00

P/PEO

X/XC	Z/W=		.089	-.181	.339	.661	.939	.911
.20			1.135	1.154	1.155	1.171	1.174	1.172
.30		1.096						
.40		1.038	1.038		1.049	1.079	1.087	1.085
.45		1.010						
.50			1.002	1.006	1.033	1.063	1.066	1.058
.55		1.087						
.60		1.000	.992	1.006	1.023	1.028	1.031	1.035
.65		1.015						
.70		1.103	1.094	1.098	1.125	1.129	1.097	1.078
.75		1.200						
.80		1.302	1.299	1.307	1.333	1.421	1.291	1.228
.85		1.393						
.90		1.498	1.477	1.486	1.511	1.549	1.498	1.483
.95		1.557						
1.00		1.606	1.600	1.603	1.633	1.651	1.644	1.541
1.05		1.647						
1.10		1.704	1.723	1.760	1.741	1.742		1.751
1.15		1.800						
1.20		1.895	1.905	1.951	1.923	1.982	1.994	2.038
1.30		2.135	2.106	2.161	2.124	2.183	2.237	2.257
1.40		2.338	2.326	2.353	2.344	2.384	2.467	2.525
1.50		2.485						
1.60		2.623			2.678	2.737	2.811	2.864
1.70		2.737						
1.80		2.814	2.814	2.888	2.831	2.833	2.954	2.965
1.90		2.833						
2.00		2.881			2.879	2.967	3.002	3.051
2.10		2.938						
2.20		2.928	2.938	2.984	2.917	3.005	3.021	3.041
2.30		2.948						
2.40		2.946						
2.50		2.965						
2.60		2.984						
2.80		2.948						
3.00		2.938						

T/T-0

	Z/W=	.062			Z/W=	.312			Z/W=	.812	
X/XC		.60	1.40	5.00	.60	1.40	5.00	.60	1.40	5.00	
INITIAL		.922	.872	.914	.914	.927	.879	.910	.920	.898	
FINAL		.92	.866	.908	.908	.921	.873	.905	.914	.893	

LAMINAR MODEL

M-INF	RE-INF	M-W	RE-XC	A.W.	ALPHA-W	P-W/P-INF
6.00	1.204E 06	6.00	2.508E 05	11.20	0	1.00

P/PEO

X/XC	Z/R=	.161	.339	.661	.839	.911
.20		1.076	1.085	1.095	1.098	1.104
.30						
.40	1.011	.997	1.043		1.034	1.037
.45	1.000					
.50		.989	1.013	1.016	1.019	1.029
.55	1.041					
.60	1.004	.997	1.024	1.012	1.015	1.018
.65	1.060					
.70	1.094	1.132	1.163	1.151	1.113	1.082
.75	1.222					
.80	1.350	1.373	1.400	1.464	1.346	1.285
.85	1.436					
.90	1.519		1.572	1.584	1.538	1.495
.95	1.583					
1.00	1.639		1.685			1.630
1.05	1.673					
1.10	1.651	1.663	1.679	1.679		1.677
1.15	1.764					
1.20	1.877	1.889	1.911	1.897	1.952	1.966
1.30	2.106	2.128	2.165	2.151	2.220	2.262
1.40	2.342	2.354	2.356	2.391	2.481	2.551
1.50	2.554					
1.60	2.716		2.758	2.772	2.833	2.889
1.70	2.699					
1.80	2.816	2.903	2.934	2.960	3.010	3.059
1.90	2.897					
2.00	2.932		3.019	3.033	3.094	3.150
2.10	2.960					
2.20	2.981	3.030	3.047	3.096	3.151	3.221
2.30	3.017					
2.40	3.045					
2.50	3.030					
2.60	3.076					
2.80	3.025					
3.00	3.081					

T/T-0

	Z/R= .062			Z/R= .312			Z/R= .812		
X/XC	.60	1.40	5.00	.60	1.40	5.00	.60	1.40	5.00
INITIAL	.88[illegible]	.917	.913	.911	.926	.906	.906	.914	.897
FINAL	.884	.912	.91[illegible]	.915	.929	.903	.908	.922	.895

LAMINAR MODEL

M-INF	RE-INF	M-W	RE-XC	A.W.	ALPHA-W	P-W/P-INF
6.04	2.403E 06	6.04	5.004E 05	11.20	.01	1.00

U/UE-O

X/XC	Z/W=	.089	.161	.337	.661	.839	.911
.2		1.076	1.102	1.111	1.136	1.141	1.142
.3							
.4	1.019	1.014	1.035	1.035	1.073	1.087	1.086
.45	1.007						
.5		1.006	1.020	1.034	1.056	1.069	1.067
.55	1.026						
.6	1.039	1.097	1.065	1.101	1.086	1.072	1.056
.65	1.220						
.7	1.340	1.332	.305	1.335	1.315	1.263	1.184
.75	1.446						
.8	1.515	1.499	1.490	1.526	1.574	1.483	1.411
.85	1.548						
.9	1.587	1.592	1.587	1.625	1.652	1.614	1.564
.95	1.615						
1.00	1.643	1.650	1.650	1.685	1.710	1.703	1.653
1.05	1.638						
1.1	1.678	1.698	1.729	1.733	1.771		1.786
1.15	1.759						
1.2	1.832	1.872	1.931	1.939	2.017	2.031	2.043
1.3	2.074	2.131	2.214	2.137	2.296	2.439	2.452
1.4	2.341	2.414	2.456	2.416	2.539	2.730	2.771
1.5	2.598						
1.6	2.839			2.841	3.020	3.138	3.309
1.7	3.056						
1.8	3.165	3.048	3.143	3.059	3.295	3.271	3.398
1.9	3.198						
2.0	3.228			3.184	3.327	3.380	3.491
2.1	3.246						
2.2	3.246	3.238	3.337	3.268	3.380	3.449	3.563
2.3	3.295						
2.4	3.311						
2.5	3.337						
2.6	3.393						
2.8	3.366						
3.0	3.400						

T/T-O

	Z/W= .062			Z/B= .312			Z/B= .812		
X/XC	.60	1.40	5.00	.60	1.40	5.00	.60	1.40	5.00
INITIAL	.933	.875	.888	.914	.926	.896	.909	.916	.874
FINAL	.931	.881	.903	.917	.935	.907	.913	.926	.891

M-INF	RE-INF	M-W	RE-XC	A.R.	ALPHA-M	P-W/P-INF
6.05	3.6 E 06	6.05	7.5 E 05	11.20	-.03	1.00

P/PEO

X/XC	Z/B=	0	.089	-.161	.339	.661	.839	.911
.20								
.30		1.021						
.40		1.007	1.005	1.018	1.071	1.064	1.073	1.071
.45		1.000						
.50			1.009	1.010	1.033	1.051	1.052	1.059
.55		1.080						
.60		1.200	1.199	1.128	1.170	1.112	1.086	1.063
.65		1.318						
.70			1.417	1.378	1.415	1.374	1.317	1.233
.75		1.480						
.80		1.530	1.536	1.528	1.565	1.[illegible]	1.513	1.449
.85		1.561						
.90		1.589	1.596	1.596	1.638	1.657	1.616	1.580
.95		1.610						
1.00		1.626	)	1.637	1.676	1.697	1.677	1.645
1.05		;						
1.10		1.632	)	)	)	)	)	
1.15		1.699						
1.20		1.793	1.801	1.847	1.878	1.967	2.010	2.083
1.30		2.073	2.079	2.152	2.219	2.292	2.417	2.540
1.40		2.404	2.434	2.468	2.574	2.669	2.750	3.081
1.50		2.723						
1.60		2.973			3.045	3.263	3.318	3.516
1.70		;						
1.80		3.235	3.227	3.305	3.300	3.444	3.501	3.597
1.90		3.244						
2.00		3.341			3.395	3.477	3.604	3.699
2.10		3.391						
2.20		3.402	3.444	3.472	3.492	3.541	3.609	3.713
2.30		3.452						
2.40		3.460						
2.50		3.455						
2.60		3.483						
2.80		3.483						
3.00		3.499						

T/T-0

	Z/B= .062			Z/B= .312			Z/B= .812		
X/XC	.60	1.40	5.00	.60	1.40	5.00	.60	1.40	5.00
INITIAL	.93[illegible]	.892	.921	.921	.941	.915	.920	.920	.908
FINAL	.93[illegible]	.893	.922	.922	.942	.916	.920	.926	.909

LAMINAR MODEL

M-INF	RE-INF	M-W	RE-XC	A.N.	ALPHA-N	P-W/P-INF
6.5	4.773E 06	6.05	9.947E 05	11.20	0	1.00

P/PEO

X/XC	Z/H=	.089	-.161	.339	.661	.839	.911
.20		1.048	1.070	1.088	1.117	1.113	1.114
.30	1.015						
.40	1.001	1.001	1.017	1.070	1.066	1.077	1.071
.45	1.000						
.50		1.024	1.007	1.036	1.052	1.056	1.059
.55	1.136						
.60	1.264	1.251	1.151	1.149	1.108	1.091	1.065
.65	1.365						
.70	1.445						
.75	1.496						
.80	1.532	1.532	1.516	1.554	1.583	1.506	1.443
.85	1.556						
.90		1.580	1.572	1.613	1.630	1.598	1.564
.95	1.590						
1.00	1.601	1.610	1.606	1.647	1.667	1.647	1.620
1.05							
1.10	1.601	1.618	1.633	1.668	1.699		1.717
1.15	1.663						
1.20	1.755	1.773	1.830	1.886	1.980	2.029	2.118
1.30		2.079	2.179	2.263	2.358	2.522	2.723
1.40	2.459	2.488	2.555	2.707	2.949	3.023	3.372
1.50	2.850						
1.60	3.080						
1.70	3.233						
1.80	3.333			3.430	3.551	3.673	3.743
1.90	3.390						
2.00	3.434			3.543	3.562	3.699	3.773
2.10							
2.20	3.470	3.530	3.544	3.588	3.634	3.701	3.755
2.30	3.506						
2.40	3.506						
2.50	3.493						
2.60	3.523						
2.80	3.517						
3.00	3.541						

T/T-O

	Z/H= .062			Z/H= .312			Z/H= .812		
X/XC	.60	1.40	5.00	.60	1.40	5.00	.60	1.40	5.00
INITIAL	.934	.891	.903	.918	.937	.909	.913	.929	.888
FINAL	.936	.893	.912	.918	.940	.914	.915	.932	.900

LAMINAR MODEL

M-INF	RE-INF	M-W	RE-XC	A.R.	ALPHA-M	P-W/P-INF
7.85	3.131E 05	7.85	6.525E 04	11.20	0	1.00

P/PEO

X/XC	Z/B= 0	.089	-.161	.339	.661	.839	.911
.20	1.345	1.331	1.384	1.308	1.332	1.310	1.345
.30	1.218						
.40	1.145	1.130	1.184	1.181	1.131	1.164	1.145
.45	1.109						
.50		1.039	1.111	1.054	1.058	1.073	1.091
.55	1.055						
.60	1.018	1.002	1.038	.981	.985	1.001	1.036
.65	1.000						
.70	1.001	.944	.984	.981	.967	.982	1.000
.75	1.001						
.80	1.019	1.021	1.020	.945		.982	.964
.85	1.074						
.90	1.165	1.148	1.184	1.126		1.110	1.091
.95	1.256						
1.00	1.383	1.367	1.384	1.344	1.387	1.401	1.273
1.05	1.297						
1.10	1.331	1.603	1.636	1.531	1.671		1.501
1.15	1.536						
1.20	1.672	1.807	1.772	1.667	1.910	1.910	1.876
1.30	1.843	1.978	1.977	1.803	2.081	1.944	2.080
1.40	1.945	2.182	2.113	2.007	2.047	2.081	2.046
1.50	2.116						
1.60	2.252			2.279	2.490	2.456	2.524
1.70	2.592						
1.80	2.626	2.626	2.659	2.449	2.558	2.558	2.728
1.90	2.660						
2.00	2.729			2.585	2.967	2.660	2.865
2.10	2.763						
2.20	2.763	2.864	2.931	2.653	2.933	2.763	2.933
2.30	2.899						
2.40	2.899						
2.50	2.999						
2.60	2.999						
2.80	2.967						
3.00	2.967						

T/T-O

	Z/B= .62			Z/B= .312			Z/B= .812	
X/XC	.60	1.40	5.00	.60	1.40	5.00	.60	1.40	5.00
INITIAL	.889	.769	.853	.879	.881	.847	.866	.864	
FINAL	.889	.769	.853	.879	.882	.848	.868	.869	

LAMINAR MODEL

M-INF	RE-INF	M-e	RE-XC	A.W.	ALPHA-W	P-w/P-INF
7.90	6.120E 05	7.90	1.275E 05	11.20	0	1.00

P/PFO

X/XC	Z/H=	0	.084	-.161	.339	.661	.839	.911
.2		1.324	1.287	1.267	1.264	1.259	1.295	1.294
.3		1.196						
.4		1.137	1.111	1.100	1.126	1.063	1.118	1.108
.45		1.088						
.5		1.039	1.042	1.021	1.028	1.004	1.050	1.059
.55		1.039						
.6		1.039	.993	.982	.960	.945	1.001	1.000
.65		1.000						
.7		1.021	.993	.972	.970	.935	.991	.971
.75		1.031						
.8		1.099	1.041	1.041	1.058		1.050	1.010
.85		1.197						
.9		1.325	1.317	1.277	1.263	1.338	1.266	1.206
.95		1.423						
1.00		1.541	1.534	1.463	1.459	1.486	1.511	1.402
1.05		1.564						
1.1		1.619	1.710	1.801	1.559	1.747		1.673
1.15		1.767						
1.2		1.895	1.912	1.985	1.779	1.915	2.097	1.894
1.3		2.098	2.096	2.205	1.963	2.152	2.207	2.115
1.4		2.263	2.335	2.426	2.183	2.281	2.373	2.336
1.5		2.424						
1.6		2.595			2.513	2.667	2.722	2.703
1.7		2.869						
1.8		2.961	2.975	3.051	2.715	2.814	2.943	2.942
1.90		3.053						
2.00		3.108			2.861	3.090	3.108	3.126
2.1		3.163						
2.2		3.200	3.197	3.308	2.916	3.182	3.163	3.218
2.3		3.255						
2.40		3.274						
2.5		3.382						
2.6		3.382						
2.80		3.236						
3.00		3.236						

T/T-0

	Z/H= .62			Z/H= .312			Z/H= .812		
X/XC	.60	1.40	5.00	.60	1.40	5.00	.60	1.40	5.00
INITIAL	.898	.777	.857	.885	.890	.852	.874	.878	.972
FINAL	.905	.782	.868	.893	.900	.862	.883	.889	.991

LAMINAR MODEL

M-INF	RE-INF	M-W	RE-XC	A.R.	ALPHA-M	P-W/P-INF
7.93	9.265E 05	7.93	1.931E 05	11.20	0	1.00

P/PEO

X/XC	Z/B= 0	.089	-.161	.339	.661	.839	.911
.20	1.260	1.243	1.262	1.246	1.244	1.254	1.253
.30	1.153						
.40	1.100	1.083	1.089	1.139	1.084	1.107	1.093
.45	1.060						
.50	1.020	1.029	1.049	1.032	1.024	1.047	1.047
.55	1.013						
.60	1.007	.996	1.008	.999	.983	1.007	1.007
.65	1.000						
.70	1.028	1.022	1.015	1.012	1.004	1.007	.987
.75	1.075						
.80	1.201	1.190	1.182	1.186		1.141	1.073
.85	1.315						
.90	1.428	1.417	1.396	1.399	1.485	1.374	1.287
.95	1.528						
1.00	1.615	1.604	1.583	1.592	1.626	1.621	1.493
1.05	1.639						
1.10	1.739	1.763	1.750	1.746	1.738		1.751
1.15	1.827						
1.20	1.965	1.976	2.000	1.983	1.964	2.064	2.013
1.30	2.190	2.226	2.250	2.220	2.226	2.276	2.276
1.40	2.446	2.463	2.475	2.457	2.451	2.526	2.501
1.50	2.640						
1.60	2.815			2.819	2.876	2.939	2.939
1.70	2.977						
1.80	3.102	3.101	3.149	3.056	3.102	3.177	3.201
1.90	3.202						
2.00	3.264			3.230	3.327	3.339	3.364
2.10	3.339						
2.20	3.352	3.338	3.399	3.268	3.364	3.427	3.414
2.30	3.402						
2.40	3.427						
2.50	3.424						
2.60	3.449						
2.80	3.413						
3.00	3.401						

T/T-0

	Z/B= .062			Z/B= .312			Z/B= .812		
X/XC	.60	1.40	5.00	.60	1.40	5.00	.60	1.40	5.00
INITIAL	.910		.885	.900	.914	.880	.889	.900	.946
FINAL	.906		.884	.896	.908	.876	.885	.887	.950

LAMINAR MODEL

M-INF	RE-INF	M-W	RE-XC	A.R.	ALPHA-M	P-W/P-INF
7.95	1.229E 06	7.95	2.561E 05	11.20	0	1.00

P/PEO

X/XC	Z/B= 0	.084	-.161	.334	.661	.839	.911
.20	1.224	1.202	1.227	1.223	1.213	1.220	1.224
.30	1.133						
.40	1.082	1.044	1.068	1.137	1.080	1.093	1.066
.45	1.046						
.50	1.010	1.013	1.017	1.030	1.014	1.036	1.031
.55	1.005						
.60	1.000	.987	.992	1.004	.983	1.006	.990
.65	1.000						
.70	1.042	1.048	1.032	1.040	1.024	1.026	.990
.75	1.134						
.80	1.267	1.263	1.242	1.259		1.205	1.112
.85	1.364						
.90	1.476	1.478	1.457	1.473	1.521	1.440	1.347
.95	1.568						
1.00	1.645	1.647	1.615	1.636	1.664	1.664	1.520
1.05	1.676						
1.10	1.762	1.780	1.798	1.795	1.771		1.751
1.15	1.886						
1.20	1.992	1.990	2.047	2.014	2.048	2.058	2.029
1.30	2.231	2.249	2.296	2.262	2.278	2.316	2.306
1.40	2.480	2.507	2.525	2.520	2.469	2.594	2.594
1.50	2.729						
1.60	2.921			2.930	2.948	3.025	3.043
1.70	3.063						
1.80	3.197	3.177	3.233	3.188	3.187	3.312	3.311
1.90	3.293						
2.00	3.350			3.312	3.407	3.455	3.455
2.10	3.398						
2.20	3.446	3.426	3.482	3.389	3.484	3.551	3.522
2.30	3.465						
2.40	3.494						
2.50	3.501						
2.60	3.558						
2.80	3.464						
3.00	3.483						

T/T-O

	Z/B= .062			Z/B= .312			Z/B= .812		
X/XC	.60	1.40	5.00	.60	1.40	5.00	.60	1.40	5.00
INITIAL	.911	.811	.889	.901	.914	.884	.888	.893	.928
FINAL	.908	.806	.881	.897	.909	.875	.887	.889	.928

LAMINAR MODEL

T-INF	RE-INF	M-∞	RE-X(	A.R.	ALPHA-M	P-W/P-INF
1.49	2.42E+06	7.99	5.04E+0[illegible]	11.20	-.02	1.00

P/P-0

X/C	Y/R=	0	.083	-.161	.339	.651	.839	.911
.2			1.167	1.159	1.154	1.138	1.153	1.152
.3		1.088						
.4		1.031	1.023	1.033	1.076	1.019	1.039	1.031
.45		1.009						
.5			.999	.999	1.009	.993	1.003	1.005
.55		1.000						
.6		1.008	1.010	1.002	1.033	.993	.991	.982
.65		1.090						
.7		1.228	1.219	1.177	1.236	1.182	1.122	1.054
.75		1.352						
.8		1.471	1.457	1.438	1.488		1.369	1.[illegible]
.85		1.548						
.9		1.618	1.602	1.593	1.638	1.635	1.547	1.485
.94		1.675						
1.[illegible]		1.714	1.703	1.704	1.741	1.715	1.697	1.619
1.[illegible]		1.737						
1.1		1.800	1.818	1.836	1.823	1.808		1.794
1.1[illegible]		1.911						
1.2		2.022	2.025	2.069	2.059	2.055	2.084	2.089
1.3		2.298	2.336	2.367	2.368	2.345	2.422	2.437
1.4		2.607	2.615	2.648	2.695	2.621	2.756	2.804
1.5		2.888						
1.6		3.135			3.221	3.157	3.312	3.355
1.7		3.336						
1.8		3.481	3.446	3.498	3.544	3.501	3.641	3.723
1.9		3.583						
2.[illegible]		3.656			3.732	3.781	3.795	3.940
2.1		3.696						
2.2		3.723	3.746	3.778	3.829	3.878	3.912	4.032
2.3		3.757						
2.4		3.771						
2.5		3.788						
2.6		3.836						
2.8		3.824						
3.[illegible]		3.886						

T/T-0

	Y/R= .62			Y/R= .812			Y/R= .812		
X/C	.60	1.40	5.00	.60	1.40	5.00	.60	1.40	5.00
INITIAL	.916	.814	.827	.917	.814	.827	.893	.898	.813
FINAL	.916	.815	.848	.748	.818	.847	.894	.911	.838

LAMINAR MODEL

[illegible]	RE=1E6	M=.8	RE=AC	ALPHA=0	P0=P0=1E6	
[illegible]	3.57ME 06	.8	7.450E 05	11.20	-	1.00

U/UE

X/XC	Z/H=						
			.062	-.161	.339	.661	.839	.911
.0			1.143	1.157	1.155	1.139	1.134	1.137
.1		1.04						
.4		1.02	1.034	1.043	1.046	1.029	1.040	1.032
.45		1.00						
.5			1.011	1.020	1.028	1.005	1.008	1.011
.55		1.04						
.6		1.12	1.113	1.072	1.130	1.061	1.024	1.007
.65		1.27						
.7		1.41	1.378	1.348	1.400	1.330	1.244	1.164
.75		1.51						
.8		1.59	1.570	1.571	1.614	1.679	1.478	1.406
.85		1.64						
.9		1.70	1.694	1.694	1.736	1.713	1.627	1.579
.95		1.74						
1.0		1.77	1.749	1.786	1.820	1.792	1.742	1.694
1.0		1.76						
1.1		1.81	1.812	1.854	1.854	1.825		1.822
1.15		1.84						
1.2		1.99	2.034	2.084	2.083	2.068	2.094	2.136
1.3		2.27	2.324	2.670	2.403	2.389	2.470	2.524
1.4		2.60	2.688	2.738	2.803	2.709	2.871	2.945
1.5		2.93						
1.6		3.21			3.429	3.438	3.503	3.725
1.7		3.44						
1.8		3.65	3.731	3.756	3.839	3.911	3.968	4.143
1.9		3.76						
2.00		3.92			4.102	4.140	4.201	4.264
2.1		4.03						
2.2		4.05	4.078	4.147	4.226	4.224	4.326	4.386
2.3		4.14						
2.4		4.15						
2.5		4.14						
2.6		4.19						
2.8		4.20						
3.00		4.22						

T/T-0

	Z/H= .62			Z/H= .312			Z/H= .812		
X/XC	.60	1.40	5.00	.60	1.40	5.00	.60	1.40	5.00
INITIAL	.933	.847	.899	.922	.939	.893	.909	.926	.880
FINAL	.933	.844	?	.921	.939	.896	.906	.919	.881

LAMINAR MODEL

M-INF	RE-INF	M-W	RE-XC	A.R.	ALPHA-M	P-W/P-INF
10.04	3.043E 05	10.04	6.341E 04	11.20	-.04	1.00

P/PFO

X/XC	Z/R=	.000	-.161	.339	.661	.839	.911
.20		1.448	1.504	1.427	1.479	1.443	1.509
.30		1.308					
.40		1.209	1.219	1.278	1.206	1.183	1.224
.45		1.118					
.50			1.144	1.126	1.137	1.122	1.160
.55							
.60		1.055	1.087	1.047	1.083	1.069	1.107
.65		1.055					
.70		1.039	1.044	1.045	1.034	1.030	1.023
.75		1.000					
.80		1.013	.986	.999	1.043	1.009	1.018
.85		1.011					
.90		1.053	1.075	1.075	1.140	1.068	1.064
.95		1.186					
1.00		1.343	1.356	1.353	1.402	1.299	1.279
1.05		1.470					
1.10		1.688		1.573	1.637	1.283	1.565
1.15		1.619					
1.20		1.788	1.840	1.823	1.893		1.788
1.30		2.053		2.038	2.085	2.040	2.014
1.40		2.209	2.250	2.260	2.275	2.204	2.183
1.50		2.396					
1.60		2.520		2.608	2.597	2.535	2.517
1.70		2.685					
1.80		2.782	2.830	2.846	2.884	2.814	
1.90							
2.00		2.952		3.049	3.131	2.982	2.982
2.10		3.022					
2.20		3.066	3.121	3.124	3.191	3.048	3.048
2.30		3.178					
2.40		3.190					
2.50		3.202					
2.60		3.221					
2.80		3.236					
3.00		3.238					

T/T-0

	Z/R= .062			Z/R= .312			Z/R= .812		
X/XC	.60	1.40	5.00	.60	1.40	5.00	.60	1.40	5.00
INITIAL		.543			.731	.648			.637
FINAL		.538			.729	.642			.632

LAMINAR MODEL

M-INF	RE-INF	M-W	RE-XC	A.R.	ALPHA-M	P-W/P-INF
10.16	6.927E 05	10.16	1.235E 05	11.20	-.01	1.00

P/PFO

X/XC	Z/R=	0	-.141	.339	.661	.839	.911
.20		1.452	1.424	1.354	1.363	1.380	1.412
.30		1.224					
.40		1.169	1.176	1.228	1.149	1.163	1.172
.45		1.081					
.50			1.113	1.084	1.091	1.082	1.125
.55							
.60		1.042	1.044	1.027	1.023	1.037	1.077
.65		1.019					
.70		1.024	1.022	1.018	.990	1.012	1.015
.75		1.000					
.80		1.021	1.006	1.012	1.005	1.022	1.010
.85		1.069					
.90		1.177	1.163	1.176	1.192	1.156	1.132
.95		1.312					
1.00		1.455	1.438	1.442	1.460	1.450	1.373
1.05		1.538					
1.10		1.559		1.667	1.691		1.672
1.15		1.712					
1.20		1.917	1.957	1.934	1.981	1.977	1.939
1.30		2.165		2.184	2.222	2.242	2.184
1.40		2.409	2.441	2.435	2.460	2.489	2.446
1.50		2.632					
1.60		2.817		2.827	2.849	2.897	2.847
1.70		2.971					
1.80		3.105	3.131	3.120	3.155	3.208	
1.90							
2.00		3.313		3.353	3.429	3.443	3.398
2.10		3.385					
2.20		3.416	3.447	3.446	3.485	3.520	3.477
2.30		3.520					
2.40		3.542					
2.50		3.542					
2.60		3.551					
2.80		3.563					
3.00		3.563					

T/T-0

	Z/R=	.062		Z/R=	.312		Z/R=	.812	
X/XC	.60	1.40	5.00	.60	1.40	5.00	.60	1.40	5.00
INITIAL		.782		.783	.776				.677
FINAL		.786		.783	.780				.669

LAMINAR MODEL

M-INF	RE-INF	M-W	RE-XC	A.R.	ALPHA-M	P-W/P-INF
10.21	8.838E 05	10.21	1.842E 05	11.20	0	1.00

P/PEO

X/XC	Z/R=	0	-.161	.339	.661	.839	.911
.20		1.347	1.391	1.322	1.329	1.318	1.372
.30		1.197					
.40		1.141	1.154	1.201	1.121	1.132	1.133
.45		1.063					
.50			1.089	1.053	1.059	1.053	1.093
.55							
.60		1.017	1.029	1.001	1.000	1.012	1.036
.65		1.000					
.70		1.002	1.008	1.001	.975	.984	.997
.75		1.006					
.80		1.050	1.034	1.044	1.031	1.024	1.002
.85		1.145					
.90		1.283	1.250	1.277	1.280	1.242	1.187
.95		1.419					
1.00		1.549	1.521	1.514	1.545	1.530	1.448
1.05		1.622					
1.10		1.505		1.737	1.769		1.739
1.15		1.797					
1.20		2.018	2.055	2.014	2.063	2.044	2.025
1.30		2.274		2.291	2.333	2.345	2.317
1.40		2.555	2.586	2.569	2.604	2.592	2.617
1.50		2.768					
1.60		2.981		2.997	3.045	3.089	3.078
1.70		3.180					
1.80		3.348	3.357	3.307	3.362	3.417	
1.90							
2.00		3.556		3.569	3.642	3.664	3.671
2.10		3.632					
2.20		3.687	3.641	3.687	3.731	3.760	3.763
2.30		3.766					
2.40		3.799					
2.50		3.813					
2.60		3.818					
2.80		3.829					
3.00		3.833					

T/T-0

	Z/R=	.062		Z/R=	.312		Z/R=	.812	
X/XC	.60	1.40	5.00	.60	1.40	5.00	.60	1.40	5.00
INITIAL		.600		.784		.643			.631
FINAL		.618		.781		.664			.651

LAMINAR MODEL

M-INF	RE-INF	M-W	RE-XC	A.R.	ALPHA-M	P-W/P-INF
10.21	1.196E 06	10.21	2.492E 05	11.20	0	1.00

P/PEO

X/XC	Z/R= 0	-.161	.339	.661	.839	.911
.20		1.352	1.283	1.295	1.276	1.313
.30	1.175					
.40	1.148		1.181	1.109	1.113	1.110
.45	1.084					
.50		1.066	1.042	1.047	1.033	1.068
.55						
.60	1.019	1.037	1.004	.997	.999	1.019
.65	1.000					
.70	1.014	1.009	.998	.981	.986	.991
.75	1.042					
.80	1.136	1.090	1.104	1.086	1.073	1.021
.85	1.242					
.90	1.394	1.354	1.362	1.378	1.332	1.268
.95	1.504					
1.00	1.626	1.588	1.579	1.613	1.592	1.517
1.05	1.696					
1.10	1.800		1.783	1.820		1.777
1.15	1.943					
1.20	2.085	2.112	2.070	2.128	2.101	2.084
1.30	2.347		2.330	2.384	2.387	2.361
1.40	2.623	2.662	2.602	2.651	2.671	2.677
1.50	2.890					
1.60	3.115		3.261	3.180	3.221	3.226
1.70	3.311					
1.80	3.521	3.501	3.458	3.537	3.587	
1.90						
2.00	3.730		3.645	3.731	3.757	3.785
2.10	3.841					
2.20	3.891	3.835	3.811	3.863	3.900	3.915
2.30	3.857					
2.40	3.919					
2.50	3.919					
2.60	3.955					
2.80	4.001					
3.00	3.987					

T/T-0

	Z/B= .062			Z/R= .312			Z/R= .812		
X/XC	.60	1.40	5.00	.60	1.40	5.00	.60	1.40	5.00
INITIAL		.744			.833			.625	
FINAL		.759			.840			.653	

LAMINAR MODEL

M-INF	RE-INF	M-W	RE-XC	A.R.	ALPHA-M	P-W/P-INF
10.24	2.392E 06	10.24	4.985E 05	11.20	.01	1.00

P/PFO

X/XC	Z/R= 0	-.161	.339	.661	.839	.911
.20	1.243	1.286	1.255	1.223	1.205	1.250
.30	1.138					
.40	1.118		1.206	1.060	1.061	1.066
.45						
.50	1.043	1.018	1.011	.992	.987	1.010
.55	1.013					
.60	1.000	.990	.983	.962	.960	.985
.65	1.015					
.70		1.044	1.094	1.029	.980	
.75						
.80	1.361	1.329	1.362	1.323		1.206
.85	1.466					
.90	1.557	1.527	1.566	1.559	1.488	1.432
.95						
1.00	1.737		1.712	1.723	1.679	1.608
1.05	1.785					
1.10	1.881		1.864	1.869		1.817
1.15						
1.20	2.178	2.152	2.134	2.166	2.138	2.132
1.30	2.453		2.417	2.441	2.441	2.441
1.40	2.801	2.793	2.758		2.808	2.833
1.50	3.152					
1.60	3.448		3.359	3.397	3.451	3.483
1.70	3.667					
1.80	3.868	3.915	3.788	3.831	3.894	3.928
1.90	4.006					
2.00	4.117		3.937	4.003	4.053	4.075
2.10	4.186					
2.20	4.243	4.351	4.156	4.258	4.320	4.314
2.30	4.186					
2.40	4.203					
2.50	4.220					
2.60	4.337					
2.80	4.360					
3.00	4.433					

T/T-0

	Z/R= .062			Z/R= .312			Z/R= .812		
X/XC	.60	1.40	5.00	.60	1.40	5.00	.60	1.40	5.00
INITIAL		.827		.860		.787	.781	.769	.821
FINAL		.837		.860		.812	.779	.796	.838

PART II
TURBULENT MODEL, θ = 30

M-INF	RE-INF	M-W	RE-XC	A.H.	ALPHA-M	P-W/P-INF
6.05	3.502E 06	6.05	4.087E 06	2.00	.05	1.00

P/PEO

X/XC	Z/B= 0	.161	.339	.661	.840
.46	1.000	1.008	1.058	1.096	1.096
.54		1.013	1.056	1.088	
.61	1.009	1.012	1.045	1.071	1.070
.64	1.014	1.012	1.043	1.070	1.066
.68	1.019	1.018		1.067	1.059
.71	1.022		1.045	1.070	1.059
.75	1.023	1.024	1.048	1.067	1.056
.79	1.025	1.030	1.048	1.067	1.051
.82	1.041	1.032	1.047	1.079	
.86	1.036	1.033	1.050	1.076	1.049
.89	1.052	1.075		1.121	1.060
.93	1.599	1.670	1.685	1.928	1.589
.96	3.047	3.106	3.161	3.171	2.903
.99	3.850	3.856	3.901	3.829	3.688
1.04	3.537	6.808	6.768	6.790	7.123
1.07	12.847	12.645	12.354	12.692	13.396
1.11	17.825	17.763	17.834	18.362	18.508
1.14	18.516	18.534	18.567	18.857	18.543
1.18	18.217	18.388	18.268	18.456	18.036
1.21	17.971	18.197	18.086	18.382	17.687
1.25	17.857	18.138	17.954	18.167	17.725
1.29	17.573	17.904	17.837	18.069	17.664
1.32	18.475	17.804	18.049	18.005	17.605
1.39	18.475	17.569	18.099	18.081	17.497
1.46	18.419	17.704	18.328	18.037	17.362
1.54	19.061	19.143	18.929	18.794	17.561

T/T-0

	Z/B= .250			Z/B= .750		
X/XC	.50	.93	1.29	.50	.93	1.29
INITIAL	.906	.912		.911	.925	.901
FINAL	.907	.914		.910	.927	.901

TURBULENT MODEL, θ = 30

M-INF	RE-INF	M-W	RE-XC	A.R.	ALPHA-M	P-W/P-INF
6.05	5.158E 06	6.05	6.019E 06	2.00	.02	1.00

P/PEO

X/XC	Z/B= 0	.161	.339	.661	.840
.46	1.000	.993	1.031	1.073	1.068
.54		.994	1.035	1.068	1.065
.61	1.012	.995	1.031	1.060	1.055
.64	1.008	.994	1.028	1.057	1.051
.68	1.008	.995		1.050	1.043
.71	1.006		1.027	1.025	1.043
.75	1.006	.996	1.025	1.048	1.040
.79	1.008	.999	1.026	1.048	1.038
.82	1.010	1.002	1.028	1.050	
.86	1.016	1.008	1.029	1.052	1.032
.89	1.378	1.368		1.130	1.037
.93	2.763	2.793	2.609	2.202	1.613
.96	3.578	3.567	3.585	3.472	3.179
.99	3.798	3.795	3.824	3.810	3.720
1.04	2.982	5.496	5.788	6.367	7.213
1.07	10.494	10.021	10.601	12.008	13.730
1.11	16.804	16.015	16.892	18.110	19.194
1.14	20.961	19.838	20.236	19.261	18.810
1.18	20.406	18.766	18.718	18.529	18.081
1.21	20.614	18.266	18.178	18.391	17.747
1.25	19.740	18.222	18.050	18.108	17.684
1.29	18.712	18.058	17.959	18.078	17.680
1.32	19.747	18.171	17.970	18.000	17.643
1.39	18.482	17.605	18.059	18.269	17.628
1.46	18.305	18.282	18.443	18.117	17.354
1.54	18.482	20.463	19.104	18.900	17.643

T/T-O

	Z/B= .250			Z/B= .750		
X/XC	.50	.93	1.29	.50	.93	1.29
INITIAL	.895	.908		.908	.920	.895
FINAL	.901	.913		.913	.922	.896

TURBULENT MODEL, θ = 35

M-INF	RE-INF	M-W	RE-XC	A.R.	ALPHA-M	P-W/P-INF
6.05	5.170E 06	6.05	6.033E 06	2.00	.05	1.00

P/PEO

X/XC	Z/B= 0	.161	.339	.661	.840
.46	1.003	.997	1.031	1.065	1.074
.54	1.001	.995	1.030	1.059	1.068
.61	1.000	.996	1.028	1.054	1.057
.64	1.003	.998	1.028	1.054	1.051
.68	1.154	1.220		1.050	1.045
.71	2.178	2.408	1.691	1.050	1.043
.75		3.512	3.098	1.158	1.040
.78	3.862	3.936	3.702	2.143	1.111
.82	4.070	4.061	3.951	3.336	
.86	4.164	4.160	4.093	3.810	3.240
.89	4.204	4.172		4.014	3.746
.93	4.217	4.184	4.175	4.101	3.915
.96	4.239	4.168	4.175	4.088	3.916
.99	4.561	4.480	4.434	4.297	4.108
1.04	4.433	4.445	4.494	4.871	5.099
1.07	5.676	5.686	6.008	7.509	8.808
1.11	7.986	7.941	8.773	12.159	15.004
1.14	11.589	11.423	13.035	18.986	23.040
1.18	16.741	16.442	18.893	26.053	28.651
1.21	22.295	22.064	25.089	30.621	27.486
1.25	27.254	26.833	29.201	30.655	24.155
1.29	30.450	30.138	31.244	25.201	23.761
1.32	31.034	31.267	28.863	24.269	23.594
1.39	24.737	24.573	24.655	23.939	22.762
1.46	26.089	24.346	25.519	25.260	23.964
1.54	23.102	23.353	22.614	22.153	20.450

T/T-0

	Z/B= .250			Z/B= .750		
X/XC	.50	.93	1.29	.50	.93	1.29
INITIAL	.880	.896		.895	.936	.852
FINAL	.890	.908		.909	.946	.851

TURBULENT MODEL, θ = 35

M-INF	RE-INF	M-W	RE-XC	A.R.	ALPHA-W	P-W/P-INF
6.05	5.160E 06	4.54	9.032E 06	1.0	11.01	4.10

P/PE.O

X/XC	Z/B= 0	.310	.679
.46	1.043		
.54	1.043		
.61	1.007		
.64	1.000		
.68	1.133		
.71	2.005	1.464	.952
.75	2.709	2.422	1.220
.79	2.919	2.782	2.160
.82	3.036	2.933	2.568
.86	3.084	3.016	1.969
.89	3.092	3.019	2.755
.93	3.086		
.96	3.090		
.99	3.414	3.246	2.879
1.04	3.312	3.344	3.245
1.07	4.214	4.460	4.742
1.11	5.691	6.226	2.410
1.14	7.660	8.592	10.100
1.18	10.137	11.677	13.606
1.21	13.311	1.484	20.522
1.25	17.056	18.503	13.903
1.29	17.852	18.868	12.984
1.32	13.529	10.039	6.907
1.39	8.509	6.715	5.748
1.44	7.124	6.432	5.146
1.54	5.955	5.961	5.675

T/T-O

	Z/B= .500		
X/XC	.50	.93	1.29
INITIAL	.885	.913	1.744
FINAL	.895	.927	1.741

TURBULENT MODEL, θ = 35

M-INF	RE-INF	M-W	RE-XC	A.M.	ALPHA-W	P-W/P-INF
6.05	3.498E 06	6.05	4.083E 06	1.0	-.01	1.00

P/PEO

X/XC	Z/H= 0	.310	.679
.46	1.000	1.003	1.041
.54	1.008	1.014	1.048
.61	1.019	1.021	1.044
.64	1.024	1.025	1.046
.68	1.027	1.025	1.043
.71	1.032	1.033	1.044
.75	1.035	1.035	1.044
.79	1.036	1.035	1.036
.82	1.122		1.039
.86	1.436	1.716	1.329
.89	3.320	3.178	2.390
.93	4.167	4.102	3.650
.96	4.402	4.296	4.122
.99	4.619	4.549	4.068
1.04	5.899	5.949	6.346
1.07	10.601	10.738	12.588
1.11	18.097	18.359	21.913
1.14	26.042	26.017	28.132
1.18	27.464	26.889	24.556
1.21	24.872	10.381	23.649
1.25	24.227	24.304	23.860
1.29	23.956	23.541	22.976
1.32	23.944	19.461	22.900
1.39	24.042	24.093	23.183
1.46	24.310	26.889	22.975
1.54	22.849	22.998	20.478

T/T-0

	Z/H= .500		
X/XC	.50	.93	1.29
INITIAL	.897	.914	
FINAL	.897	.916	

TURBULENT MODEL, $\theta = 35$

M-INF	RE-INF	M-W	RE-XC	A.R.	ALPHA-W	P-W/P-INF
6.05	5.194E 06	6.05	5.061E 06	1.0	0	1.00

P/P-0

X/XC	Z/H= 0	.310	.679
.46	1.009	.998	1.042
.54	1.003	.999	1.031
.61	1.000	.995	1.020
.64	1.003	.997	1.017
.68	1.004	.998	1.014
.71	1.004	1.007	1.018
.75	1.041	1.007	1.016
.79	1.552	1.267	1.019
.82	2.413	3.010	1.514
.86	3.653	3.527	2.887
.89	3.900	3.784	3.565
.93	4.005	3.936	3.728
.96	4.031	3.926	3.781
.99	4.236	4.180	3.893
1.04	4.638	4.816	4.983
1.07	7.464	7.900	9.258
1.11	12.600	13.368	17.016
1.14	20.116	21.084	25.912
1.18	27.030	27.781	30.219
1.21	30.766	10.338	24.633
1.25	26.703	25.333	24.237
1.29	24.292	23.864	23.105
1.32	23.618	19.404	23.176
1.39	24.408	23.880	23.140
1.46	24.511	27.781	22.796
1.54	22.814	23.054	20.069

T/T-0

X/XC	Z/H= .500 .93	1.29
INITIAL	.871	.891
FINAL	.885	.906

UNCLASSIFIED

Security Classification

DOCUMENT CONTROL DATA - R & D

(Security classification of title, body of abstract and indexing annotation must be entered when the overall report is classified)

1. ORIGINATING ACTIVITY (Corporate author)
Arnold Engineering Development Center
ARO, Inc., Operating Contractor
Arnold Air Force Station, Tennessee 37389

2a. REPORT SECURITY CLASSIFICATION
UNCLASSIFIED

2b. GROUP
N/A

3. REPORT TITLE
INVESTIGATION OF FLAT-PLATE ASPECT RATIO EFFECTS ON RAMP-INDUCED, ADIABATIC, BOUNDARY-LAYER SEPARATION AT SUPERSONIC AND HYPERSONIC SPEEDS

4. DESCRIPTIVE NOTES (Type of report and inclusive dates)
Final Report, December 10, 1969, to March 25, 1970

5. AUTHOR(S) (First name, middle initial, last name)
J. Don Gray and R. W. Rhudy, ARO, Inc.

6. REPORT DATE	7a. TOTAL NO. OF PAGES	7b. NO. OF REFS
March 1971	137	17

8a. CONTRACT OR GRANT NO.	9a. ORIGINATOR'S REPORT NUMBER(S)
F40600-71-C-0002	AEDC-TR-70-235
b. PROJECT NO. 8219	
c. Program Element 62201F	9b. OTHER REPORT NO(S) (Any other numbers that may be assigned this report) ARO-VKF-TR-70-188
d.	

10. DISTRIBUTION STATEMENT
This document has been approved for public release and sale; its distribution is unlimited.

11. SUPPLEMENTARY NOTES	12. SPONSORING MILITARY ACTIVITY
Available in DDC.	Air Force Flight Dynamics Laboratory (FDCC), Wright-Patterson AFB, Ohio 45433

13. ABSTRACT

An experimental investigation of the effects of flat-plate aspect ratio on both laminar and turbulent boundary-layer separations induced by ramps was conducted at free-stream Mach numbers of 6, 8, and 10. Reynolds numbers, based on flat-plate length, ranged from 0.06 million to 1.0 million (laminar) and from 2.6 million to 9.1 million (turbulent) at near-adiabatic model wall conditions. Local Mach number on the flat plate was varied by pitching the laminar model at all free-stream Mach numbers. Longitudinal surface pressure distributions at several spanwise stations were measured to define the lateral pressure gradients and the spanwise variation of the longitudinal extent of the separation region. Data are presented to support the conclusion that for a flat plate short enough (2.5 in.) to achieve laminar flow reattachment, it is required that the flat-plate aspect ratio be of the order of 3 to be assured of negligible effects induced by the finite span.

DD FORM 1 NOV 65 1473

UNCLASSIFIED

Security Classification

14. KEY WORDS	LINK A		LINK B		LINK C	
	ROLE	WT	ROLE	WT	ROLE	WT
boundary layer separation						
laminar boundary layer						
turbulent boundary layer						
aspect ratio						
supersonic flow						
hypersonic flow						
adiabatic flow						
flat plate models						
ramps						
surface pressure data						

AFSC
Arnold AFS Tenn